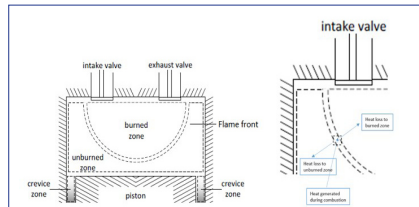
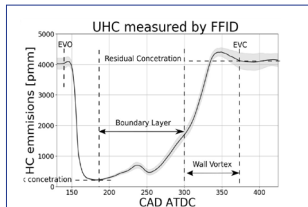


Annex 51-1



A Report from the Advanced Motor Fuels Technology Collaboration Programme

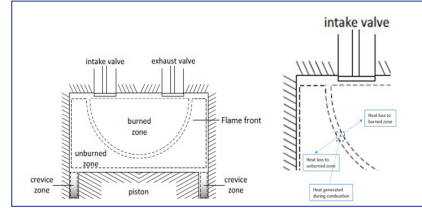
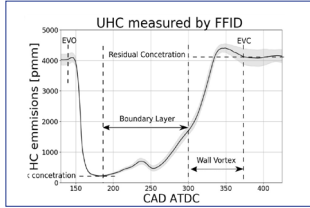
Methane Emission Control

Jesper Schramm



ADVANCED MOTOR FUELS
Technology Collaboration Programme on
Advanced Motor Fuels

Annex 51-1



A Report from the Advanced Motor Fuels Technology Collaboration Programme

Methane Emission Control

Jesper Schramm

Preface

This is the final report of IEA Advanced Motor Fuels (AMF) Technology Collaboration Program (TCP), Annex 51: “*Methane Emission Control*”. The annex was initiated partly due to the results found in the earlier Annex 39. Jesper Schramm, DTU Mechanical Engineering has been the operating agent on behalf of Denmark, and the participating countries were: Denmark, Finland, Japan, Korea, Sweden and Switzerland.

The main text of the report has been written by the Danish OA with valuable input from Japan and Sweden. Case studies 1, 2 and 4 were also prepared by Denmark. Case Study 3 was prepared by Switzerland, Case Study 5 by Korea, Case Study 6 by Finland and Case Study 7 by Sweden.

Aknowledgement

The editor would like to thank The Innovation Fund Denmark and The Danish Maritime Fund for their funding of the project through the BlueINNOship project in Denmark. Case Study 3 was supported by Swiss Federal Office of Energy (SFoE) Gasmobil AG c/o and Association of the Swiss Gas Industry (VSG). Case Study 6 was supported by CENGE, NewGas, Hercules-2 and INTENS, funded by Business Finland, European Union and several Finnish companies.

The editor of the report would like to thank the dedicated contributors from the involved countries. These were:

Denmark: Michael V. Jensen, Mads C. Jespersen

Finland: Kati Lehtoranta, Hannu Vesala, Timo Murtonen, Päivi Koponen, Rasmus Pettinen, Nils-Olof Nylund

Japan: Masayuki Kobayashi, Yutaka Takada

Korea: Chun-Beom Lee, Mi-Young Kim

Sweden: Magnus Lindgreen

Switzerland: Christian Bach, Stephan Renz

Summary

The mechanisms behind formation of unburned methane from natural gas engines were studied in this project. Furthermore, measures to address reduction of methane emissions were enlightened qualitatively and quantitatively in order to estimate the influence of different technical solutions on the effect of the emissions. These solutions includes developments during the main combustion in the combustion chamber, and catalytic after treatment of the exhaust.

The project has resulted in a detailed understanding of methane formation mechanisms. It is concluded, that there are a number of items of special importance. These include: misfire/bulk quenching, wall quenching, crevice volumes, post oxidation and valve timing/overlap. It is concluded that particularly low-pressure dual fuel engines are associated with high values of methane emissions. These methane emissions most likely off-sets the advantage of applying natural gas instead of, particularly, diesel fueled engines with respect to greenhouse gas emissions. Since the unburned methane emissions origins from areas near the combustion chamber walls the sensible way to go now is towards direct injection of natural gas/bio-methane in order to reduce emissions.

The project included 7 different case studies. In case study 1 the knowledge about the formation mechanisms was implemented in a phenomenological mathematical model, TECMU (Thermodynamic Engine Cycle Modeling of Unburned Hydrocarbons), which was used to analyze the influence of the different mechanisms. The model was used to simulate emissions from a 2014 model medium-speed 4 stroke dual fuel engine. The model results were in good agreement with experimental results, and demonstrated that all of the above mentioned mechanisms were important in relation to the resulting emissions of unburned methane. The model showed, among other things, that a straight forward way to reduce the emission could be achieved by changing the valve timing. This would reduce unburned emissions by 12-62 %, depending on the engine load, a result that was in good agreement with practical measurements on a new engine generation, where the valve timing was changed accordingly.

Further evaluation of the mechanism understanding, was carried out in case study 2 by applying a special exhaust measurement technique in a single cylinder research engine. In these experiments a so-called FFID (Fast Flame Ionization Detection) was applied to distinguish between the contribution from the different mechanisms to the unburned hydrocarbon emissions. The study focussed on investigation of the influence of different operating parameters on the unburned methane emissions from an engine operating at moderately lean air fuel mixtures. The influence of compression ratio, intake pressure and excess air ratio was studied. It was concluded that both the crevice mechanism and the quench layer mechanism was important for in the investigated operating ranges. Post oxidation seems also to play an important role in contradiction to the medium speed engine investigated in Case Study 1, where post oxidation was negligible. This most likely is due to the fact that the two engines operate at different excess air ratios - the medium speed engine operating at much leaner conditions than the engine applied in Case Study 2.

In case study 3, the influence of mixing hydrogen to the fuel was investigated. Methane was applied as fuel with and without hydrogen admixture in a Euro-4 vehicle with stoichiometric operated, naturally aspirated, manifold injected 4 cylinder engine with an engine capacity of 2.0 l. The vehicle was equipped with an external fuel supply, an access to the electronic engine control (ECU), a modified catalytic converter as well as an internal cylinder pressure measurement in the combustion chamber of the

engine. The vehicle was driven with two different driving cycles (NEDC and WLTC) on a chassis dynamometer. Emissions were measured before and after the catalytic converter.

The blending of hydrogen into the CNG is not readily feasible in terms of materials, as both the gas network and the gas-carrying components in the vehicle must be designed for this. However, operation in conventional CNG vehicles would lead to significantly lower pollutant emissions than those already present in CNG operation. NO_x emissions could be practically eliminated in the entire operating range, and T.HC emissions, which mainly consist of methane, which is primarily a strong greenhouse gas, could also be reduced by an average of one third. However, the volumetric energy density, which decreases by almost 30% with an H₂ content of 25 mole %, would be operationally disadvantageous. It could be compensated by increasing the pressure to 350 bar. For future combustion processes with diluted mixture formation (lean or EGR operation), H₂ blending could be an interesting option due to the difficult ignition of (diluted) methane gases.

In case study 4, a series of Rh/zeolite catalysts design for oxidation of exhaust CH₄ were tested. 1 wt.% Rh/zeolite catalyst had higher activity compared with the commercial catalyst under same operation condition. The activity of the Rh/zeolite catalyst can be significantly enhanced by elevating the operation temperature to 475 °C and limiting the SO₂ concentration to a low level. It seems promising to be used in the real engine exhausted gas condition where the SO₂ concentration is 1-2 ppm. Regeneration by removing SO₂ from the reaction gas can partly restore the catalyst activity, but a more efficient regeneration method is still being sought.

Case study 5 investigated the Pd based catalyst performance. Pd is believed to be the best converting precious metal for methane catalysts. In this study, some key factors were found, which led to enhance the activity and durability of current Pd-based CNG catalyst. Two critical contributions were from optimal support material and optimal characteristics of Pd. Pd dispersion were achieved by selecting support with optimal surface property. Pd-Pt alloying and the use of electronic modifiers such as OSC and promoters were effective to make CNG catalyst more durable.

SO₂ and water are known to inhibit oxidation of methane in a catalytic converter. In case study 6, a regeneration method by hydrogen was studied. With a catalyst aged to a conversion efficiency of 37%, it was possible to maintain this level, and even increase the efficiency after regeneration and ageing again applying regeneration gases containing 2,5% hydrogen.

In case study 7, a number of vehicles were tested for tailpipe methane emissions as well as other methane emissions. The amount of tested vehicles was 60. Twelve of the tested vehicles (15%) did not have any leakage. Thirty buses (50 %) did have leakage at fuel filling fittings corresponding to 2.9 ug/ day on average. There were no leakage from the gas tanks and roof fittings and only 3 % of the vehicles did have a diffuse, not quantified, increased level in the engine room. The major source of methane was inside the tailpipe corresponding to 0.88 mg /day and bus. The result indicates the major contribution of methane originates from slip during driving.

Content

1. Background	6
Methane emissions and regulations	6
Annex 39 of the Advanced Motor Fuels TCP	7
2. Unburned methane emission formation	11
Overview of formation mechanisms	11
Quench layer	14
Crevices	16
Misfire/bulk quenching	16
Post oxidation	18
Valve overlap	20
3. Outside engine emissions	21
4. Emission reduction technology	21
Combustion principle	22
Hydrogen	26
Oxidation catalysts	27
5. Case studies	
<u>Case study 1.</u> Modeling of unburned methane formation (Danish study)	30
<u>Case study 2.</u> Quantification of methane emissions from different mechanisms (Danish study)	35
<u>Case study 3.</u> Application of methane with hydrogen (Swiss study)	41
<u>Case study 4.</u> Danish catalyst study	66
<u>Case study 5.</u> Korean catalyst study.	71
<u>Case study 6.</u> Finnish catalyst study.	83
<u>Case study 7.</u> Outside engine emissions (Swedish study)	89
6. Conclusions	94
7. References	96

1. Background

The use of methane (natural gas, biogas) for transport will increase. Although diesel dual fuel (DDF) technology could bring the efficiency of gas engines close to the efficiency of diesel engines, AMF Annex 39 *“Enhanced Emission Performance and Fuel Efficiency for HD Methane Engines”* clearly demonstrated that methane slip remains a serious problem for current DDF engines. Alternatively, advanced spark ignition (SI) technologies (e.g., variable valve trains, cylinder deactivation, and high-level exhaust gas recirculation) could be applied to increase engine efficiency. However, there would still be a need for methane catalysts, due to the unsatisfactory performance and durability of current methane catalysts. Annex 51 is based on the experience of Annex 39, with the goal of improving engine-out methane emissions, methane catalyst efficiency, and methane emissions from other parts of the vehicle. Combustion engines for vehicles can be replaced by or converted to liquefied natural gas (LNG) operation. This conversion has benefits in terms of emissions of carbon dioxide (CO₂), nitrogen oxides (NO_x), and particulates. Reductions in CO₂ occur partly because the ratio between carbon and hydrogen is less for natural gas than for liquid hydrocarbons (e.g., diesel, gasoline), and partly because the LNG engines can be more efficient than the traditional ones, depending on the combustion principle chosen. With regard to greenhouse gas (GHG) effects, it is a disadvantage that LNG engines emit significantly larger quantities of unburned methane than do traditional engines. Because methane is a 20+ times more powerful GHG than CO₂, the overall result could easily be an increase in GHG emissions from vehicles if their engines were converted to run on LNG. Researchers have considerable experience in studying unburned hydrocarbons in automobile engines. This experience has motivated them to develop engines that emit very low levels of hydrocarbons. Methane, however, is a particularly stable hydrocarbon and is not converted as efficiently as are the other hydrocarbons in combustion engines. At the higher temperatures that occur during the main combustion, the methane is burned as completely as the other hydrocarbons. In colder areas near walls and in crevices, however, some unburned hydrocarbons escape the main combustion. These hydrocarbons are normally post-oxidized in the hot combustion gas, but methane molecules are probably too stable to be converted at these lower temperatures. This stability also causes problems with regard to converting methane in after-treatment systems like three-way catalytic converters. The onboard storage system for methane (either compressed or liquefied) can also be a source of vehicle methane emissions.

The scope of Annex 51 has been to give an overview/status of the NG combustion/after treatment engine technology, primarily concerned with dual-fuel technology, and the status for understanding how unburned methane is formed in a combustion engine. This latter part is given in the form of a general introduction to methane combustion in chapter 3. The status for engine technology is given in chapter 4, and the overview of AMF member countries activities is given in chapter 5.

Methane emissions and regulations

Methane is the most common hydrocarbon in the exhaust of a natural gas engine, but not found in large concentrations in gasoline engine exhaust, and the concentration is close to zero in diesel exhaust. For many years methane has not been considered as a public health concern. Therefore, emission regulations for hydrocarbons in many cases have been regulated as NMHC (Non Methane HydroCarbons) or similar. In recent years, the attention to methane’s high GHG potential has changed this situation.

Methane is a strong greenhouse gas, 84-86 times stronger than carbon dioxide according to IPCC [1], if one consider the effect on the Global Warming Potential over a period of 20 years (GWP_{20}). Over time methane is converted to carbon dioxide and water in the atmosphere, and the effect over the years is reduced. However, considering a period of 100 years, GWP_{100} for methane is still 28-34 times the value for carbon dioxide, according to IPCC.

Authorities all over the world have started the preparing process towards more stringent methane emission regulations. Euro VI regulations, for instance, includes an extra limit of 0,5 g/kWh from heavy-duty gas engines on top of the traditional THC emission standards [2].

Natural gas is particularly a potential fuel for marine applications [3]. Therefore, it is relevant to look at the status of gas engine technology for this sector. Substitution of diesel with natural gas has often been seen as an advantage in relation to the GHG emissions, since the ratio between hydrogen and carbon content in natural gas favours lower carbon dioxide emissions. However, this conclusion is only valid in some cases, if one includes the GHG effect of methane emissions.

In Figure 1 the GHG benefit of converting from diesel engine technology to natural gas engine technology is shown as a red line [2]. In the black dashed line, the result are corrected for the difference in fuel consumption to a hypothetic situation where all engines have the same Brake Thermal Efficiency ($BTE = 44\%$). In the figure, the GHG effect of methane emissions has been taken into account. There is a benefit from operating HP DF (High Pressure Dual Fuel) engines on natural gas. These engines are the large two-stroke marine engines (MAN's ME-GI), which emits very low amounts of methane. Also SI/TWC (Spark Ignited HD natural gas engines with Three Way Catalysts) for heavy duty truck purposes still have some advantages against their diesel counterparts. The engines shown here represent post 2010 technology. However, for other engine types, the GHG emission benefit from natural gas operation is negative due to the methane emissions. LP (Low Pressure) HD pre 2010 emits about 15 g CH_4 /kWh, while post 2010 LP HD emits about 8,5 g CH_4 /kWh [2].

The emission of unburned fuel in percentage of the total fuel consumption is also illustrated with the addition of the lower horizontal axis. This axis has been constructed from the assumption that all type of engines have a $BTE \sim 44\%$. It is therefore connected with some uncertainty. However, it illustrates that there is quite a potential for improving the engine efficiencies in many cases.

[Annex 39 of the Advanced Motor Fuels TCP](#)

The results of an earlier project in the AMF TCP (Annex 39 [4]) was an important part of the background for initiating the present project. In annex 39, the emission of CO_2 and $CO_2 + GWP_{100} * CH_4$ were measured/estimated for 5 different HD vehicles. The technology for the different vehicles are presented in Table 1. The table present an overview of the vehicles included in the Swedish test program. In addition, one extra vehicle is included in the figure (DDF3) as a typical representative vehicle subjected to retrofit program. Such buses have been in normal operation for several years and the intention is either to improve the emission performance or simply reduce operating cost for the vehicle.

The two dedicated gas buses represent state-of-the-art technology and are offered on the market as new buses (OEM) by manufacturers in Europe. As input from task sharing members of Annex 39 there is a wish for adding more test results and experience for vehicles using dedicated gas engines.

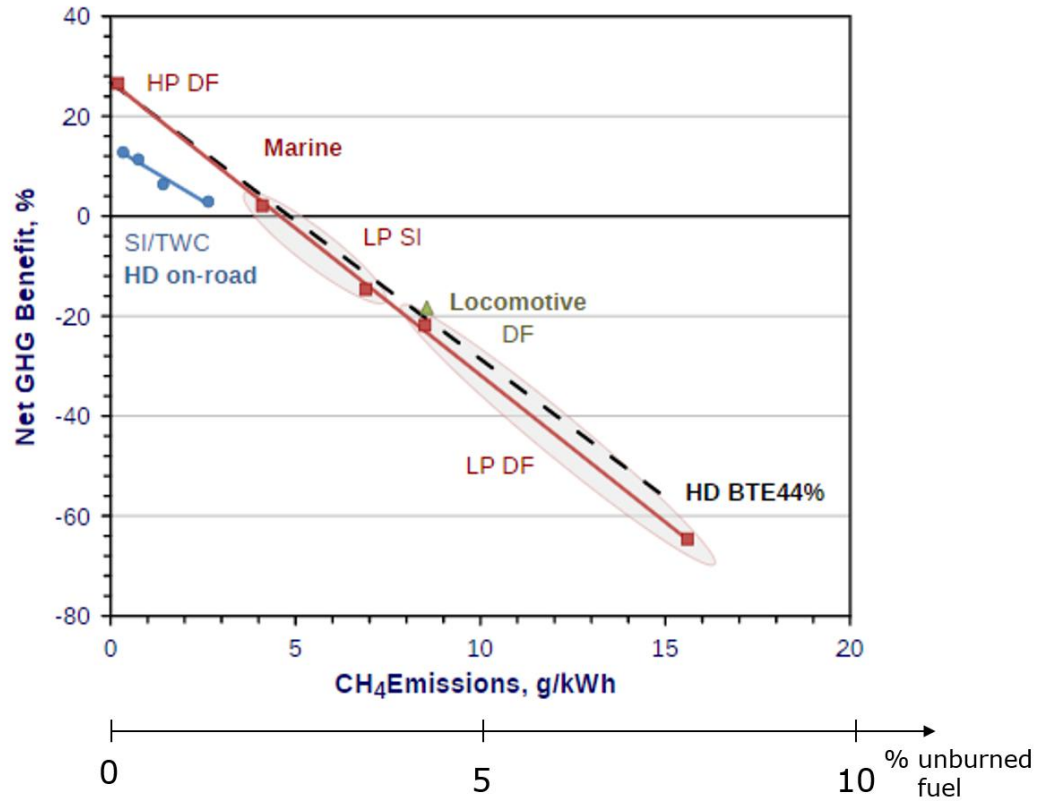


Figure 1. Net GHG emissions from different type of natural gas engines.

	DDF1	DDF2	DDF3	SI-lean burn	SI-lean/mix-burn
Model year	2011	2010	2003	2010	2010
CD Test weight (tons)	~20	-	18.8	14.1	13.8
PEMS Test weight (tons)	~20 and ~40	9.1	-	14.1	13.8
Retrofit/OEM	Retrofit/OEM	Retrofit	Retrofit	OEM	OEM
Gas system	Clean Air Power (CAP)	Hardstaff	NGV Motori	Dedicated SI	Dedicated SI
Cylinder volume (dm³)	13	7	12	9	13
Max power (kW)	345	181	250	199	228
After-treatment	DOC, SCR	SCR	CRT	DOC, SCR	TWC
Fuel	Diesel/LBG	Diesel/CNG	Diesel/LNG	CNG	CNG
Emission class	Euro V	Euro V	Euro III	EEV	EEV
Chassis	Tractor	Truck	Intercity Bus	City bus	City bus
Odometer (km)	---	22 500	n.a.	15 500	85 793
Note	Test on-road at +5°C	Test only on-road	Test only on chassis dyno	Test on-road at -2°C	Test on-road at +10°C

Table 1 Vehicle technology investigated in Annex 39.

The two trucks named DDF1 and DDF2 is offered as new vehicles (OEM) by a manufacturer in Europe. The working principal for those two engines are dual fuel technology and at the time for testing such technology could not be approved in Europe. The vehicles are therefore accepted on the road based on a national waiver. This system is commonly used in Europe for field testing of technology not mature enough for the commercial market. As input from task sharing members of Annex 39 there is a wish for adding test results and experience for DDF concepts not yet available on the European market as well as tests results from DDF vehicles that have been in normal operation for longer time.

Vehicles tested in the special program promoted by Swedish Gas Technology Centre (SGC) as well as the measurements of unregulated compounds were the following three vehicles:

1. Dedicated CNG bus with SI-lean/mix combustion, a technology alternating between stoichiometric and lean combustion. During the test program the CNG was supplied from the tank on the vehicle and was filled with gas from a commercial filling station.
2. A long haul truck using dual fuel technology. Modification of the engine and fuelling system was carried out in close cooperation with the manufacturer of the vehicle. The vehicle/engine was also modified to use liquefied biogas (LBG) as fuel. Both the bio gas and the diesel were supplied by the manufacturer of the vehicle.
3. Dedicated CNG bus with lean-burn combustion, a technology with air excess. During the test program the CNG was supplied from the tank on the vehicle and was filled with gas from a commercial filling station.

The GHG emission results are shown in Figure 2.

The results in the figure present measurement of different combustion strategies on a chassis dynamometer using the WHVC driving cycle. All tests have been carried out with a warmed up engine. The blue bars represents tail-pipe emissions of CO₂ and the red bars represents the CO₂ equivalent emissions comprising the tail-pipe CO₂ plus the emissions of CH₄ multiplied by the factor (34) for global warming potential. From the figure, it is easy to see that in all cases the lowest CO₂ emissions are found when a dual fuel engine is operating in diesel mode. Further, tail-pipe CO₂ emissions are higher for the two dedicated SI-engine methane fueled buses than for the dual fuel engines operating in diesel mode. This is mainly because the energy efficiency for engines using diesel technology is higher than for engines operating according to spark ignited technology.

When adding the emissions of CH₄ to the CO₂ emissions for a total picture of GHG, it is easy to see that the equivalent CO₂ emissions for dual fuel engines operating in dual fuel mode will increase.

The overall experience from the test program is that emissions of CH₄ will increase when the diesel replacement is increased. In reality, higher rate of diesel replacement with gas will result in higher total greenhouse gas emissions. This is in fact a serious dilemma for technology of today.

Actual CO₂ and CO₂+equivalent to CH₄ slip

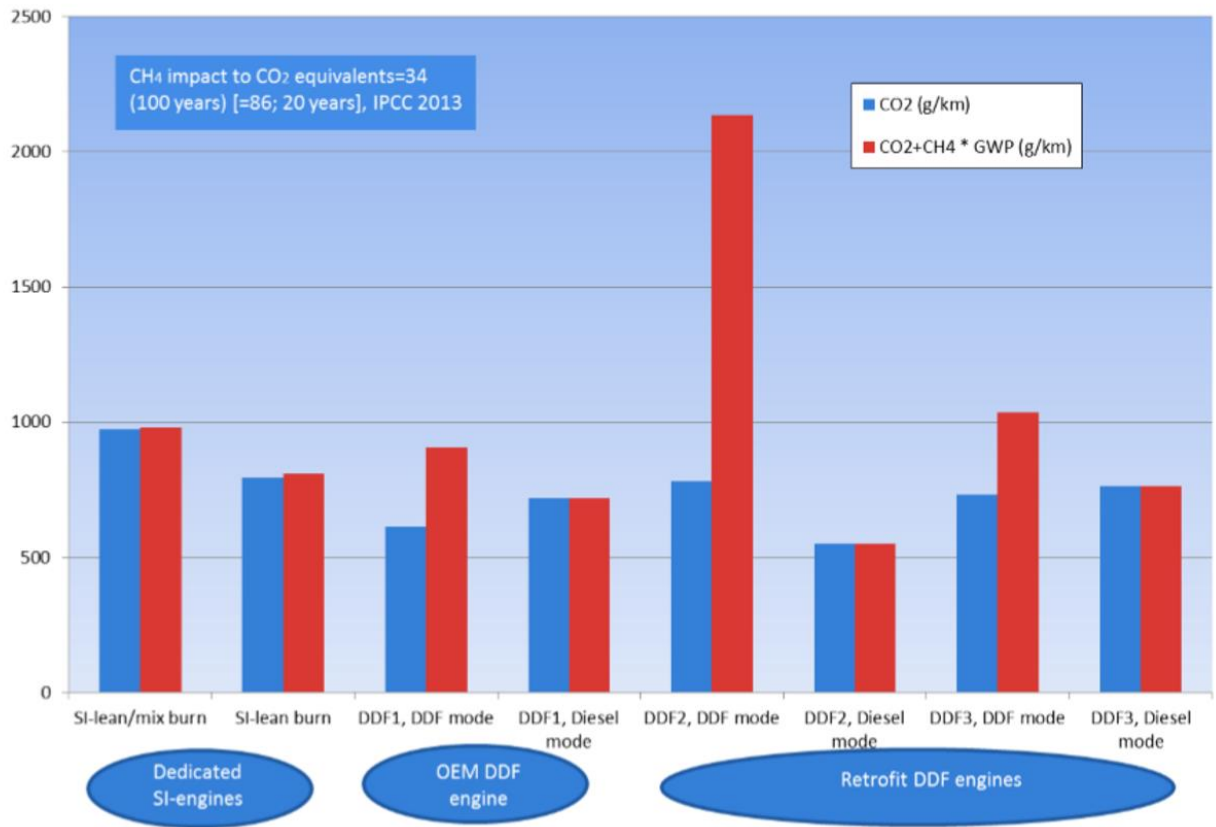


Figure 2. GHG emissions from vehicles investigated in Annex 39.

2. Unburned methane emission formation

Unburned methane formation mechanisms have been studied at The Technical University of Denmark in various projects. The knowledge obtained in this way is described in this section. The model TECMU has been developed, based on this knowledge. Applying TECMU for simulation of real engine operation will give important information about how to design future engines, in order to reduce future methane emissions. This exercise is carried out in one of the Danish case studies (case study 1 in chapter 5). The different identified mechanisms for methane formation are studied further in an experimental investigation with a single cylinder natural gas engine, where an FFID (Fast Flame Ionization Detector) instrument is applied for evaluation of the importance of the individual mechanisms (case study 2 in chapter 5).

Overview of formation mechanisms

Unburned hydrocarbons has been an issue for combustion engines since the 1950'ies. The main concern at that time was (and is still) the environment and the fuel consumption of the engines. Gasoline engines were thought to be the main problem, and the quench layer near the walls of the combustion chamber were thought to be the main reason for unburned fuel to escape the combustion processes and leave the engine unburned with the exhaust [5]. However, in the late 1970'ies, experimental studies as well as mathematical models of the combustion processes showed that the quench layer would mix rapidly with the main cylinder content and undergo post oxidation after flame extinction in a timescale short enough to maintain a temperature, high enough to allow for continued reactions [6-8].

Researchers started to look at other possible mechanism that could then be responsible. Crevices in the combustion chamber showed to be a major factor [9-11], and until today, this mechanism is thought to be of high importance. The flame will not be able to penetrate the crevices, and the unburned fuel-air mixture will be retained in the crevices for a time period long enough to prevent post oxidation of the hydrocarbons due to the temperature drop in the bulk gas. The oil layer on the cylinder wall and deposits on the combustion chamber walls were also thought to be able to absorb and retain hydrocarbons in the same manner.

As the lean burn concept gained more interest, bulk quenching and misfire became important as well. Cyclic variations needed to be avoided, by improving mixture formation, i.e. turbulence became important to improve by obtaining a better design of the engine [12].

Methane emissions have until now not been considered as a serious pollutant. The introduction of the term NMVOC (Non Methane Volatile Organic Compounds) in air pollution regulations clearly shows this. Now it is evident that methane is important since it is a very strong greenhouse gas, and therefore, is thought to be of serious concern for the global warming. Since application of natural gas has become more widespread, it is now important to look at unburned methane emissions.

Methane is a very stable molecule, compared to other hydrocarbons. Therefore, methane is expected to behave differently with respect to the established mechanisms for unburned hydrocarbon formation. One of the main tasks of the AMF Annex 51 has been to investigate the fundamental behavior of methane during the combustion inside a natural gas engine in order to propose the optimal design for f. ex. a dual-fuel, medium speed, natural gas engine, which has been involved in the Danish part of this study. However, the findings from this investigation were expected to be of general interest for all types

of engines. In order to evaluate the applicability of the fundamental studies for different kind of engines, it is important to know about the basic types of engine combustion processes.

Spark Ignition (SI) engines

In an SI engine the fuel is gaseous, and mixed with air. The charge is ignited with a spark plug, creating a flame front that protrudes the unburned charge until it reaches the walls of the combustion chamber, Figure 3.a. Gasoline, natural gas, methanol and ethanol are typical fuels for this type of engine. The fuels are characteristic by having a high octane number, which assures that the fuel does not ignite by itself. The combustion is therefore controlled by the timing of the ignition, initiated by the spark plug. This combustion process is very fast, and the piston almost doesn't move during this period.

Compression Ignition (CI) Engines.

In a CI engine the fuel is supposed to ignite by itself. Here there is no distinct flame front, the fuel rather ignites at several points in the fuel spray injected into the combustion chamber, until the cylinder content is one ocean of flames, Figure 3.b. This combustion process is rather slow, compared to SI combustion, since it involves combustion of liquid droplets, a much slower process. Typical fuels for CI engines are diesel, Heavy Fuel Oil (HFO) and DiMethylEther (DME). These fuels are characterized by a high cetane number.

Dual Fuel (DF) engines

In a DF engine we typically operate a high octane number fuel in a CI engine. This is possible because the fuel-air charge is ignited by a pilot amount of fuel with high cetane number. This type of engine is relevant in this context because natural gas is often applied in a DF engine, together with a pilot of diesel, particularly in larger engines, like truck engines or ship engines. The reason for applying this type of engine is the larger efficiency and that the engine manufacturer often chose to convert a diesel engine to DF operation. This is because of the relatively simple technical solution, and the possibility to convert to diesel operation when needed. The pilot diesel acts as a kind of spark plug that ignites the main fuel in the cylinder. Therefore the combustion process is almost as fast as in the SI engine. The process is illustrated in Figure 3.c.

The mechanisms for formations of unburned methane in a natural gas engine are very dependent on the basic engine combustion principle, as discussed in the following sections.

The knowledge about formation of unburned hydrocarbons in combustion engines is reflected in computer models, often developed in order to have a design tool for improving the engines. Whereas several models for gasoline engines have been developed, only a few investigations, have been concerned with formation of unburned methane in natural gas engines. This is because methane reduction is much more difficult to achieve and because methane has not been considered as a severe pollution until recently. However, concern about the potential as a greenhouse gas has changed this situation dramatically in the past two decades.

The computer model, TECMU, involved in this study identifies four different mechanisms, that are known to cause methane slip from the engines. Three of these mechanisms are indicated in Figure 4, which illustrates the combustion chamber of an engine without a spark plug. The ignition mechanism could be either by compression ignition of a pilot fuel or by application of a spark plug. The mechanisms are enlightened in the following sections, and the TECMU model is applied in a practical study described later in "Case study 1" in chapter 5.

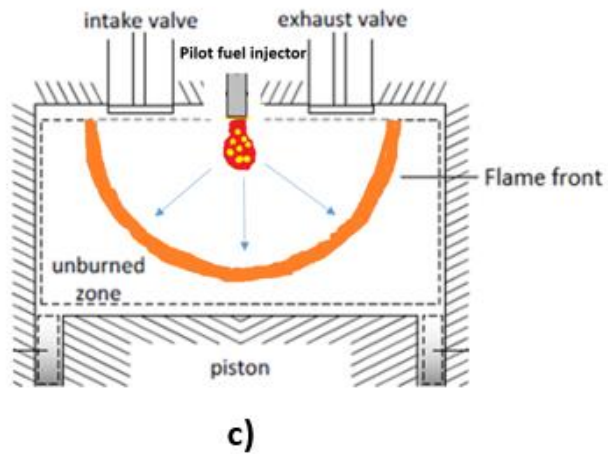
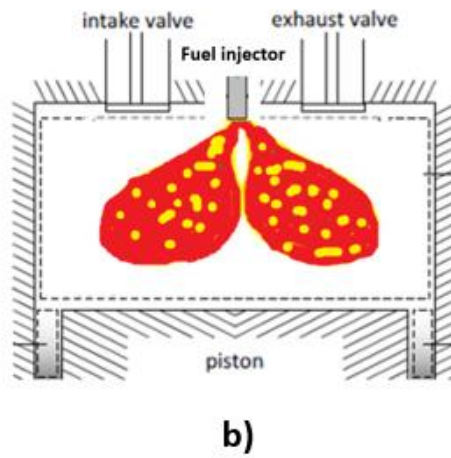
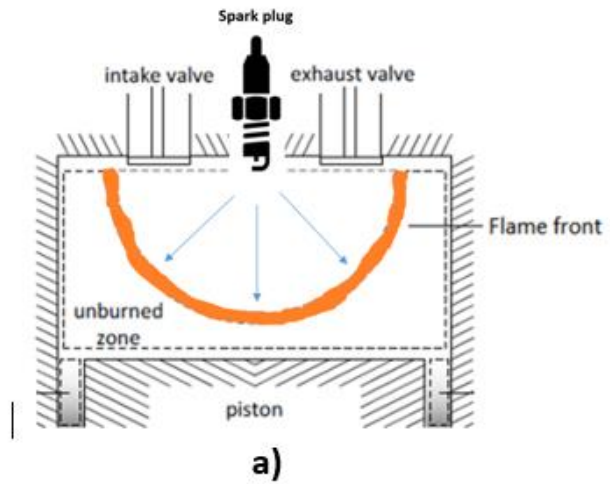


Figure 3.a-c. Schematic combustion of fuel in an SI engine (a), a CI engine (b) and a DF engine (c).

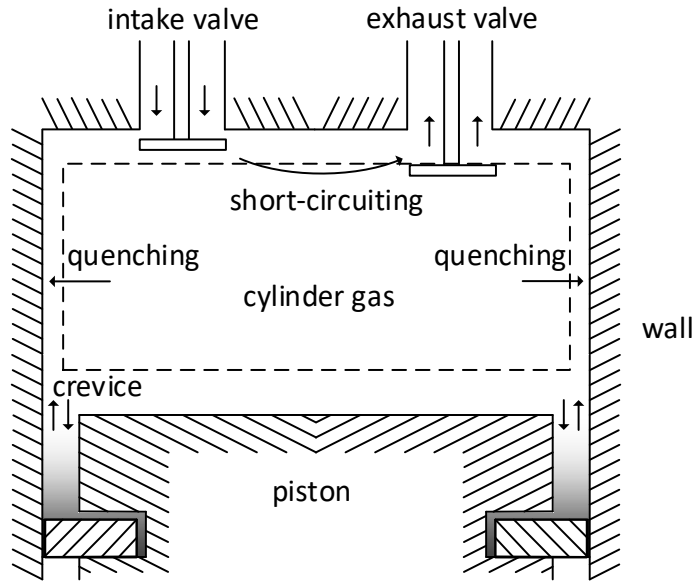


Figure 4. Methane slip sources in a combustion chamber

Quench layer

The first mechanism for the formation of unburned methane is the flame quenching near the chamber walls.

In a natural gas fueled combustion engine, the combustion process starts with a spark from a spark plug or by compression ignition in a pilot fuel spray. Both processes usually are activated from the top center of the cylinder. From there, the combustion penetrates the combustion chamber as a flame front, which in the end is quenched when the flame reaches the walls of the cylinder. Here the temperatures are too low to keep the flame alive, and some unburned charge is left near the wall in the so-called “quench layer”. In the TECMU model, an energy balance for the flame front decides when the flame is quenched. The flame is considered to be quenched, when the heat flow from the flame to the surroundings is larger than the heat produced from the combustion. This is illustrated in Figure 5.

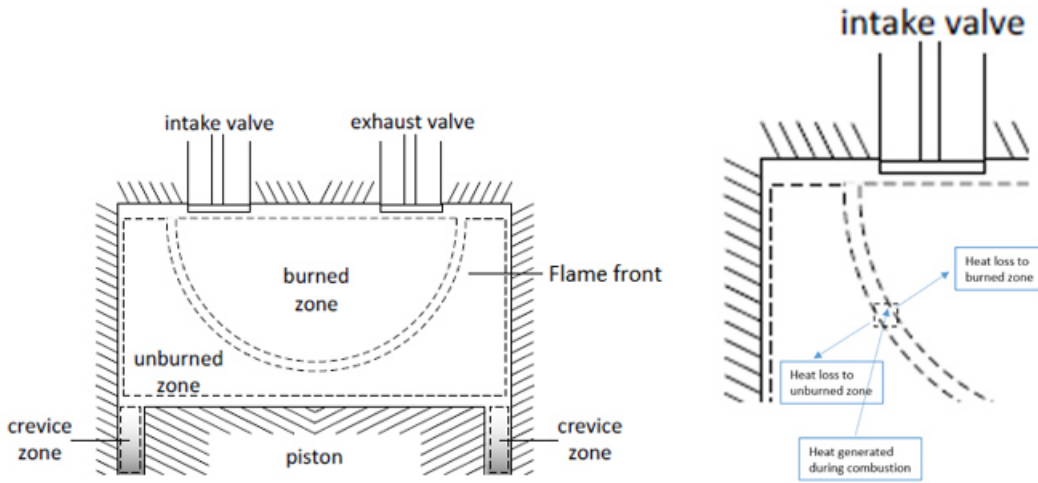


Figure 5. The flame front penetrating the combustion chamber (left) and the heat balance for an element in the flame front (right).

The heat loss from the flame to the burned gas zone in Figure 5 is assumed to be negligible, and heat loss to the unburned gas zone is assumed to happen as heat conduction through the unburned gas zone to the cylinder wall. Based on the energy balance for the flame a quench distance d_q is calculated. The flame is discretized into a number of flame elements, and at every integration time step during the combustion phase, the quench distance d_q is calculated and compared to the actual distance between each flame element and cylinder wall. If the actual distance is smaller than the calculated quench distance, the flame element is assumed to be quenched. The quench distance d_q is calculated as:

$$d_q = \frac{1}{\frac{1}{r_{bg}} - k_{ubg} \frac{(T_{bg} - T_w)}{r_{bg}^2 \dot{q}_c}} - r_{bg} \quad \{1\}$$

r_{bg} is the radius of the burned gas zone, k_{ubg} is the heat conductivity of the unburned gas, and T_{bg} and T_w are the temperatures of the burned gas and cylinder wall, respectively. \dot{q}_c is the heat production rate in the flame divided by the total flame surface area.

Considerable amounts of unburned hydrocarbons, methane or gasoline, depending on the fuel applied, is found in this layer. However, the temperature in the combustion chamber is still high at this time in the engine cycle, and a significant amount of the unburned fuel will undergo “post oxidation” at these high temperatures. However, this phenomenon has mainly been studied for gasoline, and there is a chance that methane will not follow this pattern since methane is a very stable molecule, compared to gasoline components. The activation energy for the combustion of methane may be too high for the progress of post oxidation.

This was investigated in the Danish case study described in case study 1. Here it was found for simulation of a dual fuel natural gas engine, that less than 2 % of the methane was post oxidized, whereas more than 90 % of fuel was post oxidized in the case with gasoline at medium and high load. Unburned methane could, therefore, for a large part be caused by this mechanism, since engine design so far has been adapted to the traditional gasoline.

The quench layer is very much related to the premixed charge phenomena, since the premixed charge is located near the cold walls of the combustion chamber. In a case where the fuel is injected through a nozzle directly into the cylinder, the situation is completely different. Here the fuel injection prevents too much contact with the walls. This could explain why high pressure DF engines have much lower unburned methane emissions than low pressure DF engines, as shown in Figure 1.

Crevice

The second mechanism for the formation of unburned methane is the crevice mechanism. It is anticipated that unburned charge is trapped in crevices, primarily between the piston top and the cylinder walls, during the compression of the engine cycle. The flame cannot penetrate the crevice volume since it is surrounded by cold walls. The flow of unburned charge into the crevice volumes is in the TECMU model assumed to be controlled by the ideal gas law, where the volume, temperature and pressure in the crevices decides the mass of unburned fuel in the crevices. The mass flow is thus assumed to follow the expression:

$$\dot{m}_{cr} = \frac{V_{cr}}{R_{cr} T_{cr}} \frac{dp}{d\theta} \quad \{2\}$$

The crevices are thus filled up until the maximum cylinder pressure is reached. Then the flow is reverted, and the unburned fuel enters the main combustion chamber again. Like the quench layer case, this means that the hydrocarbons undergo post oxidation, but the temperatures are too low for a complete post oxidation. This is particularly the case for methane.

This mechanism was also investigated in the TECMU model of the Danish case study. Here it was found for simulation of a dual fuel natural gas engine, that less than 2,2 % of the crevice methane was post oxidized, whereas 70-75 % of fuel was post oxidized in the case with gasoline, except at low load (25 % load) where 15,4% was post oxidized. Unburned methane is therefore, for a large part be caused by the crevice mechanism. The results show, that a significant part of unburned gasoline emissions also could be caused by this mechanism in gasoline engines, since the crevice hydrocarbons are released to the main combustion chamber very late in the exhaust stroke, preventing total post oxidation.

Misfiring/bulk quenching

The third mechanism, which is not illustrated in Figure 3, is due to so called misfire, where the thermodynamic conditions during compression prevent ignition of the fuel in some of the engine cycles, typically during lean burn conditions. This is closely related to a phenomenon called "bulk quenching" where the ignition do occur but the combustion conditions result in a very early quenching of the flame.

The phenomena usually happens gradually when the engine operation becomes leaner. This can be described as a statistical phenomenon, beginning with misfiring/“bulk quenching” in a few cycles out of many, and then with increasing frequency as the equivalence ratio decreases. The frequency of misfiring is often characterized as the COV (coefficient of variation) of the indicated mean effective pressure (imep). COV is defined as:

$$COV_{imep} = \frac{\sigma_{imep}}{x_{imep}} \quad \{3\}$$

where σ_{imep} is the standard deviation and x_{imep} is the mean value of imep over a large number of cycles. An example of COV values and the variation with the equivalence ratio is seen for a natural gas engine in Figure 6 [13]. The COV value in Figure 6 may be interpreted as something proportional to the rate of bulk quenching/percentage of misfiring cycles during operation. This pattern varies from one engine to another, but seems quite consistent for a number of investigations [13-15]. The trend line in Figure 6 is therefore taken as a good first approach. However, the coefficients of the mathematical approach will vary somewhat with the engine in question. Finding these coefficients is an essential job in model calibration against experimental results.

In the TECMU model, calibrated against results from a medium speed dual fuel natural gas engine, the mathematical description of the misfire frequency is described as:

$$cov = 0,0111\phi^{-2,944} \quad \{4\}$$

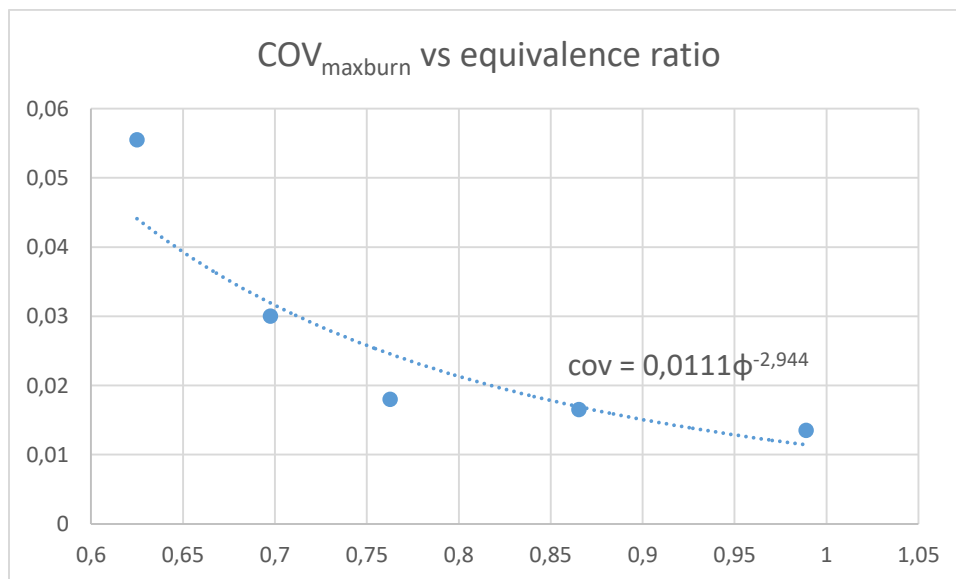


Figure 6. Example of COV values of the indicated mean pressure in a natural gas engine

Post oxidation

The unburned hydrocarbons related to the previously described mechanisms are strongly related to the combustion process inside the engine. This again determines the temperature and pressure during the engine cycle. The progress of the combustion can be divided into two phases: *the main combustion* related to the flame propagation and *the post oxidation* related to the reactions that occur due to the high temperatures after the flame quenching.

The combustion can be implemented in two different ways:

1) If the rate of heat release is known from a particular engine, then this information can be used to describe the progress of flame/combustion. For the mathematical description of the rate of heat release, so called Wiebe functions are applied. The heat release rate function can be written:

$$\dot{Q}_c = Q_c \frac{a(m+1)}{\theta_d} \left(\frac{\theta - \theta_s}{\theta_d} \right)^m \exp \left(-a \left(\frac{\theta - \theta_s}{\theta_d} \right)^{m+1} \right) \quad \{5\}$$

Q_c is the total heat released θ_s and θ_d denote the crank angle for start of combustion and the combustion duration. a and m are parameters, the so-called efficiency parameter and shape factor, which may be adjusted to fit a certain heat release rate profile.

The Q_c can then be applied in an energy balance for each of the zones (burned and unburned) of the engine cylinder, in order to estimate temperatures and pressures during the engine cycle. Equations 6 and 7 show the general form of the applied energy and mass balance, respectively.

$$\frac{dT}{d\theta} = \left(\dot{Q}_c - \dot{Q}_w - p \frac{dV}{d\theta} + \sum \dot{m} h - \sum_{i=1}^n \left(u_i \frac{dm_i}{d\theta} \right) \right) \frac{1}{m c_v} \quad \{6\}$$

$$\frac{dm_i}{d\theta} = \sum \dot{m} y_i + S_i \quad \{7\}$$

T , h and c_v are mass averaged temperature, specific enthalpy and specific heat capacity at constant volume, respectively. m is mass, p and V are pressure and volume. Index i represents gas species i out of n species. Q is heat transfer rate and \dot{m} is mass flow rate, both with respect to crank angle θ . Indices c and w are short for combustion and wall, respectively. u is specific internal energy, y is mass fraction, and S represents a source term due to chemical reactions.

The temperature and pressure estimates can thus be used to calculate the progress of the chemical reactions for hydrocarbon/methane conversion according to a quite well established chemical

combustion reaction scheme. The rate expression for the applied single step global reaction of fuel and oxidizer in the post oxidation process is:

$$r = A \exp\left(\frac{-E_a}{RT}\right) [Fuel]^a [Oxidizer]^b \quad \{8\}$$

The used values for activation energy E_a (in cal/mol), pre-exponential factor A , and concentration exponents a and b are from Westbrook and Dryer [16] and given in the table below.

	A	E_a	a	b
Methane	1.0×10^{13}	48400	0.7	0.8
Octane	4.6×10^{11}	30000	0.25	1.5

2) Alternatively the combustion progress and rate of heat release is derived from the flames speed . The flame speed can be estimated from empirical knowledge, according to the following description.

The flame speed S_f (also called the turbulent flame speed) is determined as a function of the laminar flame speed S_L :

$$S_f = f(S_L) \quad \{9\}$$

The laminar flame speed S_L is estimated using a correlation presented in [49]:

$$S_L = S_{L0} \left(\frac{T_{ubg}}{T_0}\right)^\alpha \left(\frac{p}{p_0}\right)^\beta \quad \{10\}$$

T_{ubg} is the temperature of the unburned gas and p is the cylinder pressure. S_{L0} is the laminar flame speed at reference temperature T_0 (298K) and reference pressure p_0 (1 atm). Exponents α and β are parameters which are functions of the equivalence ratio ϕ of the unburned gas. S_{L0} is calculated according to:

$$S_{L0} = W \phi^\eta \exp(-\varepsilon (\phi - \sigma)^2) \quad \{11\}$$

W , η , ε and σ are constants based on experimental data. Based on the laminar flame speed, the flame speed S_f is calculated according to the equation below which is based on the turbulent flame speed model by Keck and co-workers and presented in [50].

The flame (and thereby the combustion) is assumed to progress, at the flame speed, through the combustion chamber as a hemispherical shape from the top center of the combustion chamber, and quenches according to the energy balance for the flame front (equation 1). This now defines the rate of heat release, and the temperature and pressure during combustion can then be estimated from equation 6.

This latter method can be used as a predictive tool when the rate of heat release is not known for a specific engine. More information about TECMU is found in [17].

Valve overlap

A fourth mechanism is associated with the intake and exhaust valve timing. Particularly in situations where a 4-stroke diesel engine is converted to dual-fuel natural gas application, there will be an overlap between the time of intake valve opening and exhaust valve closing. This is convenient for diesel operation, but not for DF operation. Therefore, the valve timing is often seen to be a problem for turbocharged DF engines, because unburned charge flows directly from the intake port to the exhaust port prior to combustion. As seen in the case study 1, the correction of valve timing during DF operation, results in a significant reduction of unburned methane emissions.

The valve flow is therefore an important phenomenon in methane formation understanding. In the TECMU model, the mass flow rates through the intake and exhaust ports during the gas exchange process are calculated according to equation 12 assuming a one-dimensional quasi-steady compressible flow of an ideal gas with constant heat capacity ratio [17]. If the flow is choked equation 13 is applied. Choked condition occurs if the pressure ratio over the ports exceeds the critical pressure ratio r_c determined by equation 14

$$\dot{m} = C_D A_r \frac{p_0}{\sqrt{R T_0}} \left(\frac{p_1}{p_0} \right)^{\frac{1}{\gamma}} \left[\frac{2\gamma}{\gamma-1} \left(1 - \left(\frac{p_1}{p_0} \right)^{\frac{\gamma-1}{\gamma}} \right) \right]^{\frac{1}{2}} \quad \{12\}$$

$$\dot{m} = C_D A_r \frac{p_0}{\sqrt{R T_0}} \gamma^{\frac{1}{2}} \left(\frac{2}{\gamma+1} \right)^{\frac{\gamma+1}{2(\gamma-1)}} \quad \{13\}$$

$$r_c = \left(\frac{\gamma+1}{2} \right)^{\frac{\gamma}{\gamma-1}} \quad \{14\}$$

In the flow rate equations indices 0 and 1 refer to upstream and port conditions, respectively. R is the specific gas constant of the gas. A_r is the minimum geometric flow area (reference area) which is, depending on the actual valve lift, either the port area (equation 15) or the valve curtain area (equation 16). D_v and D_{vs} are valve and valve stem diameter, respectively. l is the actual valve lift.

$$A_p = \frac{\pi}{4} (D_v^2 - D_{vs}^2) \quad \{15\}$$

$$A_{vc} = \pi D_v l \quad \{16\}$$

The discharge coefficient C_D in the flow equations is defined as the ratio between the effective flow area A_e and the geometric flow area A_r (equation 17). The effective flow area is smaller than the geometric flow area due to separation of the flow from the valve surfaces [17].

$$C_D = \frac{A_e}{A_r} \quad \{17\}$$

3. Outside engine emissions

Very little is known about methane emissions sources from natural gas vehicles other than the engine exhaust. AVL MTC AB has on the commission of The Swedish Transport Administration (STA) carried out measurements of methane leakage from methane fueled city busses. The Swedish study is described in more details in case study 7 in chapter 5. The amount of tested vehicles was 60. Twelve of the tested vehicles (15%) did not have any leakage. Thirty buses (50 %) did have leakage at fuel filling fittings corresponding to 2.9 ug/ day on average. There were no leakage from the gas tanks and roof fittings and only 3 % of the vehicles did have a diffuse, not quantified, increased level in the engine room. The major source of methane was inside the tailpipe corresponding to 0.88 mg /day and bus. The result indicates the major contribution of methane originates from slip during driving.

4. Emission reduction technology

As mentioned previously, the major emission concern regarding unburned methane emissions is associated with premixed charge dual fuel engines. In practice this means heavy duty vehicles/busses for road vehicles application and medium speed 4-stroke engines for marine applications.

Reduction of unburned methane in general can be achieved in three different ways:

- By the introduction of a better suited (advanced) combustion principle
- By introduction of a more suited natural gas formulation. Addition of hydrogen to the basic natural gas fuel seems to be a way forward

- By exhaust gas after treatment in an oxidation catalyst

Combustion principle

A recent investigation from Hokkaido University [14] has systematically shown how basic engine parameters influences the emissions and fuel consumption of a dual fuel natural gas engine. The engine system as well as the engine specifications are shown in Figure 7. In these experiments, the influence of the equivalence ratio of natural gas changed with intake throttling or supercharging, and the intake oxygen concentrations with cooled EGR were systematically examined to establish the conditions for clean, silent, and efficient combustion. The influence of the compression ratio was investigated as well.

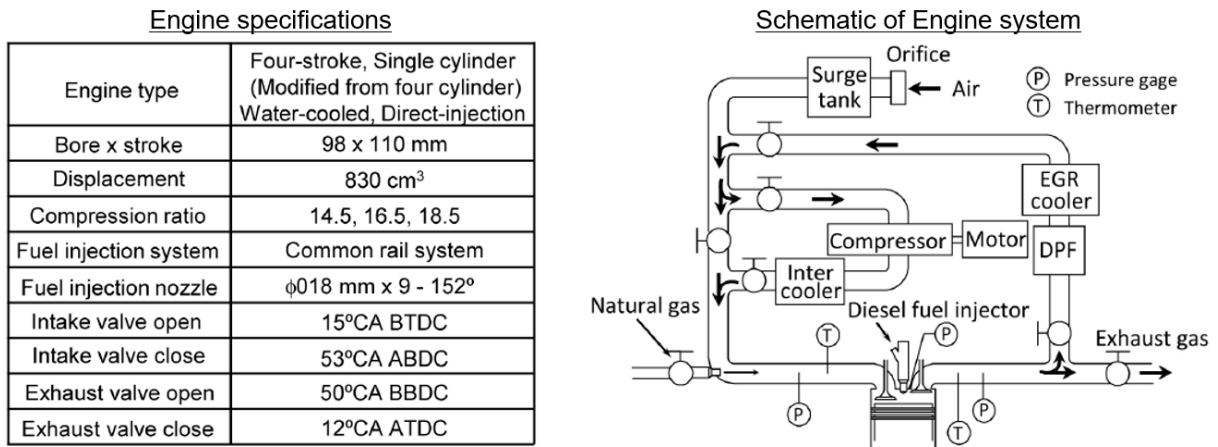


Figure 7 Engine setup and specifications from [14].

Results of varying the compression ratio and the equivalence ratio at low engine loads ($imep=0,3$ MPa) are shown in Figure 8. Increasing the equivalence ratio of natural gas by intake throttling is an effective technique to decreasing the THC, CO and NO_x emissions as well as to improvements in both the combustion efficiency (η_u) and the indicated thermal efficiency (η_i). Increasing the equivalence ratio (or lowering the excess air ratio) would mean higher amounts of unburned hydrocarbons in the boundary layer and in crevices, according to the discussion in chapter 3. Therefore, the beneficial effects of increasing the equivalence ratio must lie in a more complete combustion process, which is also reflected by the combustion efficiency results. The combustion efficiency could be a result of misfiring (cycle to cycle variations) being more important as the equivalence ratio is lowered. This is often seen at very low equivalence ratios.

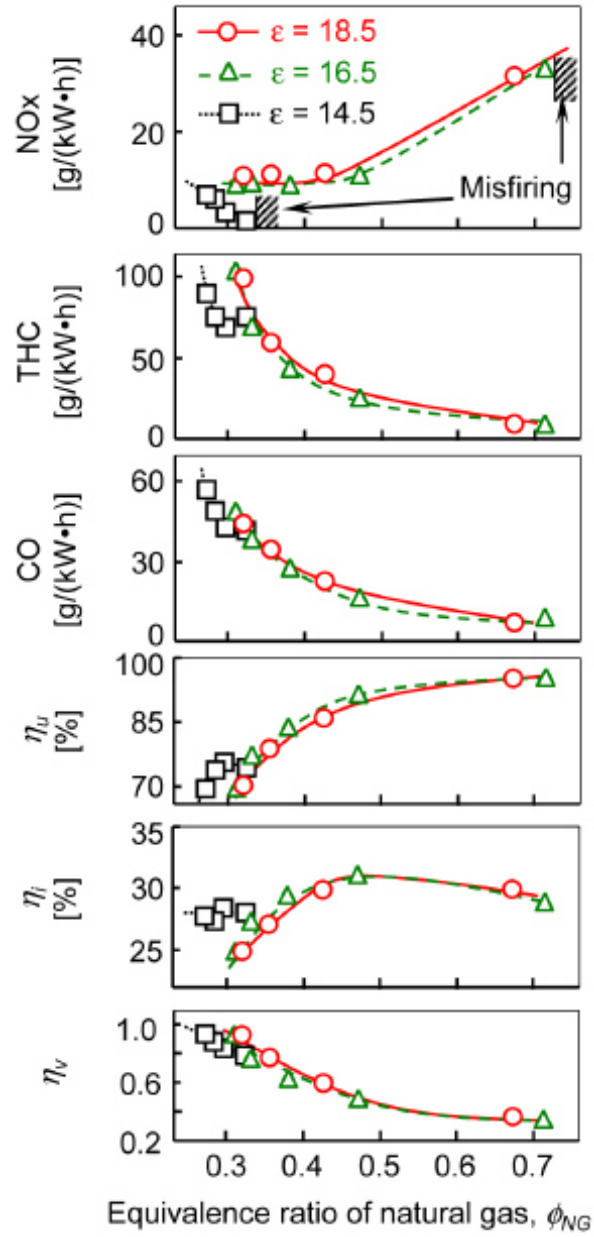


Figure 8. Results from varying the compression ratio and the equivalence ratio at low engine loads ($i_{mep}=0,3$ MPa) [14].

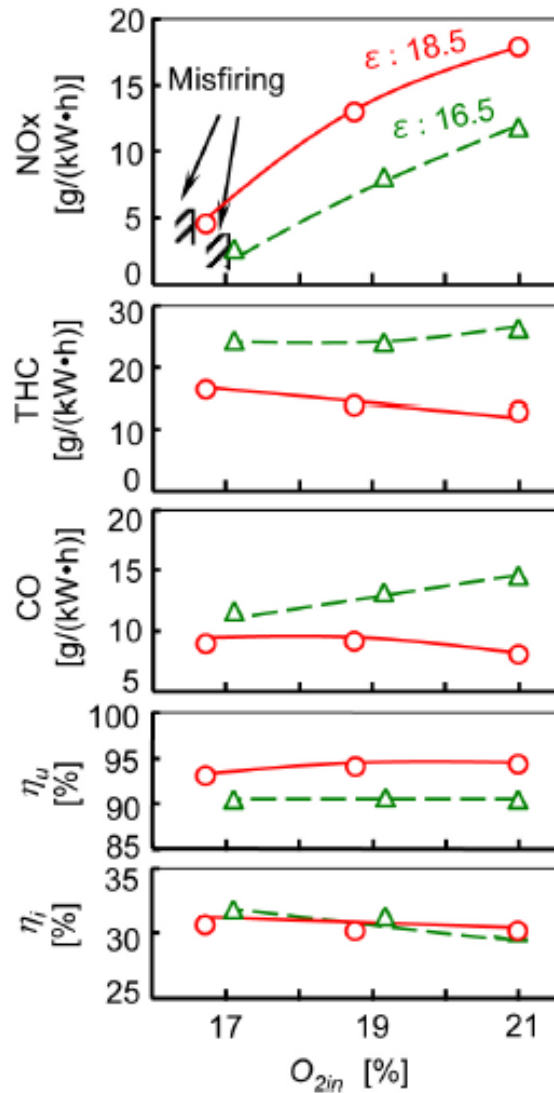


Figure 9 The EGR (characterized by the exhaust O_2) is an effective technique to reduce NOx without increasing THC and CO emissions [14].

The EGR is an effective technique to reduce NOx without increasing THC and CO emissions as shown in Figure 9.

Results of varying the compression ratio and the equivalence ratio at high engine loads ($i_{mep}=0,8$ MPa) are shown in Figure 10. Reducing the equivalence ratio of natural gas by increasing the boost pressure moderates the combustion and reduces the NOx, but increases the THC and CO emissions with deteriorations in the thermal efficiency. The tendencies are the same as for low loads. However, the combustion efficiencies are higher, meaning lower level of misfiring and unburned hydrocarbons.

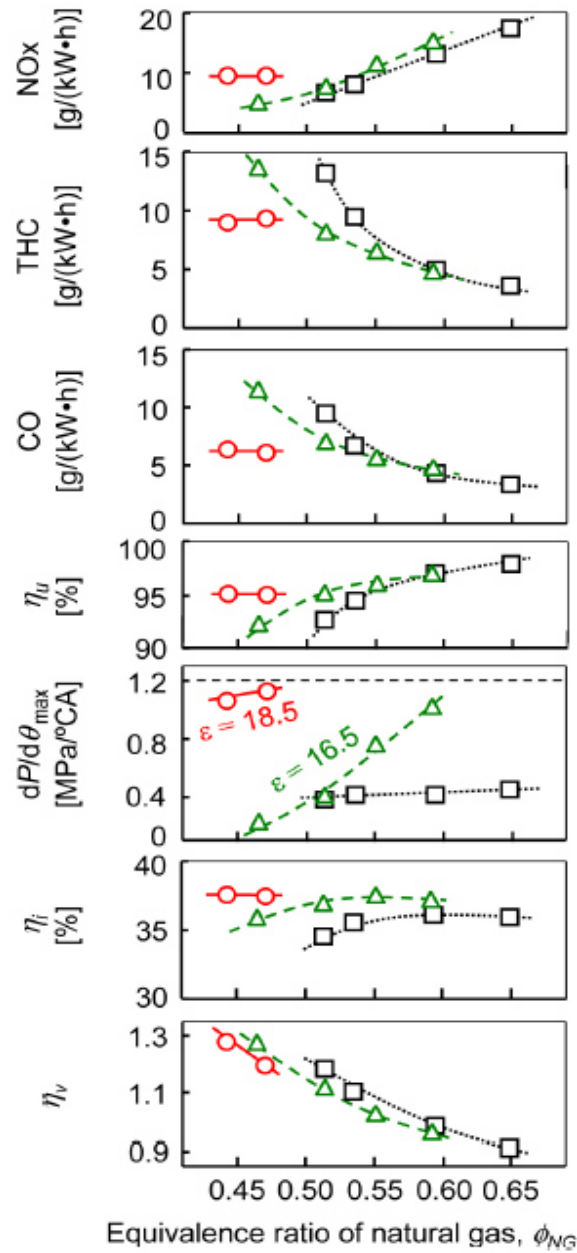


Figure 10. Results from varying the compression ratio and the equivalence ratio at high engine loads ($imep=0,8$ MPa) [14].

From the results shown here, it seems as running with higher equivalence ratio is a beneficial technique for lowering unburned hydrocarbon emissions. However, the NOx emissions are seen to increase at the same time, which is not desired. Furthermore, the authors observed that at lower equivalence ratios than 0.7, misfiring occurred due to a too low inlet pressure, causing trouble for the diesel pilot spray ignition.

The indicated efficiencies of a dual fuel natural gas engine can be increased, as shown by researchers at Waseda University, Japan [18], by applying a special injection strategy. In this investigation, a

combustion strategy is proposed based on engine tests to utilize “high dispersed pilot diesel injection” to promote flame propagation of premixed natural gas in a heavy-duty Dual Fuel natural gas engine. The results indicate that the combustion strategy proposed in the present study can achieve higher thermal efficiency than that of conventional diesel combustion at low load. The results show, that the indicated efficiency can be increased from about 35% to over 40% at medium load and an EGR ratio of 30%. This is shown in Figure 11. However, since NO_x and THC levels are high, after treatment of the exhaust will be required.

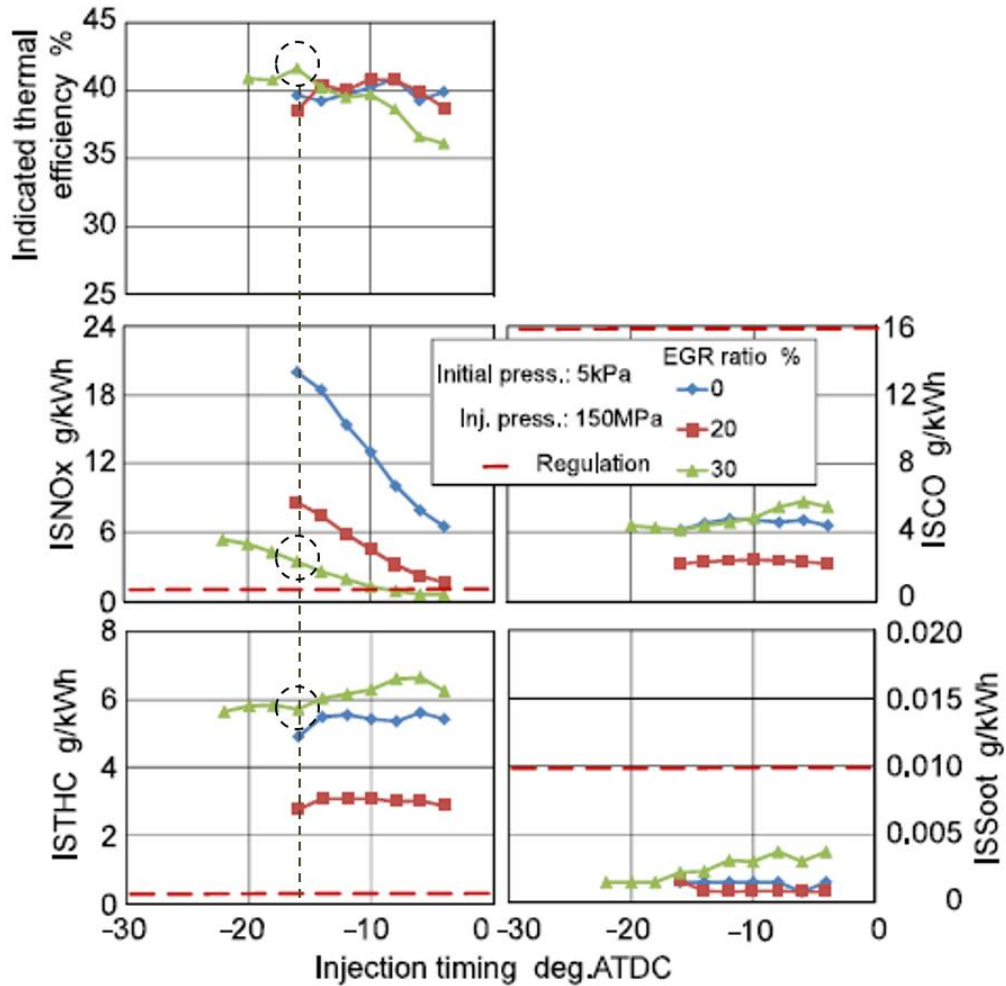


Figure 11. Results from applying a special injection strategy: “high dispersed pilot diesel injection” [18]

Hydrogen

The use of hydrogen enriched fuels, in particular in the form of hydrogen enriched methane, has already been studied in various fuel process studies [20-24]. These studies show that in particular the flammability behavior is accelerated by the hydrogen admixture. This is a basically welcome effect, as methane has a slower inflammation behavior than gasoline due to its short-chain molecular structure without C-C double bonds.

The motor investigations on hydrogen-enriched, methane-based fuels in this project have also shown that the high knock resistance of methane does not decrease due to the hydrogen admixture (at least until admixture rates of up to 25% by volume). This is explained in such a way that the effects of the H₂ admixture are practically completely limited to the ignition phase (0 - 5% fuel conversion), in which the knocking behavior is generally uncritical due to low internal cylinder pressures. The following combustion phase (5 - 100% fuel conversion), on the other hand, is hardly influenced by the admixture in stoichiometric operation.

There are only a few studies on the use of hydrogen-enriched methane in vehicles³. In the case of vehicles with stoichiometrically operated gas engines and three-way catalytic converters, these show significantly lower values, especially for NO_x emissions.

The following questions are investigated in this project:

- Can the effects on fuel consumption and engine-out emissions determined in combustion process studies on the engine test bench be confirmed in a vehicle in transient operation?
- To what extent is the correction of the fuel-induced shift in the center of gravity of the combustion needed in order to use the full potential of the hydrogen enrichment?
- How can the strong increase in the NO_x conversion rate in the catalytic converter in HCNG operation, shown in literature, be explained?

Without countermeasures, the increasing expansion of PV and wind farms leads to the production of electricity, which cannot be used in the electricity market or cannot be sold economically due to oversupply (hereinafter referred to as "excess electricity"). This excess electricity must be stored and used at other times (e.g. pumped storage power plants or batteries), transferred to mobility by power-to-gas/liquid plants or have to be curtailed. Although this curtailment is cost-effective, it should be prevented as it could limit the expansion of renewable electricity production.

The production of hydrogen from excess electricity in power-to-gas plants with feeding into the gas grid would be a technically relatively simple, under certain conditions even economical and somewhat energy-efficient way of harnessing excess electricity. This could mean that in the future natural gas will contain not only biogas but also hydrogen.

Oxidation catalysts

Methane emission from the engine exhausted gas can be mitigated by installing an oxidation catalyst in the after treatment system to fully oxidize CH₄ to CO₂ and H₂O. The engine exhausted gas can be characterized by low CH₄ concentration, high concentration of water vapor, large excess of oxygen and presence of SO_x and NO_x [25-30]. The temperature is lower than 500-550 °C, at which the high water content and presence of SO_x species are two main problems for the lifetime and efficiency of the catalysts. Water caused deactivation to the catalyst which leads to lower CH₄ conversion at the same temperature compared with the dry condition. While it is possible to get stable conversion in the presence of H₂O. The addition of SO₂ caused more detrimental deactivation to the catalyst which significantly decreased the lifetime. A catalyst with good performance at low temperature, good thermal stability, and high poisoning resistance is still urgently needed [31]. Catalysts for methane oxidation can be classified into two groups (see Fig.12), noble metal supported catalysts (Pd, Pt, Rh and Au supported

catalyst) and transition metal oxides catalysts (including single metal oxides and mixed metal oxides) [32-33].

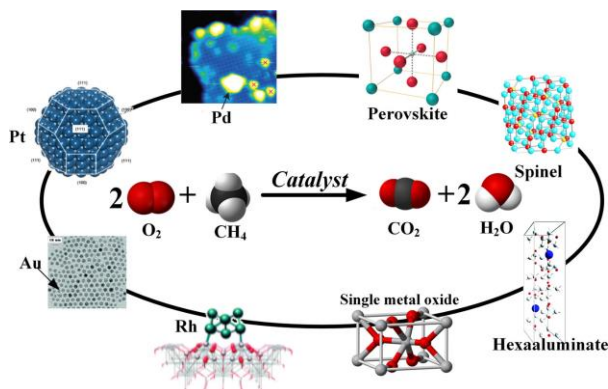


Fig.12. Catalysts for methane catalytic oxidation [32].

Noble metal catalysts, especially palladium based catalysts, show high catalytic activity towards CH₄ oxidation while the deactivation caused by sintering at operation temperature and poisoning by water and SO_x limited its application in the real process. The active phase of Pd supported catalyst was under debated for a long time and recently proved to be the PdO nanoparticles using the time resolved in situ DXAFS (dispersed X-ray absorption fine structure) method [34]. They found that the oxidation of CH₄ occurred by reduction of PdO and the activation energy for nucleation of metallic Pd (121 kJ/mol) is similar to the C-H dissociation energy of CH₄ on PdO (100) (131 kJ/mol). They also found that the presence of metallic Pd can accelerate the reaction which is consistent with other researchers. The performance of Pd catalyst was influenced by the support materials it dispersed on, the addition of promoters, as well as the operation conditions. Compared with the traditional support materials like Al₂O₃ and SiO₂, using an oxide with high oxygen storage and release ability like ZrO₂, CeO₂, and TiO₂ due to the changeable valance of the Zr, Ce, and Ti could provide oxygen for Pd in the reaction redox and the supports can then be reoxidized by the gas phase oxygen.¹¹ Ce and Zr oxides supported Pd catalysts were found to be less initially active but more stable in the long term activity test compared with Pd/Al₂O₃ catalyst [35-36]. Pd/TiO₂ catalyst was less active compared with others and also less studied in the literature [37]. Besides being used as a support material, ZrO₂, CeO₂, and TiO₂ were more usually used as a promoter for Pd/Al₂O₃ catalyst to improve the stability, water resistance, and SO₂ tolerance. While the promotion of CeO₂ cannot be used in the water existing condition due to the water caused aggregation of CeO₂ nanoparticles [38]. Based on the atomic layer deposition technique, Pd@ZrO₂/Si-Al₂O₃ catalyst with a core-shell structure was found to be promising to be used in the SO₂ present condition, while the performance of the catalyst in both water and SO₂ present condition is still unknown. The promotional effect of TiO₂ was reported to be a higher activity in the subsequent run after removing of SO₂, which was actually not realistic in the real engine condition [39]. Addition of Pt to the formula of Pd/Al₂O₃ catalyst as a bimetallic catalyst was also studied to improve the performance of the Pd catalyst under real condition. Andreas et al [40] found that it is possible to get CH₄ converted using a Pd-Pt/ Al₂O₃ catalyst in the presence of both H₂O and SO₂. The conversion of CH₄ was influenced by the SO₂ concentration in the reaction gas and the operation temperatures (see Fig.13) At 450 °C, the conversion of CH₄ decreased from 100 % to 20 % and 12 % with addition of 2.5 ppm and 5 ppm SO₂, respectively. As a lower operation temperature, 400 °C, the conversion of CH₄ in the absence of SO₂ was 55 % and the conversion dropped to 0 % within 25 h with addition of SO₂. They verified that the activity

of the Pd-Pt/Al₂O₃ catalyst was dependent on the operation temperature and the SO₂ amount that passed through the catalyst bed. Higher operation temperature can lead to higher CH₄ removal activity while it caused more irreversible deactivation shown by lower activity after removal of SO₂ compared with the catalyst had been run under same condition but lower temperature. More test need to be done to find the optimized operation condition and an efficient regeneration method for the poisoned catalyst.

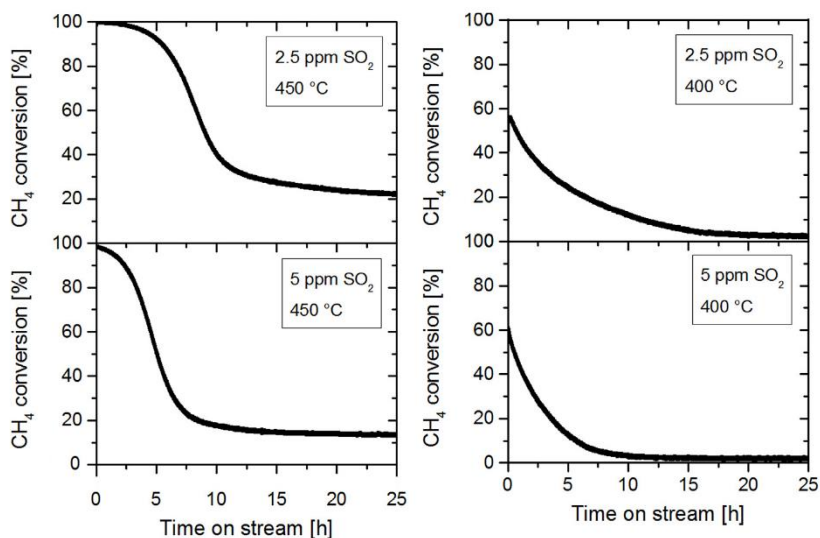


Fig. 13. CH₄ conversion as function of time on stream over Pd-Pt/Al₂O₃ at two different temperatures (400 and 450 °C) and two SO₂ concentrations (2.5 and 5 ppm). 3200 ppm CH₄, 10 % O₂, 12 H₂O, 2.5 or 5 ppm SO₂, in N₂. GHSV=30,000 h⁻¹ (40).

Except for the existed catalysts, designing a new catalyst with higher SO₂ tolerance is also of great importance to solve the CH₄ emission problem. Zeolites, mainly consisting of Si, Al, O and the cations elements (H⁺, Na⁺, and NH₄⁺), were also found as a promising support for noble metal supported catalysts due to its microporous structure and acid-base properties. Yang et al. [41] found that Pd supported on H-ZSM-5 with a loading of 1 wt.% could reach 100 % conversion at a temperature as low as 320 °C. Comparing with mostly studied Pd catalyst, Rh was reported to be more sulfur resistant and can be promising to be used under real engine condition [42].

5. Case studies

Case study 1. Modeling of unburned methane formation (Danish study)

A computer model, TECMU, has been developed. TECMU in this case study is used to simulate the engine process of a four-stroke dual-fuel medium speed engine. Engine design parameters, such as engine geometry and operation conditions, are given as input, and the model then calculates results for the expected engine performance and unburned methane emission level under the given conditions.

The computer program includes modeling of four different mechanisms that are known to cause methane slip from the engines. Three of these mechanisms are illustrated in Figure 4 in chapter 2 which is an idealized picture of the combustion chamber of an engine. One mechanism is the short-circuiting where methane flows directly from the intake port to the exhaust port. This occurs because an overlap period exists where both valves are open at the same time and during this period a pressure difference across the combustion chamber is present due to the turbocharging of the engines.

Another mechanism is the crevice mechanism whereby methane is forced into crevices in the combustion chamber during the pressure rise caused by the compression and combustion of the gas in the chamber. The propagating flame in the chamber is not able to penetrate into the crevices, and therefore methane in the crevices escapes combustion. During the pressure decrease in the chamber after the combustion has ended, crevice gas, and thereby unburned methane, re-enters the chamber. The unburned methane may be partly post-oxidized in the main combustion chamber after leaving the crevices but, unlike gasoline, most of it is expected to exit the combustion chamber unburned when the exhaust valve opens.

A third mechanism is the flame quenching near the chamber walls. When the flame propagates through the combustion chamber it will at some point be quenched near the walls because the heat loss to the walls will exceed the heat released in the flame. Therefore, some of the methane located near the walls will not be reached by the flame and will be left unburned. The near-wall methane may subsequently be partly post-oxidized, like the re-entering crevice gas, but some of it is expected to exit the combustion chamber unburned during the gas exchange process.

A fourth mechanism, which is not illustrated in Figure 4, is due to so called misfire, where the thermodynamic conditions during compression prevent ignition of the fuel in some of the engine cycles, typically during lean burn conditions. This is closely related to a phenomenon called “bulk quenching” where the ignition do occur but the combustion conditions result in a very early quenching of the flame.

The developed model can be used as an assisting tool for analyzing existing engine designs and operating conditions in order to gain a better understanding of the mechanisms, which lead to slip of unburned methane through the engines. The model can be used as well in the work of developing new and improved engine designs with respect to lower methane slip.

A calibration of the model against measured data from a 4-stroke medium speed Dual-Fuel engine, 2014 version, has been carried out. The methane slip from the engine from different load cases was afterwards analyzed to obtain a better understanding of the reason for the slip and to suggest possible improvements. Results for the methane slip are shown in Table CS1.1.

Table CS1.1. Calculated and measured (in red) methane emissions from a 4-stroke medium speed Dual Fuel engine

Load			100%	75%	50%	25%
Methane as fuel						
Specific emission	Calculated	[g/kWh]	26.3	16.8	37.6	71.8
	Measured	[g/kWh]	26.3	16.5	38,0	70,5
Relative emission		[kg/kg]	0.164	0.093	0.178	0.295
Relative contributions						
Short-circuiting			34.7%	61.4%	21.2%	12.14%
Crevice			23.9%	30.8%	17.1%	12.53%
Quenching			41.4%	7.8%	61.7%	75.33%
Post oxidation						
Fraction of fuel in crevice at EOC			0.55%	2.22%	0.30%	0.015%
Fraction of fuel in cylinder at EOC			0.23%	1.38%	0.22%	0.008%
Fraction of fuel in cylinder and crevice at EOC			0.28%	1.83%	0.23%	0.009%
Octane as fuel						
Specific emission		[g/kWh]	9.25	10.85	8.17	64.89
Relative emission		[kg/kg]	0.061	0.061	0.042	0.271
Relative contributions						
Short-circuiting			93.6%	93.3%	89.9%	13.2%
Crevice			6.4%	6.7%	10.1%	12.7%
Quenching			0%	0%	0%	74.1%
Post oxidation						
Fraction of fuel in crevice at EOC			70.2%	75.6%	67.5%	15.4%
Fraction of fuel in cylinder at EOC			100%	99.6%	100%	8.1%
Fraction of fuel in cylinder and crevice at EOC			95.7%	86.8%	96.4%	8.5%

Data in the table **Fehler! Verweisquelle konnte nicht gefunden werden.** indicate a good agreement between methane emission level obtained with the developed model and the measured level. This follows from comparison of the two upper rows, which deviate for all load case by less than 2%. The relative contributions to the methane slip from the different sources, indicated by the model, suggested that short-circuiting in the engine is important to address, particularly at 75% load.

Changes in the valve timings could lower the valve overlap period and thereby reduce the short-circuiting contribution. New valve lift profiles for the intake and exhaust valves have been adopted to the engine, and these are shown in Figure CS1.1 together with the old valve lift profiles. The valve overlap period is substantially reduced for the new valve lift profiles, and it was expected that this will accordingly reduce the short-circuiting of methane through the engine significantly. This result was

certainly obtained, as seen in Table CS1.2, where TECMU is used to calculate emissions from the new valve profile engine. The results indicate furthermore that although the total methane slip could be reduced to some extent by addressing the short-circuiting, it is also important to counteract the contributions from crevices and quenching.

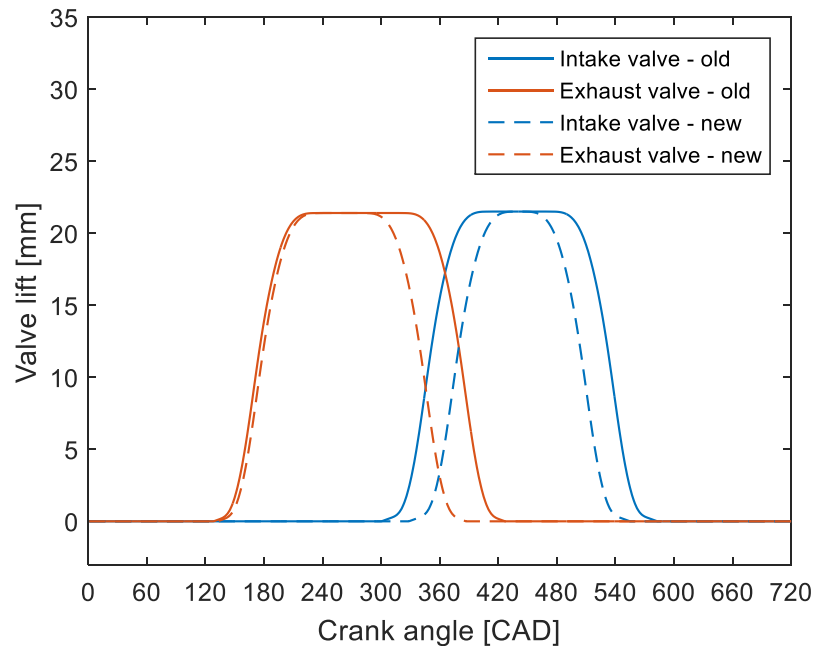


Figure CS1.1 Valve lift profiles for a MAN L28/32 Dual-Fuel engine.

The TECMU model clearly illustrates that crevices do play an important role in unburned methane formation after almost eliminating the valve overlap mechanism. However, wall quenching and bulk quenching/ misfire are the dominating contributors. This fact becomes more outspoken as the load decreases, which is seen in Table CS1.1 and CS1.2.

In these simulation cases, it is not possible to distinguish between quench layer mechanism and bulk quenching/misfire, since the rate of heat release curves from engine measurements have been used as input to the TECMU model. This in one hand eliminates the possibility of estimating all the individual emission contributors. On the other hand, it gives a result which complies more exactly with the engine in question.

After modification of the valve timing it is clear, that crevices, and particularly quenching is important to address in order to achieve lower emissions. Crevices is the most important mechanism at 75% load, whereas quenching is the most significant contributor at all other operating conditions.

According to the theory for methane formation, given in chapter 2, the quench layer thickness increases at leaner operation, which gives an increasing contribution to the total emissions at lower loads. The

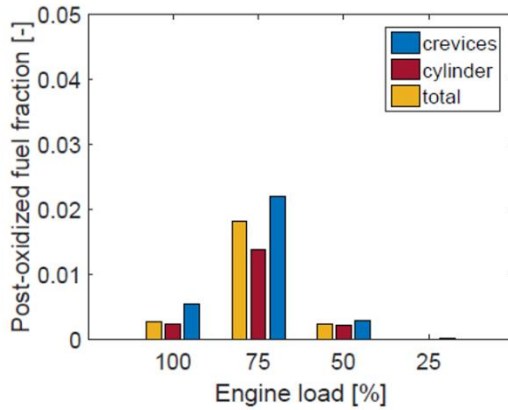
bulk quenching/misfire mechanism follows the trend seen in Figure 6., where cyclic variations occur with an increasing tendency at leaner operation. This also indicates higher emissions at lower loads.

Table CS1.2. Calculated and measured (in red) methane emissions from a 4-stroke medium speed Dual Fuel engine with reduced valve overlap.

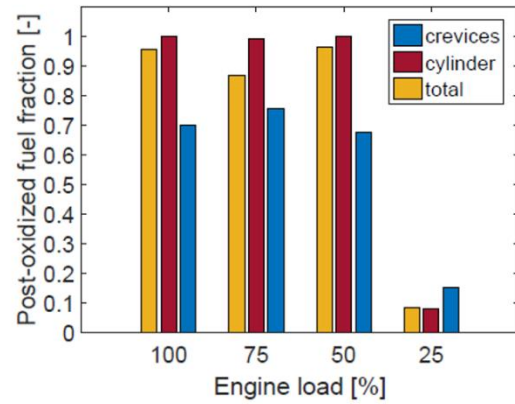
Load			100%	75%	50%	25%
Methane as fuel						
Specific emission	Calculated	[g/kWh]	17.8	6.22	30.3	65.2
	Measured	[g/kWh]	17.0	6.0	30.5	64.0
Relative emission		[kg/kg]	0.117	0.036	0.147	0.275
Relative contributions						
Short-circuiting			0%	0%	0%	0%
Crevice			36.4%	83.1%	21.9%	14.2%
Quenching			63.6%	16.9%	78.1%	85.8%
Post oxidation						
Fraction of fuel in crevice at EOC			1.64%	4.66%	0.71%	0.037%
Fraction of fuel in cylinder at EOC			0.77%	2.36%	0.51%	0.022%
Fraction of fuel in cylinder and crevice at EOC			0.90%	3.59%	0.53%	0.023%

The influence of post oxidation was investigated, since it was expected, that this mechanism would be clearly different for methane, compared to other high octane fuels. The model was therefore used to recalculate the post oxidation as if the fuel was octane (gasoline like fuel). The reaction constants for octane, used in equation 8, were thus applied. Results in these cases are seen in the lower part of Table CS1.1. This had the effect that post oxidation changed dramatically. When methane is the fuel, almost no post oxidation occurs for the quenching mechanisms. This changes to close to 100% when octane is the fuel. Only part of the crevice hydrocarbons is emitted – about 30% of the crevice hydrocarbons are emitted after post oxidation. Only at low load the post oxidation is very limited with octane, 15.4%.

The post oxidation effect changes the engine emissions completely. The unburned hydrocarbon emissions seems to be reduced with a factor of about 2. However, this is very dependent on the load. The post oxidation would be very improved with addition of hydrogen to methane, since hydrogen enhances the reactions at lower temperatures. This is an effect that has been investigated in case study 3. The fractions of unburned methane that are post oxidized in the two cases are compared in Figure CS1.2. The results are further discussed in Case Study 2.



(a)



(b)

Figure CS1.2 The post oxidized fuel fractions for methane reactions (a) compared to octane reactions (b).

Summary:

A mathematical model, TECMU, which calculates the contribution of unburned methane from different mechanisms, has been developed and tested against measurements on a 4-stroke medium speed Dual Fuel engine. The comparison revealed that all described mechanisms: valve overlap, crevices, quenching and post oxidation are important for the engine out emissions

Reduction of valve overlap reduced the methane emissions with about from 12 to 62%, depending on engine load. Post oxidation was shown to be very limited with methane as fuel, compared to octane. This indicates the importance of hydrogen, which could enhance post oxidation of unburned methane. In order to address methane emissions from the engine, after modifying the valve timing, it is necessary to look at both crevices and quenching mechanisms.

[Case study2. Quantification of methane emissions from different mechanisms](#)
(Danish study)

In order to further evaluate the methane formation model, TECMU, an experimental research facility was established. This facility enabled us to operate an engine according to a typical Otto combustion cycle on various natural gas fuels. This research engine is spark ignited. However, the thermodynamics of the combustion processes is similar to the MAN dual-fuel combustion engine, both operating according to the Otto-cycle process.

The experimental engine was a traditional CFR engine with the specifications as found in Table CS2.1

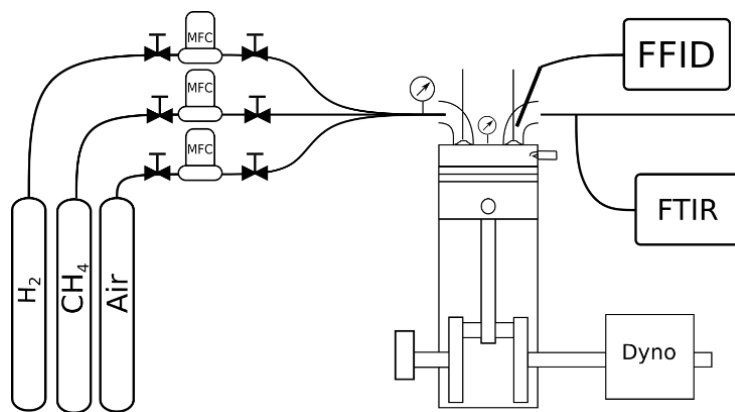


Figure CS2.1. CFR test setup schematic drawing. MFC: Mass Flow Control, FFID: Fast Flame Ionisation Detector, FTIR: Fourier Transform Infrared spectroscopy.

Table CS2.1 Experimental engine data.

CFR engine	
Bore	82.775 mm
Stroke	114.3 mm
Compression ratio	4.5 - 15
Ignition	NGK 2910 AB-6 (gab 1mm)
Max intake pressure	2 bar
Valves	Shrouded vales

The purpose with the experiments was to be able to vary essential engine/fuel parameters and estimate the influence on the different unburned methane formation mechanisms. The basic parameters that were varied were the compression ratio (CR), the excess air ratio ($\lambda=1/\phi$) and the intake pressure (p_{in}) The distinction between the different hydrocarbon formation mechanisms was done by the use of the Fast Flame Ionization Detection (FFID) equipment [51]. In this method a sample probe is installed just

downstream of the exhaust valve, and the fast principle enables us to follow the variation of unburned methane emissions as a function of time, with a few crank angle (CA) degrees resolution. Therefore, we are able to relate the emissions to the different mechanism, since they occur at different CA's. A picture of the engine with the essential installations is shown in Figure CS2.1, and a schematic figure showing a typical picture of the FFID measurement [51], is shown in Figure CS2.2.

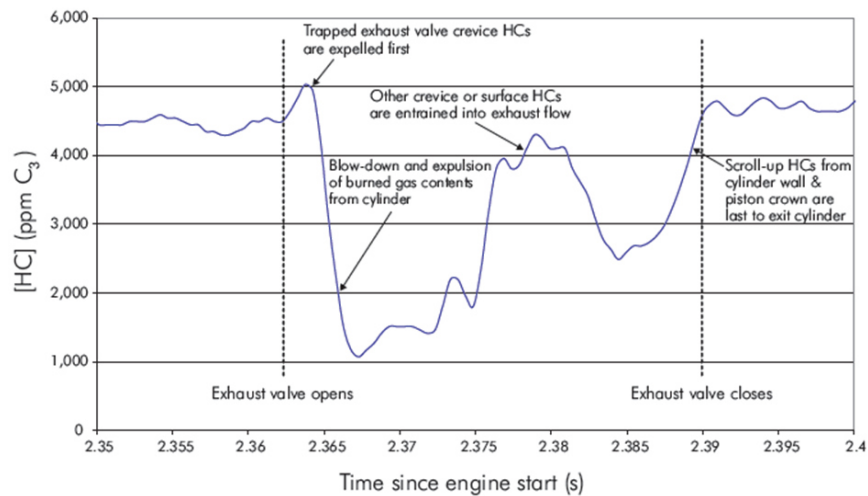


Figure CS2.2. Example of a measured output signal from the FFID sensor.

From the figure we follow the concentration (by volume) from the opening of the exhaust valve until the closing of the valve. Right after opening a small peak is seen. This is interpreted as the unburned fuel trapped in the crevice around the exhaust valve. Thereafter, the concentration drops dramatically, reflecting the content of the bulk gas, which is very low due to the effective combustion. This comes out as the first part of the exhaust. Then hydrocarbons from boundary layers and other crevice material enters the exhaust port. At the end of the period, the so called roll-up vortex material enters the exhaust port. This vortex scrapes of the cylinder liner boundary layer quenching material and also a part of the unburned material trapped in the crevice between the liner and the piston crown.

A typical example of the measurements from the present investigation is shown in Figure CS2.3.

Here we clearly see the initial increase after EVO, reflecting material coming from the valve crevice. As the bulk gas enters the exhaust valve, the concentration drops to a very low level due to the efficient combustion of the main cylinder gases. Thereafter, the unburned methane, diffusing out of the boundary layer is emitted. Finally, the roll up vortex enters the exhaust reflected by a clear increase in the rate of concentration.

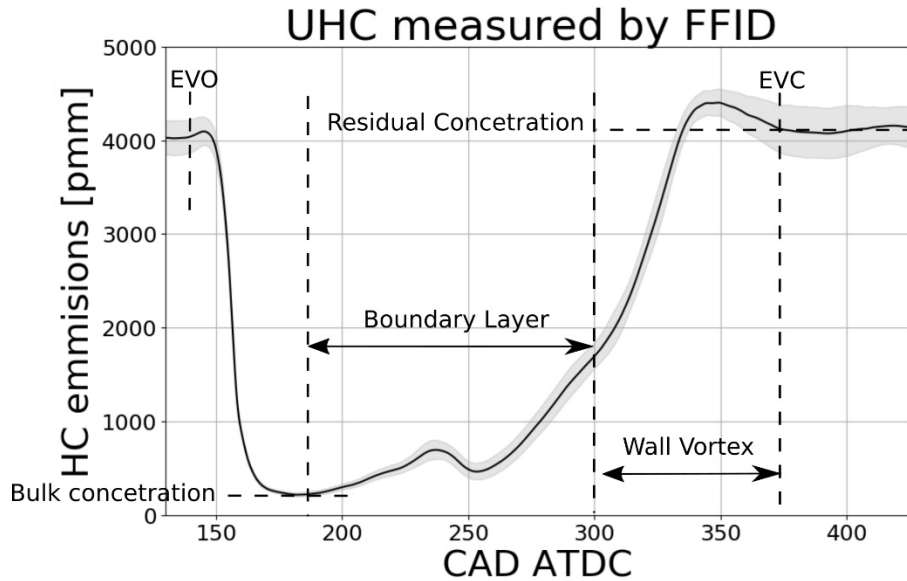


Figure CS2.3. FFID signal output example from the CFR engine.

The total emissions of unburned methane was measured in the exhaust by using an FTIR (Fourier Transform InfraRed) instrumentation. The measurements of unburned methane are shown in Figure CS2.4 for varying compression ratio, excess air ratio and intake pressure. The Figure shows that the methane slip increases with increasing compression ratio and excess air ratio, whereas the slip decreases with increasing intake pressure (load). The variation with the excess air ratio is opposite to what is seen in gasoline engines [5]. The reason for this could be that in gasoline engines the crevice mechanism is dominating whereas in natural gas engines the quench layer mechanism is the most important, at least at leaner operation. Post oxidation also plays a quite different role with gasoline compared to natural gas, These tendencies were also shown in case study 1 (Table CS1.2, Figure CS1.2).

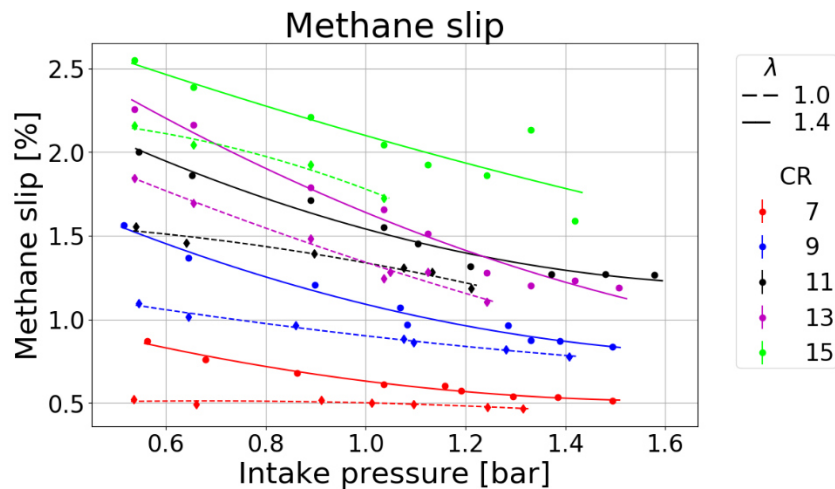


Figure CS2.4. Unburned methane emissions measured in the exhaust of the CFR engine.

In order to investigate further the influence of crevice material, we calculate the expected amount of engine out emissions from the crevices alone, M_{CR} , by integrating equation {2} from chapter 2 until the maximum pressure during compression. This is then a measure of the crevice material/methane we would find if there were no post oxidation of methane in the cylinder (in case study 1 it was found that there was almost no post oxidation in the 4-stroke medium speed dual fuel engine, which operates at leaner mixtures). The results from these calculations are shown in Figure CS2.5. We notice, that the calculated emission level is much higher than measured. Therefore, there must be significant post oxidation in the CFR engine. Furthermore, the calculated emissions increases with intake pressure, which is opposite to the measured tendency.

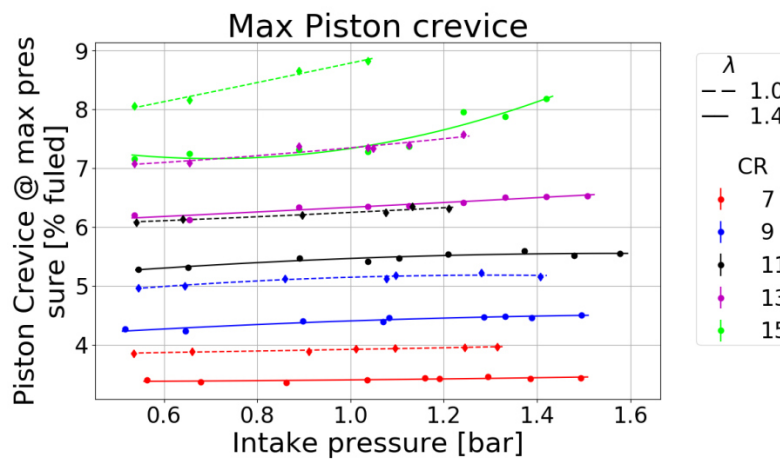


Figure CS2.5. Variation of unburned methane in crevices at maximum cylinder pressure.

In order to investigate the influence of post oxidation, a model for the crevice material flow into the cylinder was established [15]. It was furthermore assumed that all crevice material that flows out of the crevices according to this model was post oxidized completely if the temperature of the bulk gas was above a certain temperature. Otherwise, it was assumed that there was no post oxidation. Using this method the results in Figure CS2.6 were achieved. With the assumption of 1700 K as the critical post oxidation temperature the emission levels are in good agreement with the measured values. The TECMU model indicates that this is a threshold temperature for the post oxidation. Below 1700 K the post oxidation becomes ineffective. Now the influence of excess air ratio also shows the correct tendency. However, the influence of intake pressure is still wrong, indicating other important mechanisms.

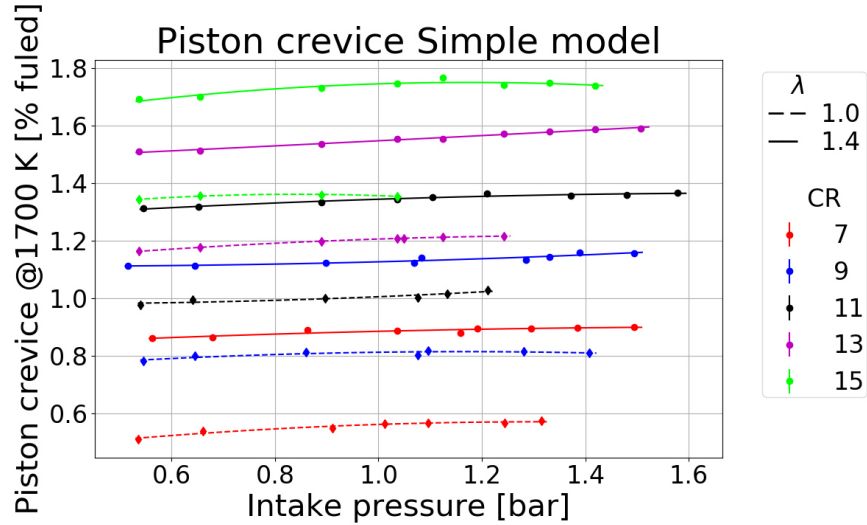


Figure CS2.6. Variation of unburned methane in crevices after postoxidation at 1700K.

This calls for further investigation of the UHC near the walls, including the quench layer and crevices. As the UHC from crevices, for most of the expansion, is exiting the crevice with low speed, the UHC from the crevice is dragged on the liner as a thin layer, as seen in Figure CS2.7. Therefore, the post oxidation for both crevices and quench layer can be treated the same.

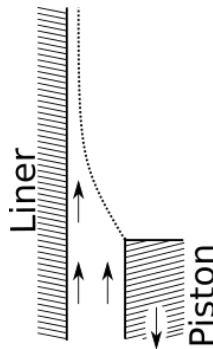


Figure CS2.7 Crevice material is dragged on the liner as a thin layer.

In order to confirm the importance of the UHC near the walls, the variation of the residual methane concentrations in Figure CS2.3 were investigated. This concentration is closely related to the unburned methane emitted from the quench layer and the crevice material from the piston/wall crevices (the bulk gas concentrations in the lower left corner of the figure is then assumed to be ~ 0). The variation of this concentration is seen in Figure CS2.8.

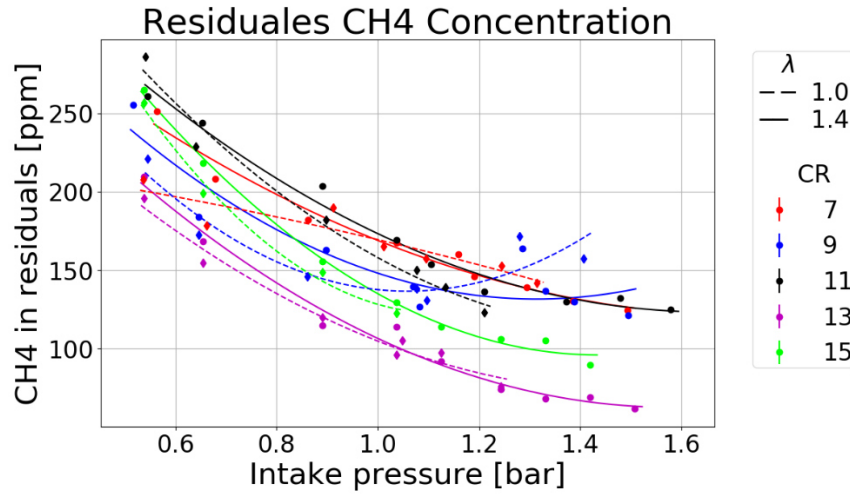


Figure CS2.8 Unburned methane in the residual fraction, measured with the FFID.

This clearly gives the right variation with intake pressure and also with the excess air ratio, whereas the variation with the compression ratio is more unclear.

A conclusion from the experimental work in Case Study 2 is then that both the crevice and the quench layer mechanisms are important for the engine methane slip, and the post oxidation is certainly important, at least in relation to the crevice material. In case study 1 it was found that the quench layer mechanism is very important at lean operation, and the post oxidation was almost eliminated at all conditions. The explanation for this is that the engine in case study 1 operated at more lean conditions than the engine in case study 2.

Case study 3. Application of methane with hydrogen (Swiss study)

Test setup

In the context of this project, methane was measured as fuel with and without hydrogen admixture in a Euro-4 vehicle with stoichiometric operated, naturally aspirated, manifold injected 4 cylinder engine with an engine capacity of 2.0 l. The vehicle was equipped with an external fuel supply, an access to the electronic engine control (ECU), a modified catalytic converter as well as an internal cylinder pressure measurement in the combustion chamber of the engine. The vehicle was driven with two different driving cycles (NEDC and WLTC) on a chassis dynamometer with road load simulation and combustion parameters, consumption and gaseous emissions were measured before and after the catalytic converter.



Fig. CS3.1 Project vehicle on chassis dynamometer

Modifications on the catalytic converter

At the beginning of this project, a new original catalytic converter was installed in the vehicle. This new catalytic converter was run in on the test bench with 400 km of motorway driving subjected to a so-called "degreening". In order to ensure that the emission values measured after the catalyst were not too close to the detection limit of the respective analysis systems, the effectiveness of the catalyst was artificially impaired by shortening it by approx. 1/3 of its length (Fig. 2).



Fig. CS3.2 Shortened catalytic converter - only the left part (2/3 of the length) was used.

Fig. 3 shows the sampling points before and after the catalytic converter in the underbody of the project vehicle.

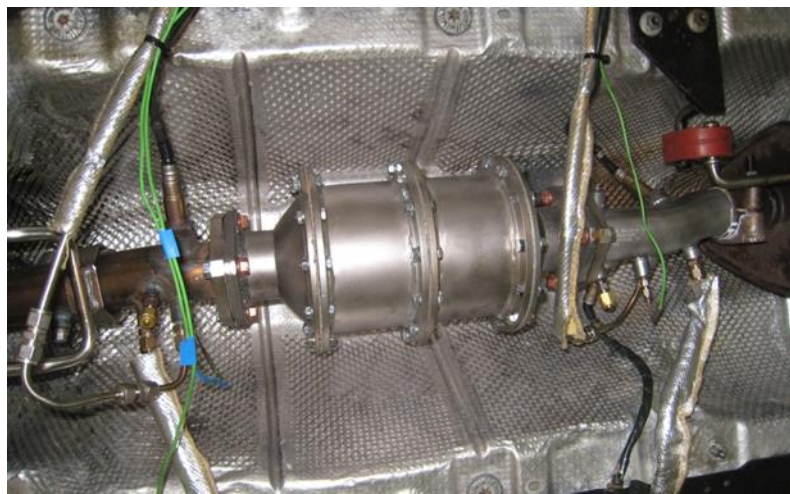


Fig. CS3.3 Catalytic converter in vehicle underbody with for exhaust gas, probe and exhaust gas sampling points

Driving cycles

For the emission measurements, the vehicle was tested in the currently valid and in the future legislative driving cycle.

- NEDC -> Official driving cycle until Autumn 2017 (Fig. 4, red curve)
- WLTC -> Official driving cycle from Autumn 2017 on (Fig. 4, blue curve)

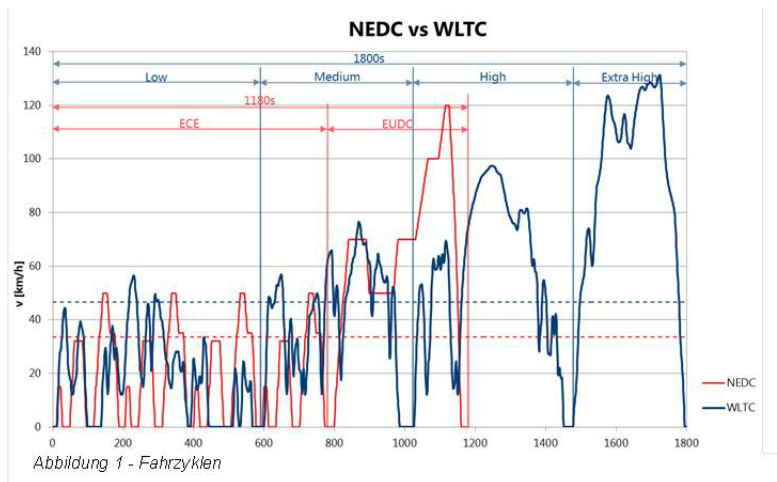


Fig. CS3.4 Driving patterns NEDC and WLTP

In contrast to official measurement, the engine was warmed up before the measurements and the test was started with the engine at operating temperature.

Used fuels

Designation	CH ₄ -share [Mol%]	H ₂ -share [Mol%]	Energy% H ₂ [Mol%]	Density [kg/m ³]	NHV [MJ/kg]	CWF (mass%)
CNG	100	0	0	0.6785	50.01	74.9
HCNG ₁₅	85	15	5.1	0.5895	51.58	73.2
HCNG ₂₅	75	25	9.3	0.5302	52.92	71.9

Table CS3.1 Fuel specifications (density at 15°C and 1'013 mbar) /
NHV = Net heating value, CWF = Carbon Weight Fraction

Measurement technology and exhaust gas sampling

A 2-line exhaust gas analysis system (Horiba Mexa-7400H) and a dilution system with critical venturi (Horiba CVS-9400T) were used to determine the legally limited pollutants.

The non-limited pollutants (NO₂, NH₃) were measured using an FTIR infrared spectrometer (Gaset CR-2000S) and a hydrogen mass spectrometer (V&F H-Sense). In addition, the hydrocarbons were recorded with a fast 2-line flame ionization detector (Cambustion Fast-Response-FID HFR500) for pre- and post-catalyst measurements.

To ensure that the measured emissions can be assigned correctly to the underlying events of engine operation, a Bosch LSU-4 broadband lambda sensor was installed at each of the two sampling points

before and after the catalyst. These fast measuring oxygen sensors thus served as a time reference at the respective sampling connection.

A so-called "open" engine control unit - ECU with emulator probe (ETK) - enabled the adaptation and adjustment of the ignition timing and supplied the data acquisition with further measured variables which served to control and characterize the engine operating status and combustion.

A cylinder pressure indexing system (Kistler KiBox) with a piezoelectric pressure sensor integrated in a spark plug was used to measure the cylinder pressure, which is indispensable for assessing the combustion and its center of gravity.

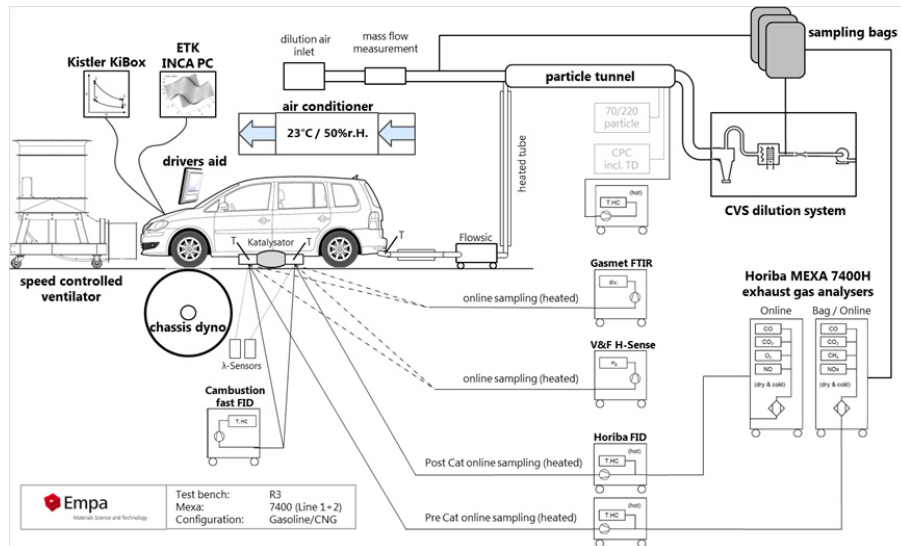


Fig. CS3.5 Experimental setup and measurement technology

Ignition timing and position of the center of gravity

Ignition timing

The addition of H₂ to the CNG fuel accelerates the combustion phase, resulting in an early shift of the combustion center of gravity, defined as 50% energy conversion. In order to correct this early shift, the ignition point (IgnP) in HCNG operation must be shifted by the corresponding amount to "late". The test vehicle is equipped with an applicable engine control, which makes such an adjustment possible.

In order to determine the parameters for adapting the IgnP map, the center of gravity was first determined in CNG operation with the original ignition map at various constant speeds using a cylinder pressure indexing system. After switching to the hydrogen enriched fuels (HCNG₁₅ and HCNG₂₅), the combustion center of gravity was corrected by shifting the ignition time to "Late" to the original center of gravity position previously determined with the standard fuel. For the sake of clarity, only the measurements with admixtures of 25 mol% hydrogen are listed below. The effects of the measurements with 15 mol% hydrogen admixture are practically everywhere approximately in the middle between CNG and HCNG₂₅ operation.

The ignition timing corrections, measured in degrees crank angle ($^{\circ}\text{KW}$), were converted into a corresponding time delay and then extrapolated to the relevant speed range of the ZZP map (see Fig. 6 left). Since the influence of the load on the shift of the center of gravity position is small, a load-dependent adjustment of the ignition timing was dispensed with. This resulted in the offset curve shown in Fig. 6 on the right, which was applied to the original map over the entire load range. With this correction of the ZZP map, it was possible to keep the center of gravity in the original position in HCNG₂₅ operation.

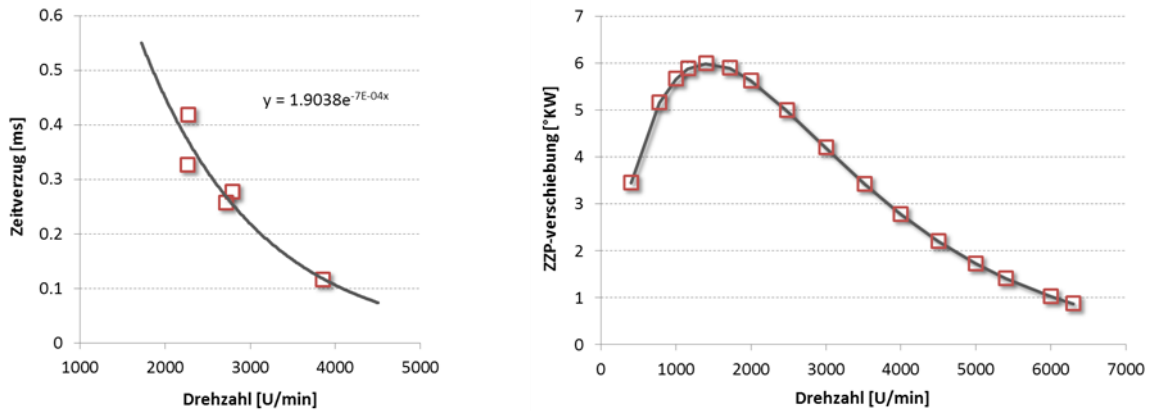


Fig. CS3.6 left: Determined time delay in the NEDC constant speeds in HCNG₂₅ operation

Fig. CS3.6 right: Extrapolated ignition timing shift for the HCNG₂₅-Operation in degrees crank angle ($^{\circ}\text{CA}$)

In order to determine the sensitivity of the ignition timing variation, additional measurements were carried out with other IgnP map adjustments in which the correction according to Fig. 6 (hereinafter referred to as "mod2") was only corrected by 50% (referred to as "mod1") and with a IgnP map in which the ignition timing was overcorrected by 50% ("mod3").

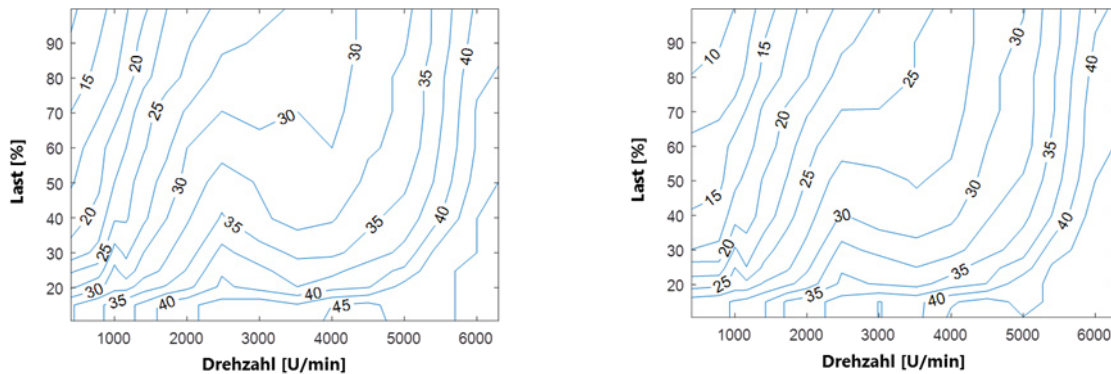


Fig. CS3.7 left: Original ignition map for CNG operation. The lines and values correspond to the ignition timing (ZZP) in degrees crank angle ($^{\circ}\text{KW}$) before top dead center (v.OT).

Fig. CS3.7 right: Adapted ignition map for HCNG₂₅ operation with optimum ZZP adjustment (mod2)

Centre of gravity position over various driving cycles

In addition to the emission values, some control unit sizes and the combustion parameters determined with the cylinder pressure indexing system were also recorded during the measurements. The analysis of the data in the positive load range of the engine (positive wheel power and accelerator pedal >1%) shows that the ignition timing correction achieved the desired effect (Figs. 8 - 11). With the original characteristic map in CNG operation, over 45% of the centres of gravity are in the ideal range of 6 - 10°KW according to OT. In HCNG25 operation, over 45% of the combustion centres are also in this range (see graphs). There are several reasons why not all the focal points are in this area

- In dynamic operation, a constant center of gravity position seldom occurs, since load and speed can change continuously. This also influences the position of the center of gravity.
- The later the IgnP is set, the more unstable the center of gravity position becomes (expressed as an increase in standard deviation), probably due to ignition at higher pressures [43].
-

Combustion center of gravity in CNG operation

Fig.8 shows the frequency distributions of the combustion center of gravity in CNG operation over the crank angle to TDC in the NEDC (left) and in the WLTP (right). The mean combustion center of gravity position with original ignition map (org) is 8-9°KW n.OT (mean value from 6 measurements) both in the NEDC and in the WLTC and shifts with the IgnP map corrections (mod1, mod2, mod3) as expected to "late".

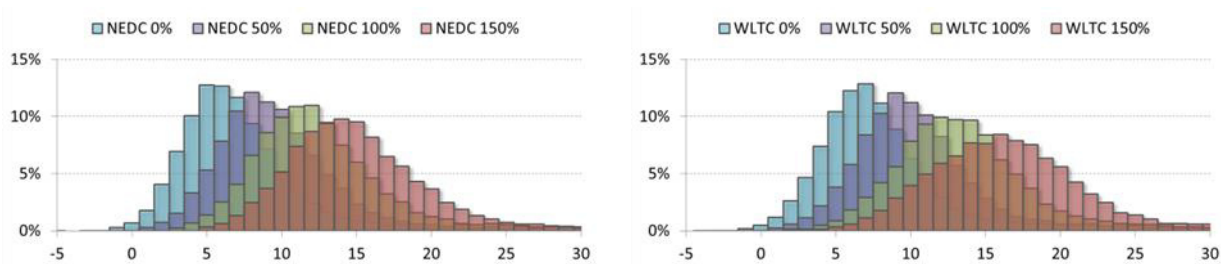


Fig. CS3.8: Distribution of the combustion center of gravity in CNG operation in the NEDC (left) and in the WLTC (right) with original ZFP map (light blue) and the IgnP variations mod1, mod2 and mod3.

Fig. 9 shows the distributions without IgnP correction (0%) and with the variations mod1 (50%), mod2 (100%) and mod3 (150%) individually. It can be seen that the IgnP corrections lead to a shift of the center of gravity as well as a slight widening of the distribution in both the NEDC and the WLTP.

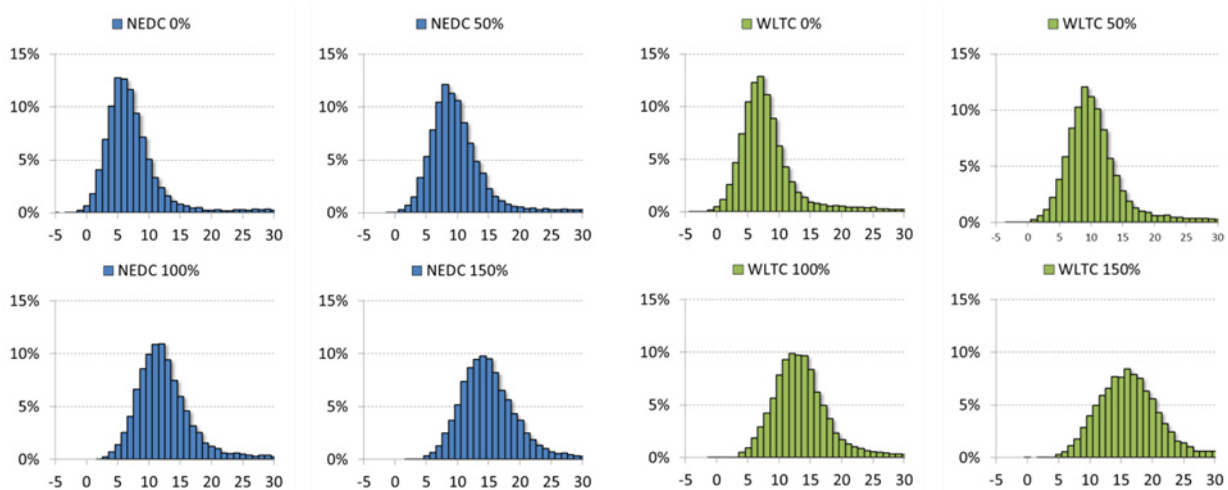


Fig. CS3.9: Verteilung der Verbrennungsschwerpunktlage im CNG-Betrieb im NEFZ (links) und im WLTC (rechts) mit originalem ZCP-Kennfeld (hellblau) und den ZCP-Variationen mod1, mod2 und mod3.

Centre of gravity of combustion in HCNG₂₅ operation

Fig. 10 shows the frequency distributions of the combustion center of gravity in HCNG₂₅ operation over the crank angle to TDC in the NEDC (left) and in the WLTP (right). Without IgnP correction, there is an early shift in the position of the combustion center of gravity. On average, this is 4-5°KW a.TDC (mean value from 6 measurements). The IgnP corrections mod1, mod2 and mod3 shift the distributions back to "late", whereby the correction "mod2" comes closest to the original values in CNG mode.

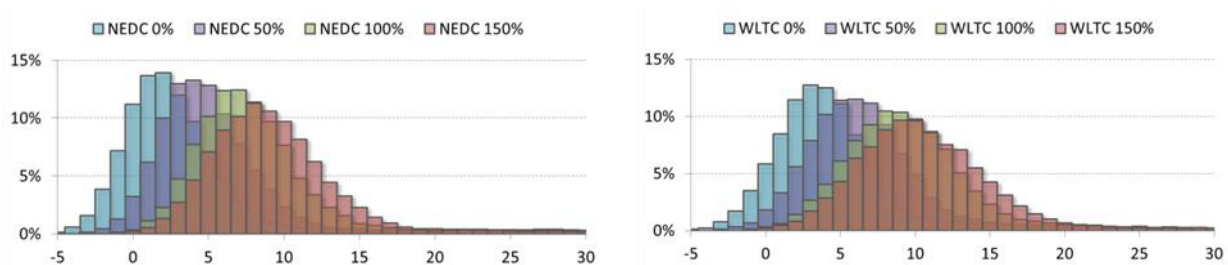


Fig. CS3.10: Distribution of the combustion center of gravity in CNG operation in the NEDC (left) and in the WLTC (right) with original ZCP map (light blue) and the IgnP variations mod1, mod2 and mod3.

Fig. 11 shows the distributions in HCNG₂₅ operation without IgnP correction (org) and with the variations mod1, mod2 and mod3 individually. It can be seen that the IgnP corrections also lead to a slight widening of the distribution in HCNG₂₅ operation, as in CNG operation (see Fig. 9).

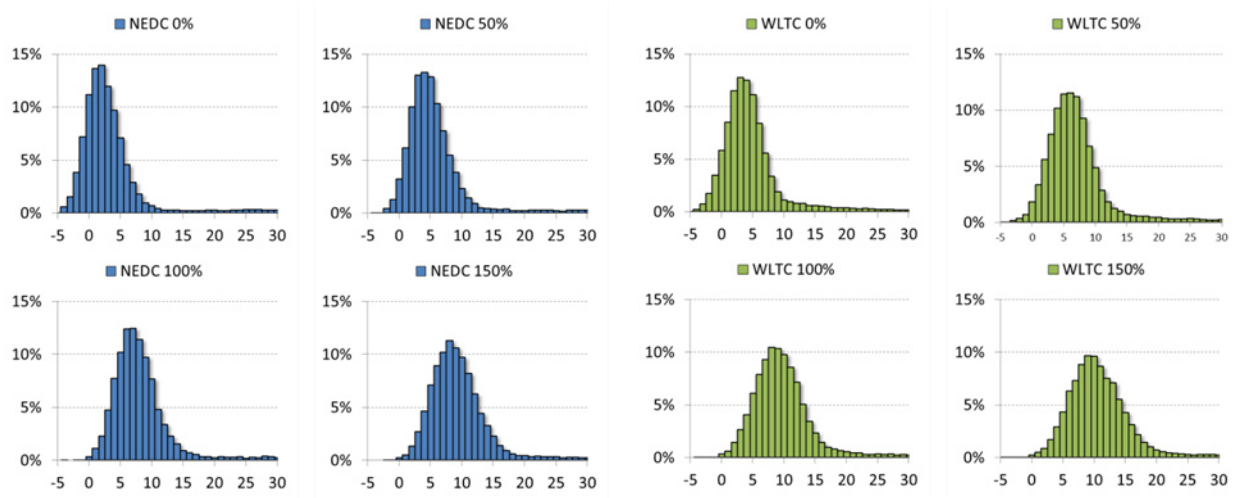


Fig. CS3.11: Distribution of the combustion centre of gravity in CNG operation in the NEDC (left) and in the WLTC (right) with original ZP map (light blue) and the IgnP variations mod1, mod2 and mod3.

Results

Influence of H₂ blending on energy consumption

a) Basic fuel consumption measurements in CNG operation

To ensure that not the IgnP variation but really the H₂ blending is responsible for the effects on exhaust emissions and fuel consumption, a first series of measurements was carried out to investigate how the corrections to the IgnP map in CNG operation affect the NEDC and WLTC driving cycles.

Fig. 12 shows the energetic fuel consumption in MJ/km in CNG operation in the NEDC and WLTC in the individual partial cycles (green markings) as well as the percentage deviation from the original IgnP map (yellow markings). This showed that all IgnP variations in CNG operation led to an increase in consumption. It can therefore be assumed that the original data for the IgnP map were determined for optimal fuel consumption and that the following measurement results can be attributed solely to the H₂ admixture.

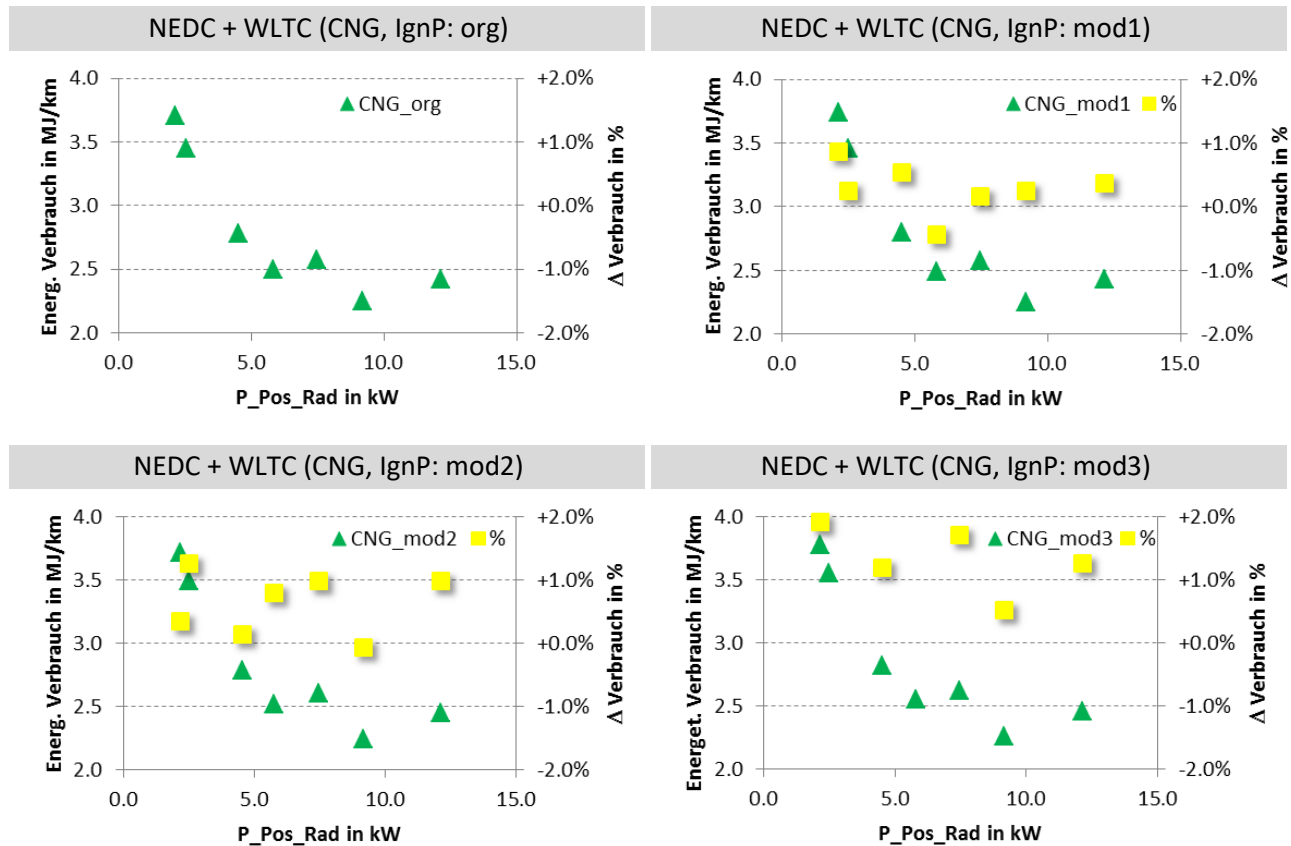


Fig. CS3.12 Energetic fuel consumption in the NEDC and in the WLTC (green markings) as well as consumption changes compared to the original IgnP map (yellow markings) for the IgnP variations (mod1, mod2, mod3) in CNG operation with engine at operating temperature (oil temperature at engine start = 80°C).

The effects of the IgnP correction in the individual partial cycles differ due to their different load profiles. However, the changes due to the IgnP variation are similar proportionally over the entire operating range. If the ignition map is shifted slightly to late (mod1), the changes in consumption are in the range of -0.5 to +1%, if the IgnP map is optimal for HCNG₂₅ operation (mod2) they are in the range of

0 to 1% and if the IgnP map is shifted even further to late (mod3), changes in consumption are measured in the range of 0.5 to 2%. By trend, low-load partial cycles showed a slightly higher percentage deterioration than the higher-load partial cycles.

b) Comparative consumption measurements in HCNG₂₅ operation

The comparison measurements in HCNG₂₅ operation are listed below. Fig. 13 shows the energy consumption values determined in the NEDC and WLTC with original ignition maps in CNG operation (orange markings), with modified ignition maps in HCNG25 operation (blue markings) and the percentage changes (yellow markings).

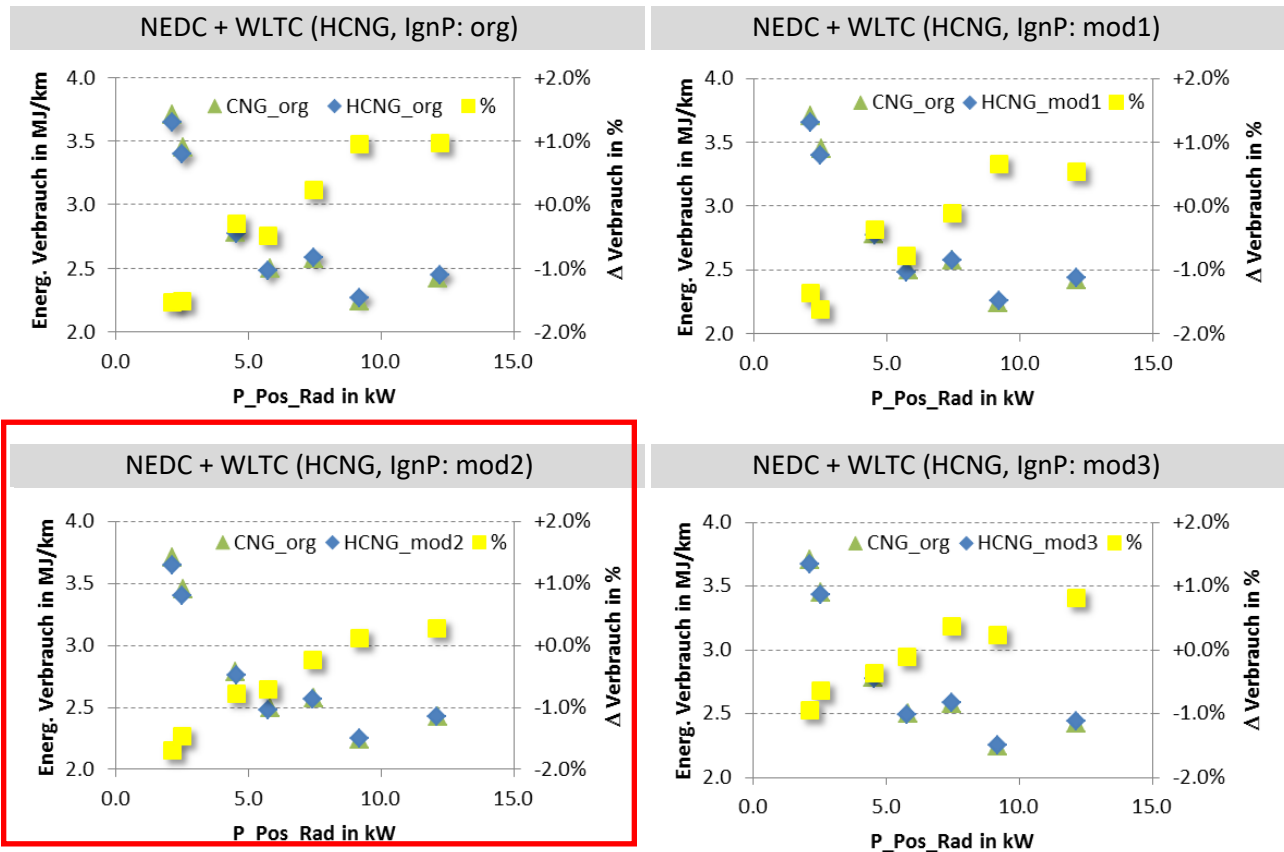


Abb. CS3.13 Energy consumption in NEDC and WLTC in CNG mode (green markings) and in HCNG mode (blue markings) as well as changes in consumption (yellow markings) compared to the original IgnP map for the IgnP variations (mod1, mod2, mod3) in HCNG₂₅ mode with warm engine (oil temperature at engine start = 80°C).

The H₂ blending with original IgnP map leads to energy consumption savings of up to 1.5% on low load journeys (average positive wheel power <7 kW); on higher load journeys, however, an increase of up to 1%. The average deviation over all partial cycles is -0.24%. The half corrected shift of the combustion center of gravity (IgnP map mod1) reduces the energy consumption slightly compared to the original IgnP map. For driving cycles with higher average positive wheel power, however, there is still a slight increase in consumption of up to 0.5%. The average deviation over all partial cycles is -0.44%.

The optimum correction of the IgnP map (IgnP map mod2; framed in red in Fig. 13), which returns the center of gravity of the combustion to the original values, reduces energy consumption the most. Even in driving cycles with higher average positive wheel power, this does not lead to a significant increase in fuel consumption. The average deviation over all partial cycles is -0.64%.

Excessive late adjustment of the IgnP map (mod3) leads to a slight increase in energy consumption compared to complete correction of the IgnP map. This results in an additional consumption of up to 1% for driving cycles with higher average positive wheel performances. The average deviation over all partial cycles is -0.1%.

1.1. Influence of H₂ blending on CO₂ emissions

CO₂ emissions depend on energy consumption and the carbon content of the fuel. According to Fig. 13, the H₂ blending with 25 mol% leads to a consumption reduction of 0 - 2%. According to Table 2, this H₂ admixture corresponds to an energy content or a corresponding reduction in carbon content of 9.3%. Thus a CO₂ reduction in the range of 9.3 - 11.3% can be expected.

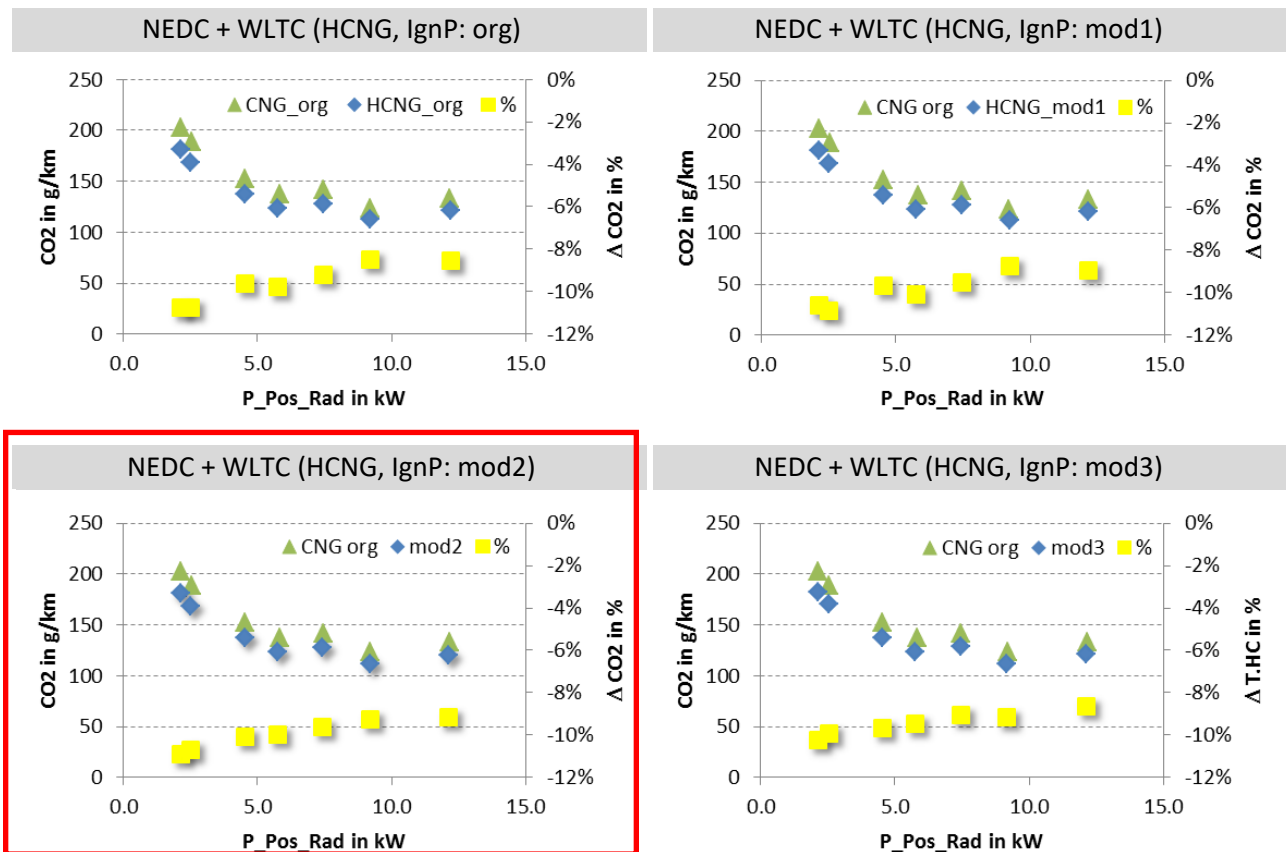


Fig. CS3.14 CO₂ emissions in NEDC and WLTC in CNG mode (green markings) and in HCNG₂₅ mode (blue markings) as well as changes (yellow markings) compared to the original IgnP map for the IgnP variations (mod1, mod2, mod3) in HCNG₂₅ mode with warm engine (oil temperature at engine start = 80°C).

As Fig. 14 shows, the CO₂ emissions of the vehicle in HCNG25 operation are, as expected, 9.3 - 11.3% lower than in CNG operation with correct IgnP correction (mod2, framed in red).

Influence of H₂ blending on T.HC emissions

a) Tailpipe T.HC emissions in CNG operation

Fig. 15 shows the T.HC emissions in CNG operation with original IgnP map (orange markings) and with variation of the IgnP map (green markings). The changes compared to the original IgnP map are represented by the yellow markings.

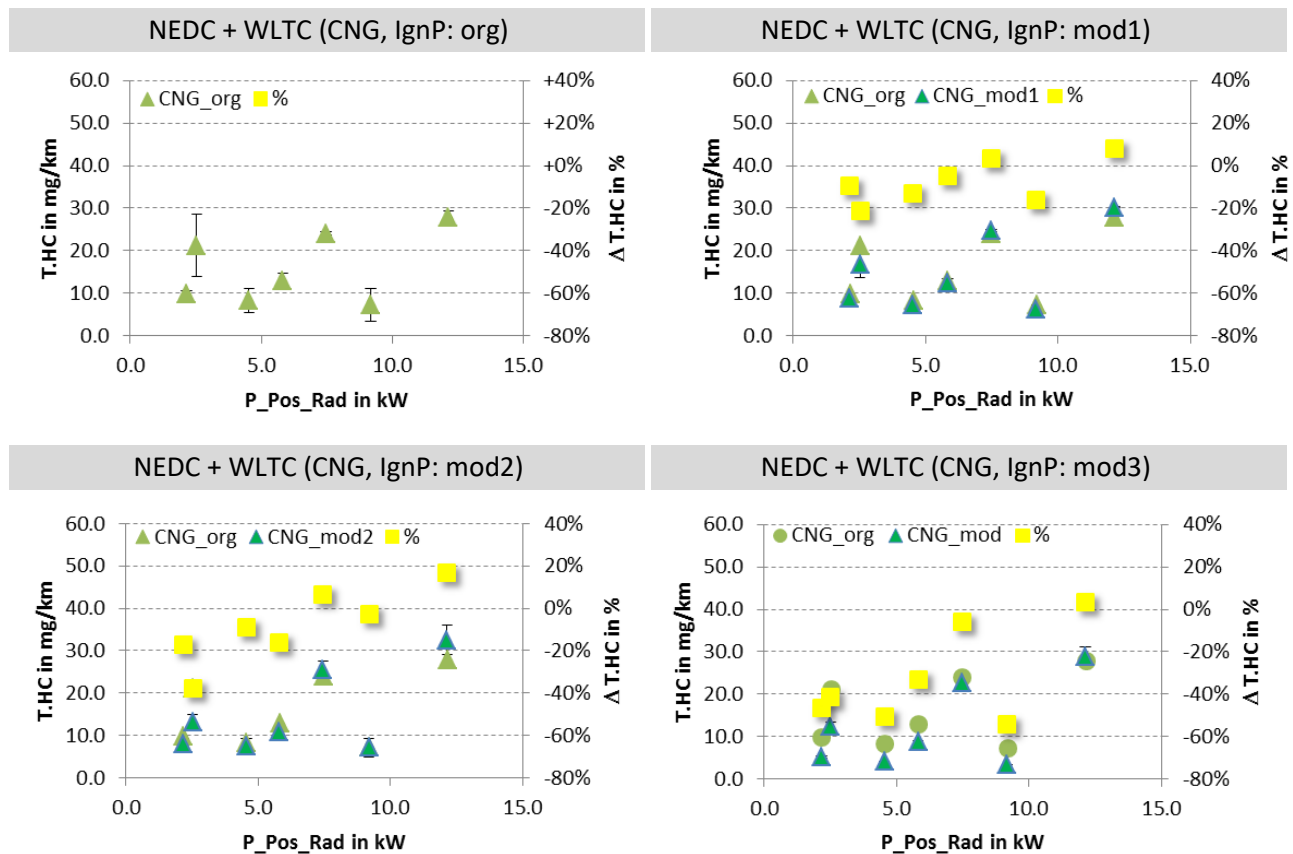


Fig. CS3.15 T.HC emissions in NEDC and WLTC in CNG operation with original ZP map (light green markings) and in CNG operation with modified IgnP maps (dark green markings) as well as changes (yellow markings) compared to the original IgnP map for the IgnP variations (mod1, mod2, mod3) in CNG operation with warm engine (oil temperature at engine start = 80°C).

Fig. 15 shows that the late shift of the IgnP map already leads to a reduction of T.HC emissions in CNG operation. However, this alone causes a deviation from the optimum combustion center position and therefore a deterioration in efficiency (see Fig. 12).

b) Tailpipe T.HC emissions in HCNG₂₅ operation

In HCNG₂₅ operation, 10 - 50% lower T.HC emissions were measured, depending on the map correction. With the optimum ZPP map correction (mod2, framed in red), these values were on average 35% lower than with CNG operation with the original ZPP map.

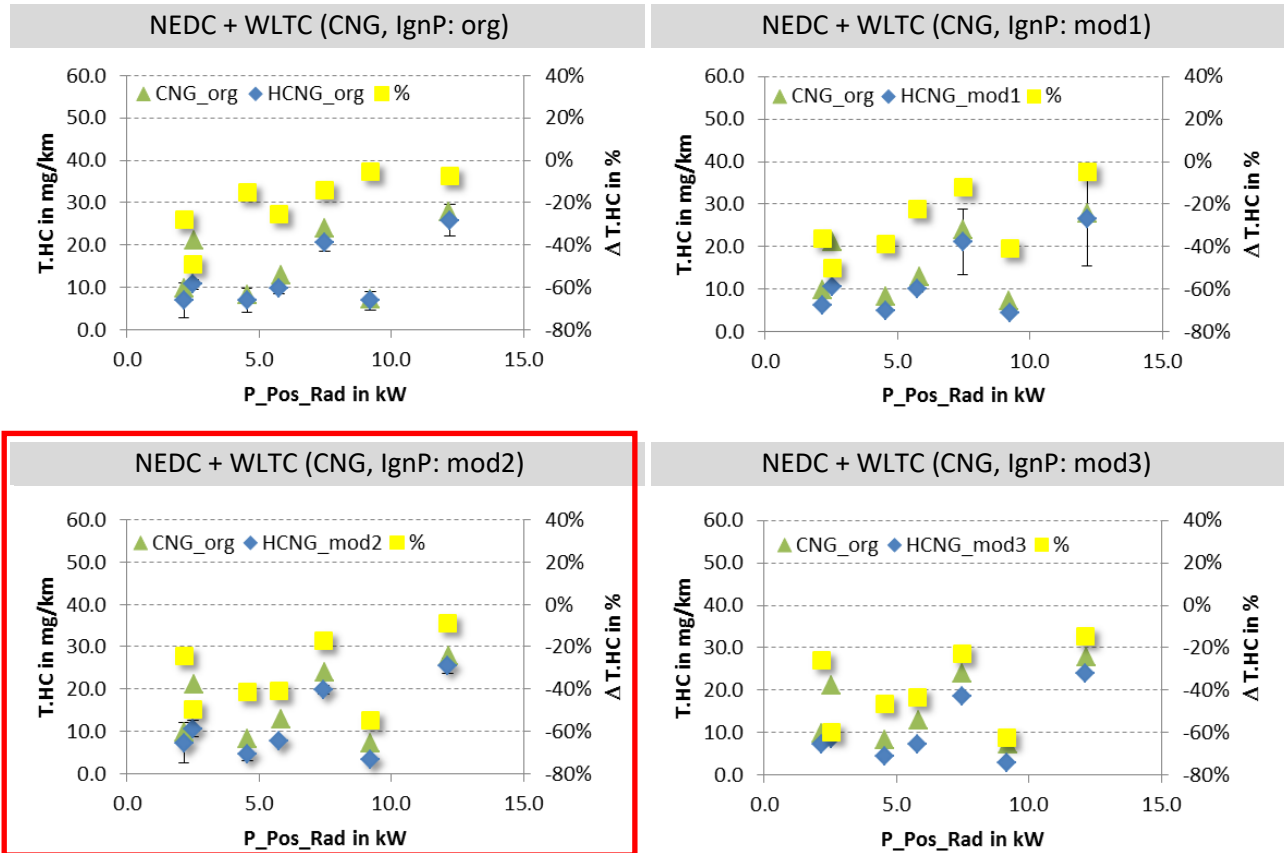


Fig. CS3.16 T.HC emissions in NEDC and WLTC in CNG mode (green markings) and in HCNG₂₅ mode (blue markings) as well as changes (yellow markings) compared to the original IgnP map for the IgnP variations (mod1, mod2, mod3) in HCNG₂₅ mode with warm engine (oil temperature at engine start = 80°C).

In HCNG₂₅ operation, a reduction in T.HC emissions was observed in the entire operating area. With an optimum IgnP map (framed in red) for the combustion center of gravity, a reduction in T.HC emissions of almost 60% (see yellow markings) could be measured, depending on the partial cycle.

c) Engine-out T.HC emissions in CNG and HCNG operation

In order to understand the reduction of T.HC tailpipe emissions as shown in Fig. 16, engine-out measurements were carried out in CNG operation with original IgnP map and in HCNG₂₅ operation with fully corrected advance adjustment (IgnP map mod2) with engine at operating temperature.

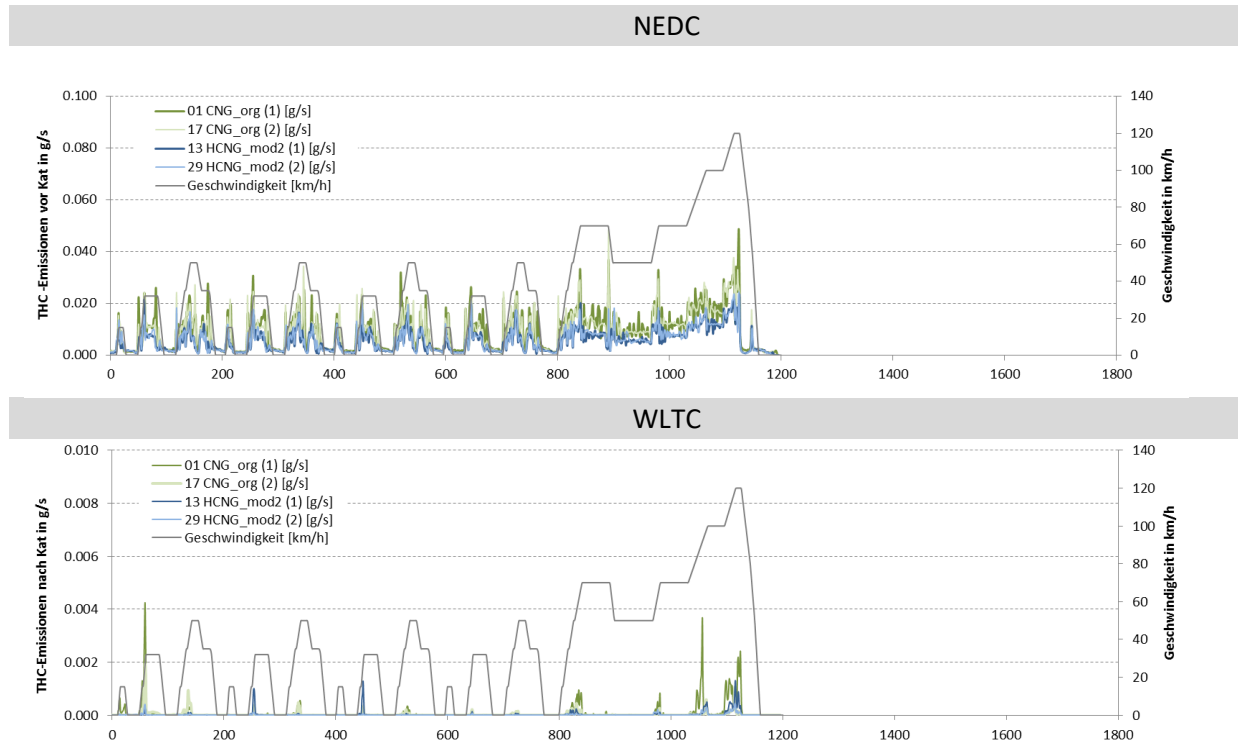


Fig. CS3.17 T.HC engine-out emissions in CNG operation (green) and in HCNG operation with 25 mol% H₂ blending (blue) in NEDC (top) and WLTC (bottom)

The T.HC engine-out emissions are generally 20 - 40% lower in both driving profiles in HCNG₂₅ operation than in CNG operation. An important source of T.HC emissions are the flame extinguishing zones on the combustion chamber walls. Ma et al give a flame extinguishing distance 3 - 4 times shorter for pure hydrogen than for methane. Against this background, the T.HC reduction shown in Fig. 17 in HCNG operation can very probably be attributed mainly to the shorter flame extinguishing distance of the HCNG₂₅ mixture.

d) T.HC tailpipe measurements in CNG and HCNG₂₅ operation

Tailpipe T.HC measurements were carried out in CNG mode with original and in HCNG₂₅ operation with fully corrected advance adjustment (ZZP map mod2) and engine at operating temperature. As described in chapter 2, the catalytic converter was shortened by 1/3 for these tests. This explains the sharp increases in emissions after the catalyst at high exhaust mass flows..

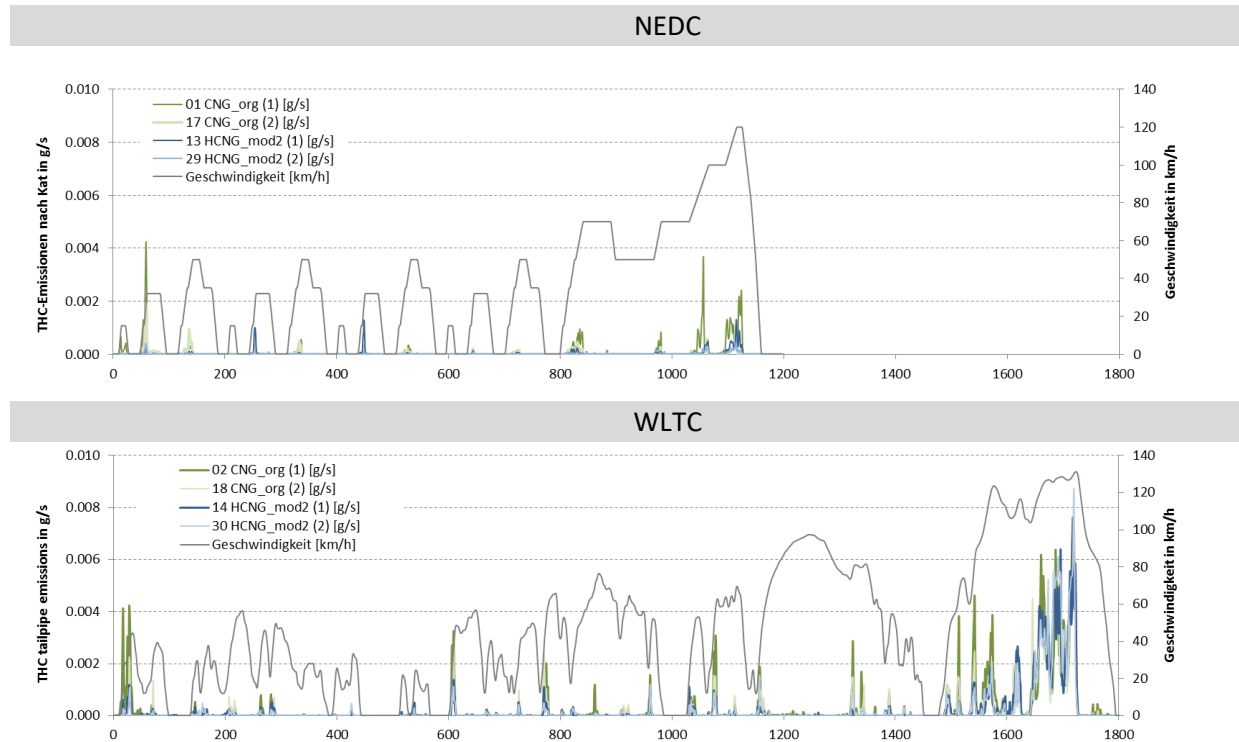


Fig. CS3.18 T.HC emissions after catalyst in CNG operation (green) and in HCNG operation with 25 mol% H₂ blending (blue) in NEDC (top) and WLTC (bottom)

The T.HC tailpipe emissions are at a very low level. At speeds <100 km/h, only individual T.HC peaks can be detected when starting up or after load changes. These are probably related to the difficult mixture formation process at accelerations after a fuel cut-off. This is derived from the fact that these T.HC peaks occur both in CNG and HCNG₂₅ operation at the same location and therefore have to be assigned to a control event rather than to the catalyst behavior. Fig. 18 also shows that the T.HC peaks in HCNG₂₅ operation - analogous to the engine-out emissions - are significantly lower than in CNG operation.

At speeds >100 km/h, a significant reduction in the conversion rate or an increase in T.HC emissions can be seen. This can be attributed to the 1/3 reduction in the catalytic converter.

A comparison of the cumulated T.HC engine-out and tailpipe emissions in the NEDC and the WLTC (Fig. 19) shows that the H₂ blending leads to a significant T.HC reduction in both the NEDC and the WLTC as well as for engine-out (left Y-axis) and tailpipe emissions (right Y-axis).

The increase in tailpipe T.HC emissions at speeds >100 km is due to the reduction of the catalyst by 1/3 (see chapter 2).

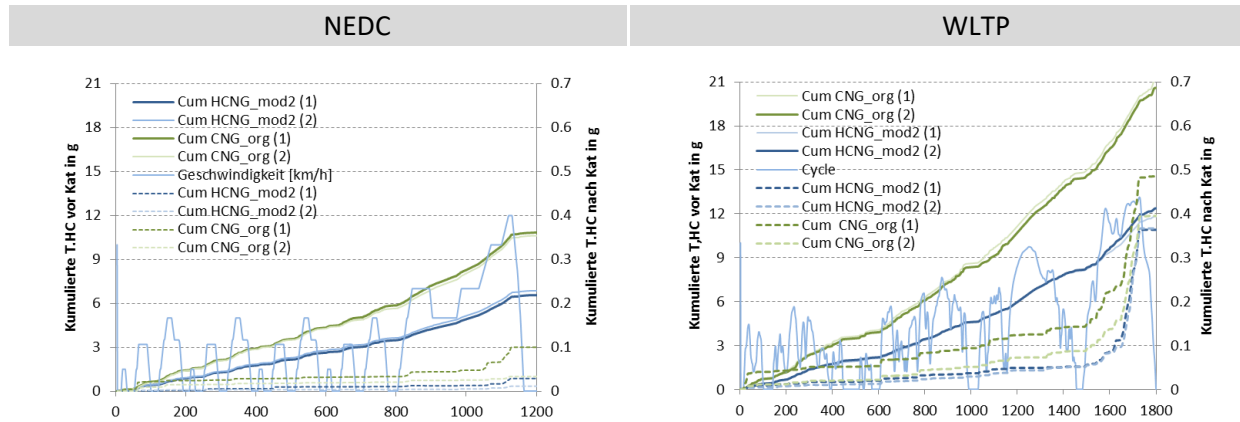


Fig. CS3.19 Cumulated T.HC engine-out and tailpipe emissions (2 measurements each) in NEDC (left diagram) and WLTP (right diagram)

Influence of H₂ blending on NO_x emissions

a) Tailpipe NO_x emissions in CNG operation

Fig. 20 shows the NO_x tailpipe emissions in CNG operation with original IgnP map (light green markings) and with variation of the IgnP map (dark green markings). The changes compared to the original IgnP map are represented by the yellow markings.

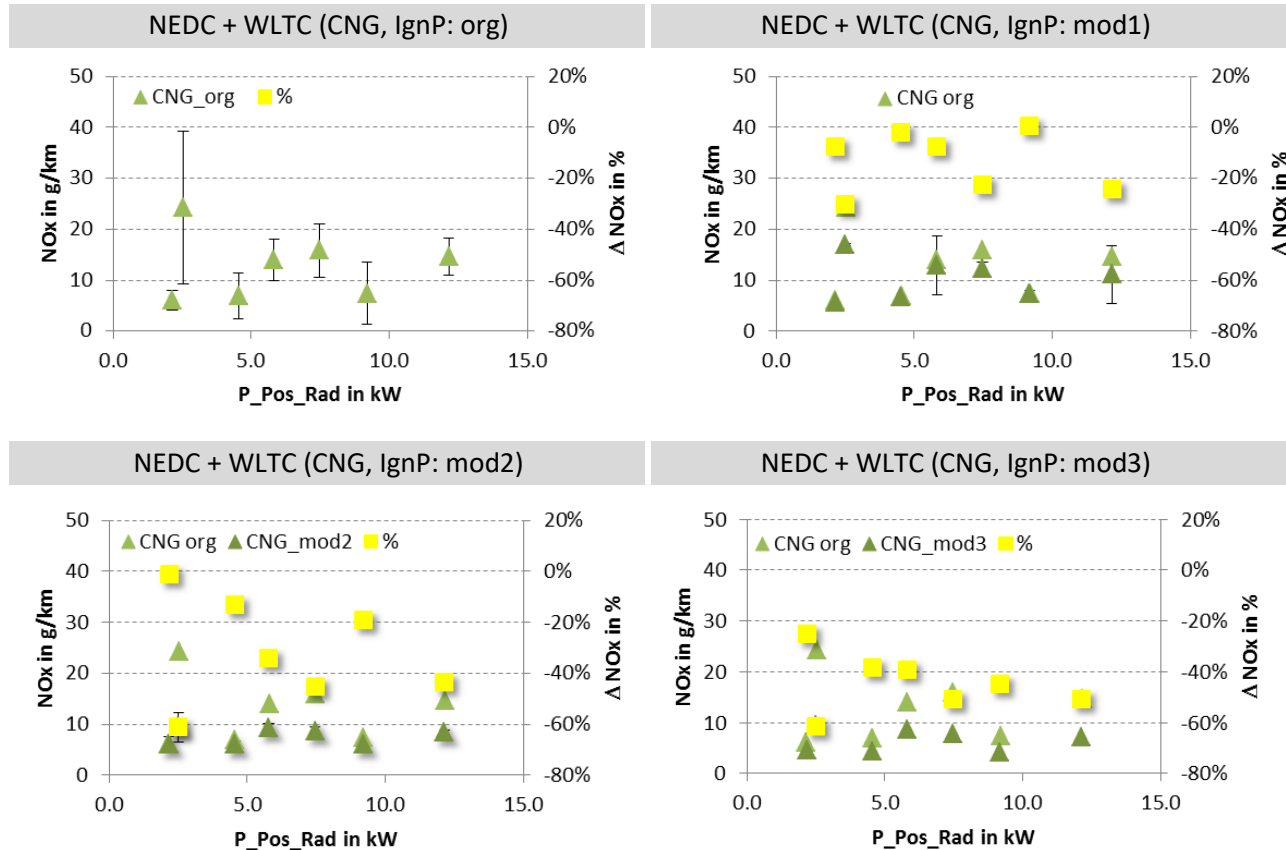


Fig. CS3.20 NO_x emissions in NEDC and WLTC in CNG operation with original IgnP map (light green markings) and in CNG operation with modified IgnP maps (dark green markings) as well as changes (yellow markings) compared to the original IgnP for the IgnP variations (mod1, mod2, mod3) in CNG operation with warm engine (oil temperature at engine start = 80°C).

Fig. 20 shows that the late shift of the IgnP map already leads to a reduction of NO_x emissions in CNG operation. However, this causes a deviation from the optimum combustion centre position and therefore a deterioration in efficiency (see Fig. 11). However, in contrast to T.HC emissions, the decrease is somewhat more constant over the entire wheel power range.

b) Tailpipe NOx emissions in HCNG₂₅ operation

In HCNG₂₅ operation, up to 60% lower NOx emissions were measured depending on the catalyst and the map correction. With the optimum IgnP map correction (mod2, framed in red), these values were on average 42% lower than with CNG operation with the original IgnP map.

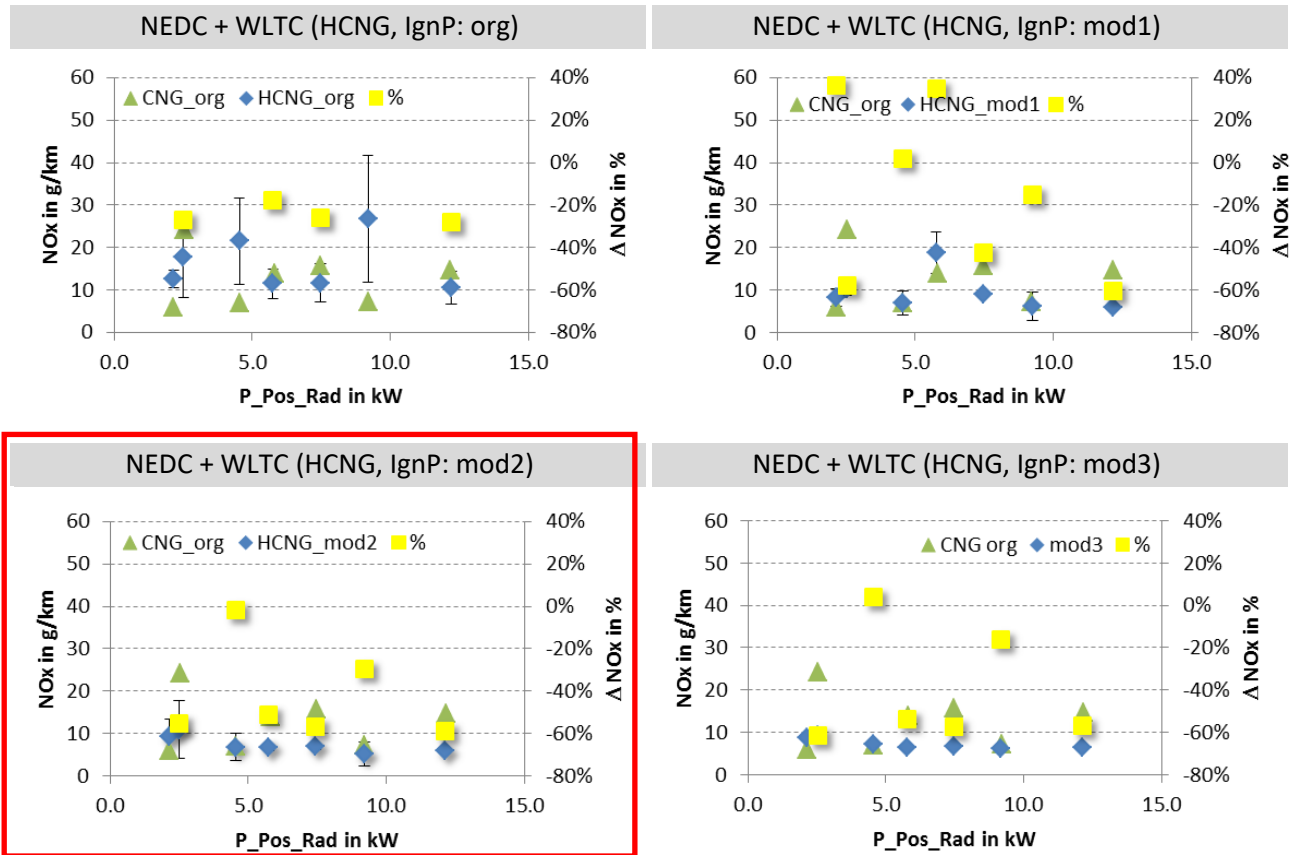


Fig. CS3.21 T.HC emissions in NEDC and WLTC in CNG mode (green markings) and in HCNG₂₅ mode (blue markings) as well as changes (yellow markings) compared to the original IgnP map for the IgnP variations (mod1, mod2, mod3) in HCNG₂₅ mode with warm engine (oil temperature at engine start = 80°C)

In contrast to T.HC emissions, the high reduction in NOx tailpipe emissions cannot be derived from combustion, as the following explanations show. The NOx emissions before catalyst in CNG operation with original IgnP map and in HCNG₂₅ operation with optimized IgnP map (mod2) are practically identical.

c) Engine-out NOx measurements in CNG and HCNG operation

The measurements were carried out in CNG mode with original and in HCNG₂₅ operation with fully corrected advance adjustment (IgnP map mod2) and engine at operating temperature.

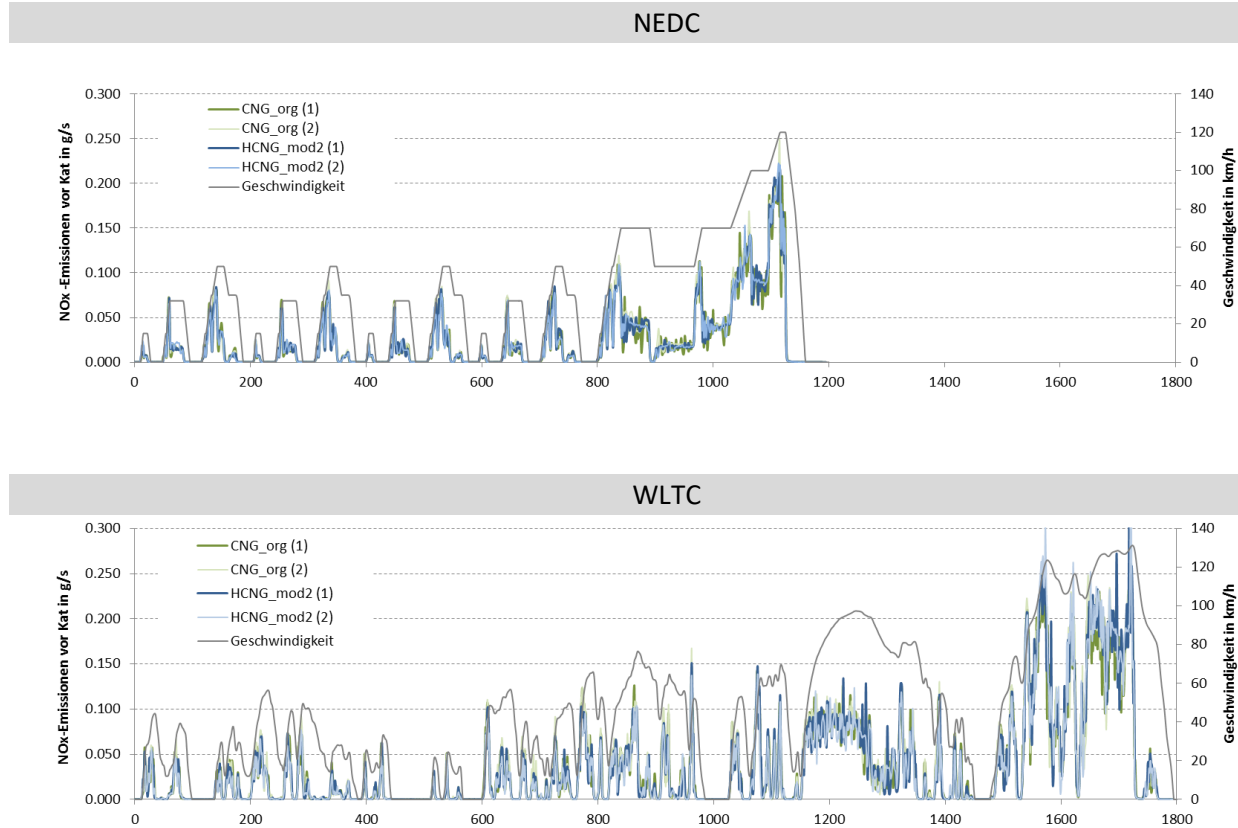


Fig. CS3.22 Engine-out NOx emissions in CNG operation (green) and in HCNG₂₅ operation (blue) in NEDC (top) and WLTC (bottom)

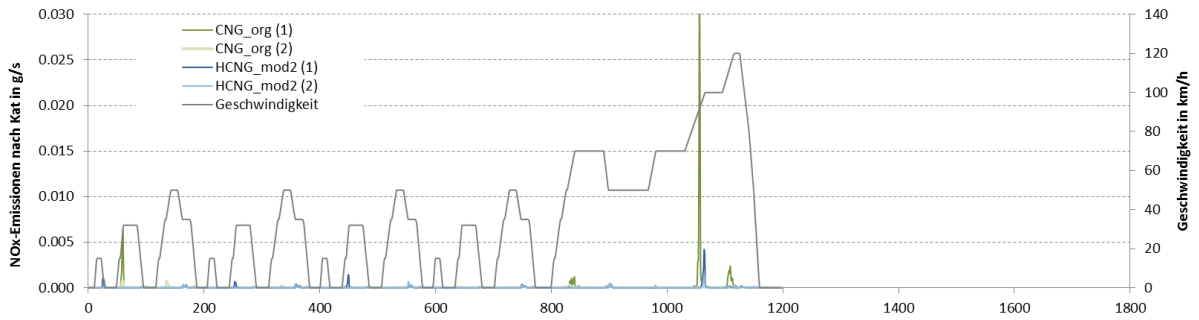
The engine-out NOx emissions are at the same level for both driving profiles in CNG and HCNG₂₅ operation. The NOx emissions in the combustion engine are mainly formed thermally. The measurements show that the correction of the IgnP map in HCNG operation to the same combustion center as in CNG operation leads to constant raw NOx emissions upstream of the catalytic converter.

Thus the NOx emissions in CNG and HCNG₂₅ operation are - in contrast to the T.HC emissions - at almost the same level before the catalytic converter.

d) Tailpipe NOx measurements in CNG and HCNG operation

The measurements were carried out in CNG operation with original and in HCNG₂₅ operation with fully corrected advance adjustment (IgnP map mod2) and warm engine. As explained in Chapter 2, the catalyst for these tests was shortened by 1/3.

NEDC



WLTC

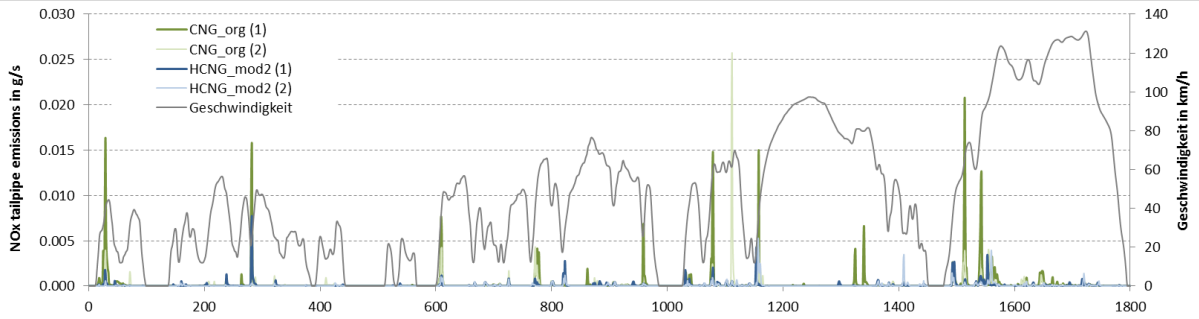


Fig. CS3.23 Tailpipe NOx emissions in CNG operation (green) and in HCNG₂₅ operation (blue) in NEDC (top) and WLTC (bottom)

Tailpipe NOx emissions are at a very low level in both CNG and HCNG₂₅ operation. As with T.HC emissions, individual NOx peaks can only be detected during start-up or after load changes.

Looking at the cumulated engine-out and tailpipe NOx emissions (Fig. 24), it can be seen that the engine-out emissions (Fig. 24, extended lines) in CNG and HCNG₂₅ operation are very similar in both cycles. However, the tailpipe emissions (Fig. 24, dotted lines) in HCNG₂₅ operation are significantly (up to 60%) lower than in CNG operation.

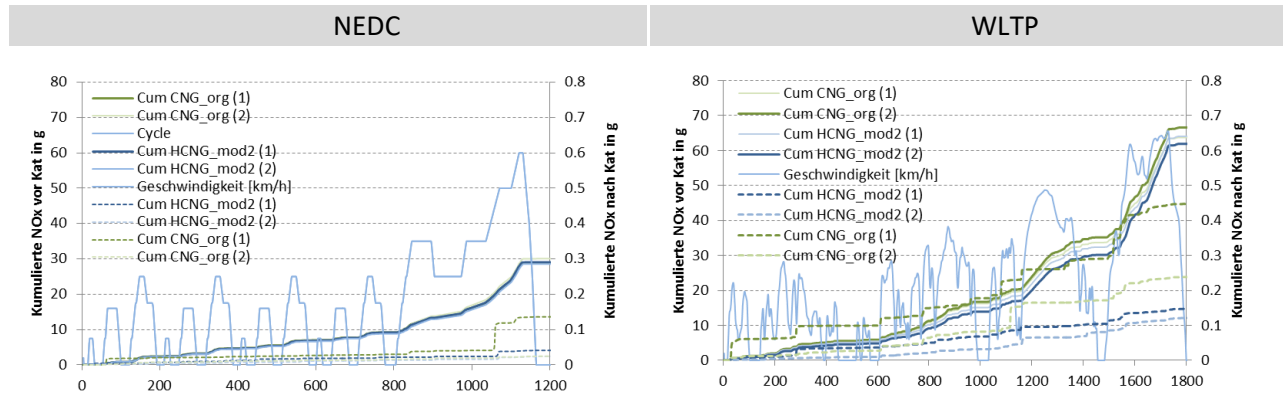


Fig. CS3.24 Cumulated engine-out and tailpipe NOx emissions (2 measurements each) in NEDC (left diagram) and WLTP (right diagram)

In contrast to T.HC emissions, tailpipe NOx emissions in HCNG₂₅ operation do not simply reflect the lower engine-out values, but an additional increase in conversion resulting in the catalyst can be observed.

To explain this effect, various analyses of kinetically based hypotheses (higher temperature, higher proportions of more reactive exhaust components) were carried out in a first attempt. Corresponding parameters such as temperatures before the catalyst, proportions of non-limited pollutant compounds such as NO₂, NH₃ or H₂ were measured and rapid NOx analysis was used. However, the differences in all these aspects were rather small and could not explain the significant reduction in NOx tailpipe emissions.

The only difference was that slightly higher H₂ concentrations were measured at low exhaust mass flows (i.e. at low loads) (Fig. 25). If the potentials of this temporarily slightly increased H₂ content are converted to a chemical reduction of NOx emissions (SCR reaction), the NOx reduction can only be explained to a small extent. We can therefore exclude a kinetic or chemical reason for the increased NOx reduction in HCNG₂₅ operation.

Fig. 25 shows that the H₂ concentrations in CNG and HCNG₂₅ operation in the NEDC as well as in the WLTC are in the range 4'000 – 5'000 ppmV practically independent of the current driving condition, except after fuel shut-off phases, where the concentration in CNG operation rises to around 15'000 ppm and in HCNG₂₅ operation to 17'000 – 18'000 ppm.

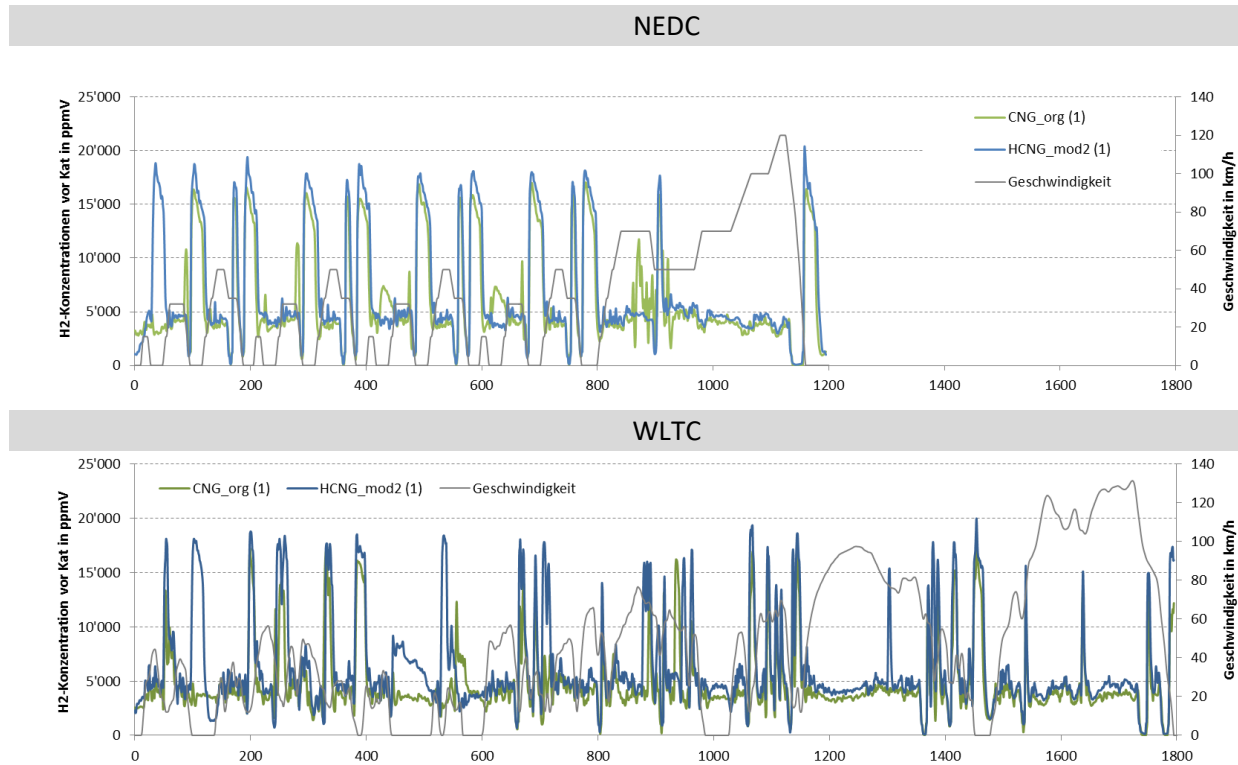


Fig. CS3.25 Engine-out H₂ concentrations in CNG operation (green) and in HCNG₂₅ operation (blue) in NEDC (top) and WLTC (bottom)

After deceleration phases with a fuel shut cut-off and a corresponding filling of the catalytic converter with oxygen, the engine control system is providing a rich air/fuel mixture with correspondingly increased engine out CO emission to reduce the oxygen level in the catalytic converter (also known as oxygen removal in the catalytic converter). In the catalytic converter, the CO reacts to CO₂ and thus at least partially breaks down the chemically bound oxygen on the porous catalyst surface, the so-called "washcoat". Without this "oxygen removal", the catalytic conversion efficiency would be massively reduced for NO_x conversion after fuel shut-off phases, since the oxygen required for the oxidation reactions for the conversion of HCs and CO would be removed from the washcoat and not from the nitrogen oxides.

In a second attempt, therefore, a hypothesis based on control technology was put forward, which includes the above-mentioned observation of the increased H₂ concentration during idling phases and after thrust shutdown.

The question is, whether the increased H₂ concentration compared to CNG operation could accelerate the oxygen removal and thus positively influence the NO_x conversion in the catalytic converter after fuel shut-off phases.

The oxygen storage takes place during vehicle deceleration through the oxidation of Ce₂O₃ with O₂. This reaction takes place very quickly. At 300°C, the Ce₂O₃ is completely saturated in the washcoat in less than 1 second.

Regeneration or "oxygen removal" takes place in rich operation by chemical reduction of CeO₂ with CO or H₂ in Ce₂O₃ (+CO₂ respectively H₂O).

Fig. 26 shows that the engine-out CO emissions in the NEDC and in the WLTC are very similar in CNG and HCNG₂₅ operation.

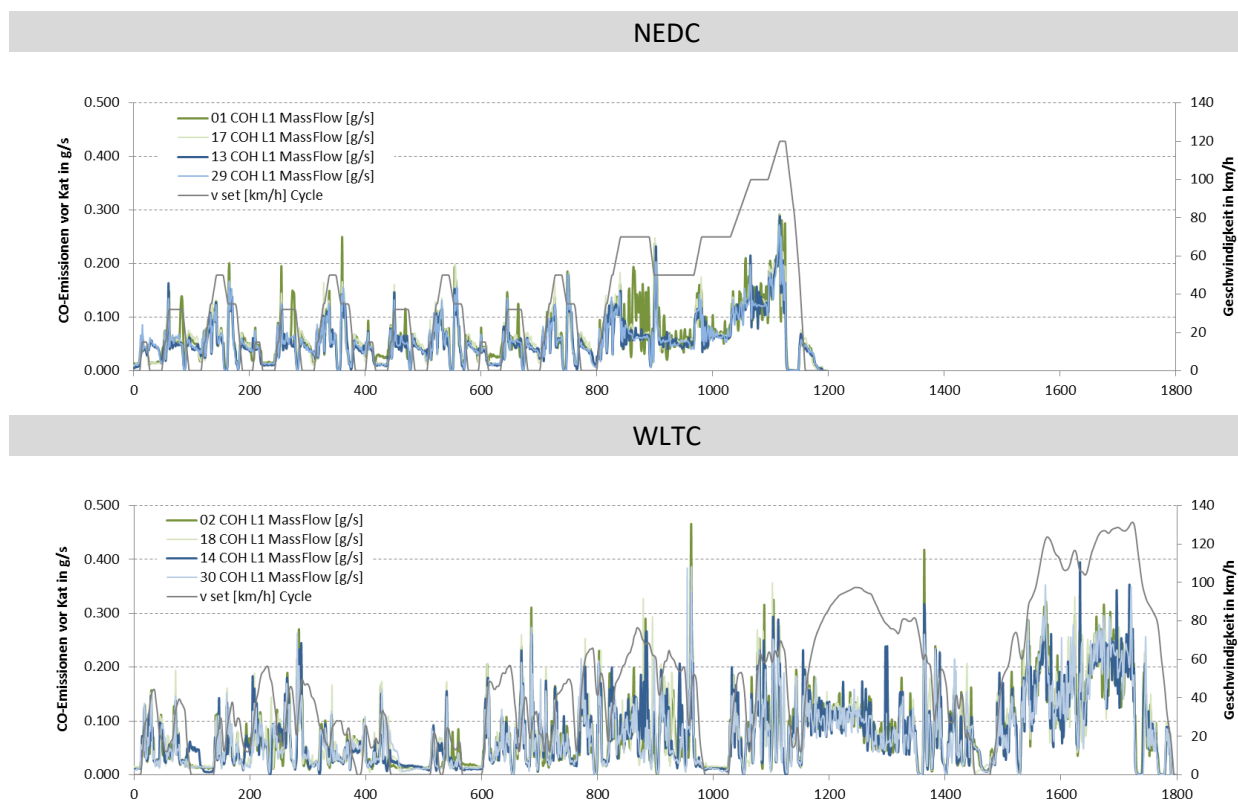


Fig. CS3.26 CO emissions in exhaust gas upstream of catalytic converter in CNG operation (green) and in HCNG₂₅ operation (blue) in NEDC (top) and WLTC (bottom)

It can therefore be assumed that CO emissions do not play a role in this context, which focuses on the H₂ content of exhaust emissions.

It is known that H_2 has a positive influence on conversion behaviour in the catalyst. For example, the water gas shift reaction (1) and steam reforming (2) but also the oxygen storage from steam at Ce_2O_3 (3) increase the hydrogen content in the catalyst, which is known to increase the catalytic conversion efficiency:

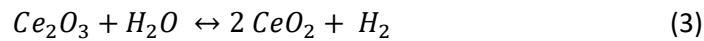
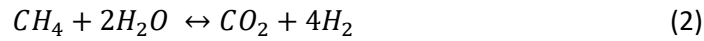


Fig. 27 shows by how much NO_x emissions could be reduced in $HCNG_{25}$ operation by adding H_2 . The emission profiles of the two measurements in CNG and $HCNG_{25}$ operation were averaged and the difference (NO_x in $HCNG_{25}$ operation - NO_x in CNG operation) was calculated.

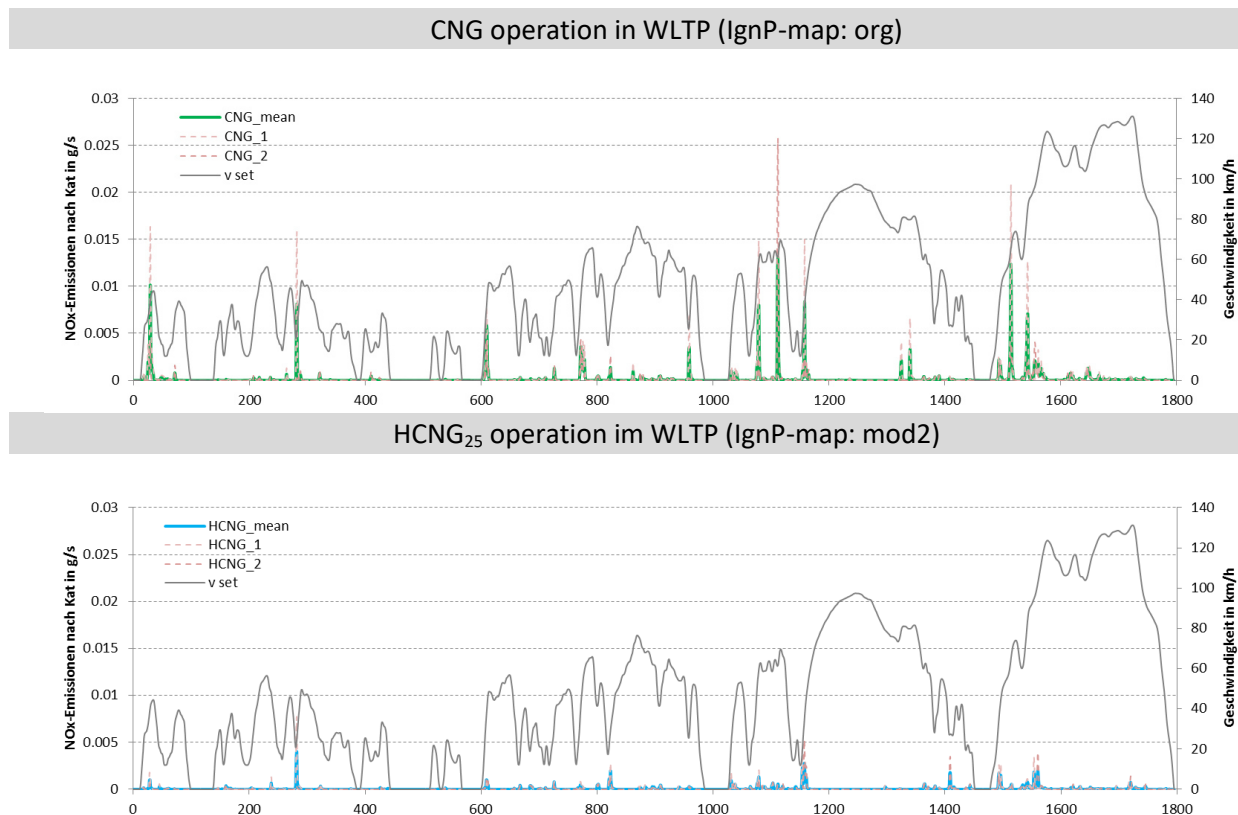


Fig. CS3.27 Average NO_x emissions in exhaust gas after catalyst in CNG operation (upper diagram) and in $HCNG_{25}$ operation (lower diagram) in WLTC

Fig. 27 shows that tailpipe NO_x emissions consist almost exclusively of NO_x peaks after fuel shut-off phases and that the dispersion is very low in both CNG and $HCNG_{25}$ operation.

If we now form the difference between the two NO_x curves (without any temporal corrections), it can be seen that the H_2 admixture in $HCNG_{25}$ operation significantly reduces all NO_x peaks after deceleration

phases compared with CNG operation. This reduction can be identified by the exclusion procedure as a contribution of the H₂ admixture.

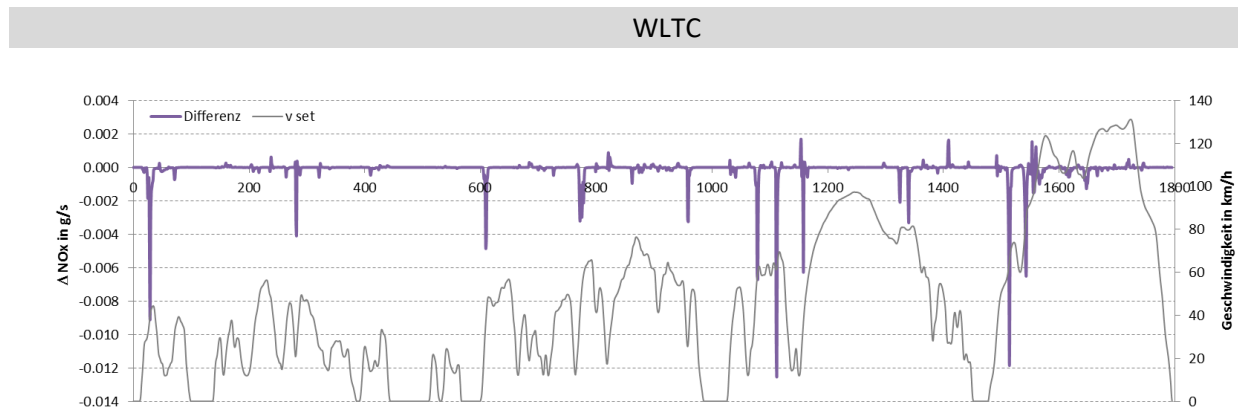


Fig. CS3.28 Engine-out CO concentrations in CNG operation (green) and in HCNG₂₅ operation (blue) in NEDC (top) and WLTC (bottom)

The hypothesis that the slightly increased H₂ content of the exhaust gas upstream of the catalyst after thrust phases could be responsible for the increased NO_x conversion in the catalyst in HCNG operation has thus at least been empirically confirmed. This is due to the reactivity of H₂ for the reaction with O₂.

Due to the complex oxygen storage with material, temperature and ageing dependencies in the washcoat of the catalytic converter and the strong dependencies on control engineering functions and the data of the engine control during cat removal and the O₂ level control of the catalytic converter, as well as finally the occurrence of other H₂-forming reactions in the catalytic converter, scientific proof of this hypothesis can only be provided by detailed modelling. This was not the subject of this project. It is currently being examined whether such work could be undertaken, for example, as part of a follow-up project.

Summary of the results

The blending of hydrogen to the CNG is not readily feasible in terms of materials, as both the gas network and the gas-carrying components in the vehicle must be designed for this.

However, operation in conventional CNG vehicles would lead to significantly lower pollutant emissions than those already present in CNG operation. NO_x emissions could be practically eliminated in the entire operating range, and T.HC emissions, which mainly consist of methane, which is primarily a strong greenhouse gas, could also be reduced by an average of one third.

However, the volumetric energy density, which decreases by almost 30% with an H₂ content of 25 mol%, would be operationally disadvantageous. It could be compensated by increasing the pressure to 350 bar.

For future combustion processes with diluted mixture formation (lean or EGR operation), H₂ blending could be an interesting option due to the difficult ignition of (diluted) methane gases.

[Case study 4. Danish catalyst study](#)

Summary

Catalysts study in this work aimed at a solution for the SO₂ tolerance of CH₄ oxidation catalyst. This work designed a series of Rh/zeolite catalysts for oxidation of CH₄. 1 wt.% Rh/zeolite catalyst had higher activity compared with the commercial catalyst under same operation condition. The activity of the Rh/zeolite catalyst can be significantly enhance by elevating the operation temperature to 475 °C and limiting the SO₂ concentration to a low level. It can be promising to be used in the real engine exhausted gas condition where the SO₂ concentration is 1-2 ppm.

Experimental and method.

A series of noble metal supported catalysts were synthesized and studied for oxidation of methane under simulated exhausted gas condition in this work. The catalysts were prepared by Incipient Wetness Impregnation (IWI) method followed by calcination in air at 600 °C. A fixed-bed plug-flow quartz reactor was used to test the activity of the synthesized and commercial catalysts under different atmospheres. A three-zone heated furnace was used to heat the catalytic bed to the reaction temperatures (250-600 °C). The gas atmospheres studied in this work are SO₂ absent atmosphere (2500 ppm CH₄, 10 vol.% O₂, 5 vol.% H₂O, balanced with N₂, total flow: 300 Nml/min) and SO₂ present atmosphere (2500 ppm CH₄, 10 vol.% O₂, 5 vol.% H₂O, 1-20 ppm SO₂, balanced with N₂, total flow: 300 Nml/min). Each time, 0.12 g (or 0.24 g) catalyst was diluted with 1.08 g (0.96 g) inert sand to give a gas hourly space velocity (GHSV) of 150,000 (or 75,000) ml/h·g_{cat}. Before sending to analysis, the effluent gas was firstly condensed in a condenser and passing a filter to remove H₂O from the stream. The dry exit gas was further analyzed with an online IR gas analyzer to monitor CO₂, CO, O₂, and SO₂ concentrations, and a Micro GC for CH₄ concentration. The CH₄ concentration measured by the micro GC was used to calculate the CH₄ conversion.

The active noble metals studied in this work include Palladium (Pd), Platinum (Pt), Rhodium (Rh), and bimetallic Palladium-Platinum (Pd-Pt), and the supports include alumina (g-Al₂O₃), silica (SiO₂), titanium oxide (TiO₂), alumina-manganese spinel (AlMgO_y), and zeolites. Tungsten oxide (WO₃), cerium oxide (CeO₂), and cobalt oxide (Co₃O₄) were also studied as promoters to improve the SO₂ resistance of alumina supported catalysts. The comparison between the catalysts stated above indicates that Rh/zeolite catalyst can be the most promising catalyst system for methane oxidation under real engine exhausted gas condition with the presences of H₂O and SO₂. A commercial Rh-Cr-Al catalyst supplied by Haldor Topsøe was also tested in the presence of H₂O and SO₂ as a reference for the new designed catalysts. The concentration of SO₂ in the simulated exhausted gas was chosen to be 20 ppm to accelerate the SO₂ caused deactivation and shorten the experimental time.

Results and discussions

Comparison between the commercial catalyst and the home made catalyst

The performance of the commercial Rh-Cr-Al catalysts is shown in Fig.1.

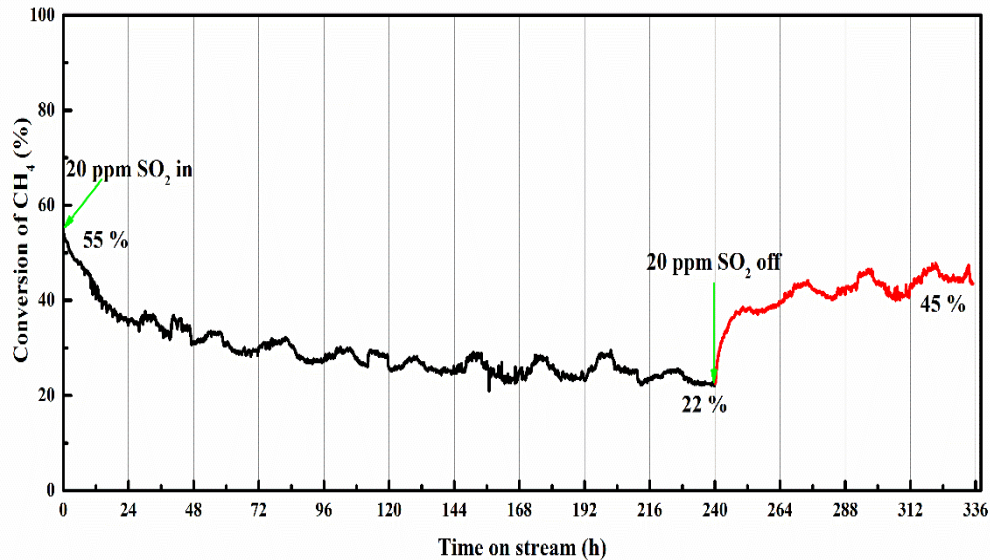


Fig. CS4.1 Deactivation of commercial Rh-Cr-Al catalyst in the presence of 20 ppm SO₂ at 450 °C and the conversion recovery after removal of SO₂. 2500 ppm CH₄, 10 vol.% O₂, 5 vol.% H₂O, 20 ppm SO₂ when present balanced with N₂. GHSV= 75,000 ml/h g_{cat}.

As shown in Fig.1, at an operation temperature of 450 °C, the conversion of CH₄ over the commercial Rh-Cr-Al catalyst decreases as addition of 20 ppm SO₂, while it reaches a stable level of around 22 % after running in the presence of 20 ppm SO₂ for 10 days. After removal of SO₂, the conversion of CH₄ can be restored to around 45 % without extra heating. It indicates this catalyst is able to remove CH₄ under realistic exhaust gas conditions, but it is limited by the content of toxic Cr in the formula. A homemade 1 wt.% Rh/zeolite catalyst was compared with this commercial catalyst under same condition in the absence of SO₂, and the result is shown in Fig.2.

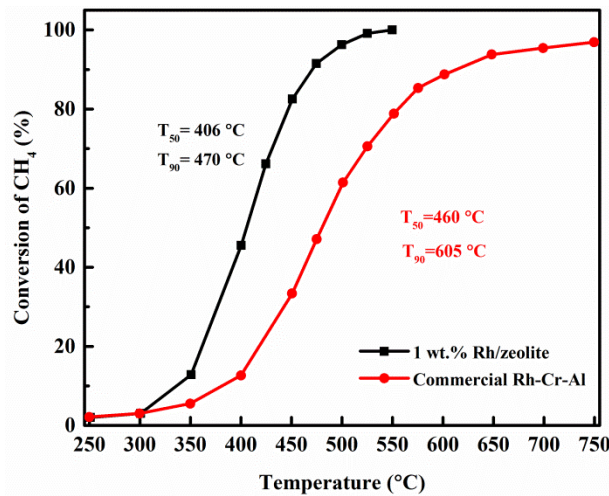


Fig. CS4.2 Comparison between commercial Rh-Cr-Al catalyst and homemade 1 wt.% Rh/zeolite catalyst. 2500 ppm CH₄, 10 vol.% O₂, 5 vol.% H₂O, 20 ppm SO₂ when present balanced with N₂. GHSV= 150,000 ml/h g_{cat}.

As shown in Fig.2, in the absence of SO_2 , the home made 1 wt.% Rh/zeolite catalyst is more active than the commercial Rh-Cr-Al catalyst, with a temperature for 50 % conversion 54 °C lower and 90 % conversion 135 °C lower. There is one uncertainty that the commercial catalyst here was crushed from a monolithic form and the homemade catalyst was in the synthesized powder form. It can be a composition difference after formulating a powder form catalyst to a real monolithic catalyst, and the activity of the monolithic is always lower than that in powder form.

Influence of Rh loading and operation condition.

The homemade Rh/zeolite catalyst was further studied in terms of influence of Rh loading, and deactivation caused by the presences of 5 vol.% H_2O and 20 ppm SO_2 . The results are shown in Fig. 3.

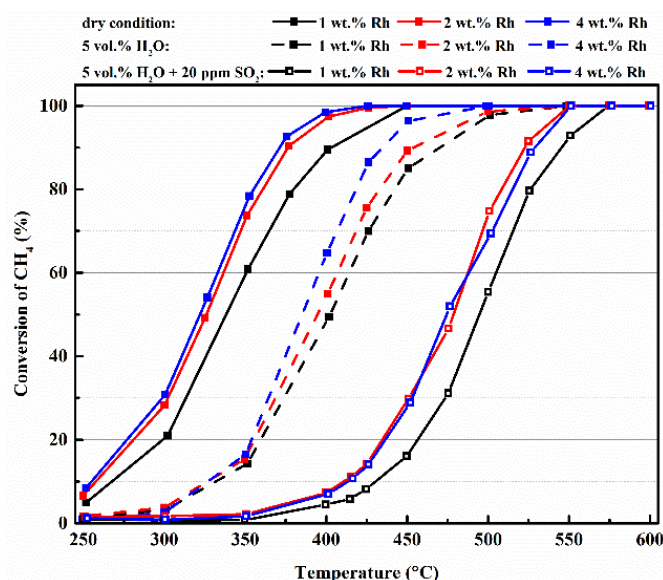


Fig. CS4.3 Activity of Rh/zeolite catalyst with Rh loading of 1 wt.% (black), 2 wt.% (red) and 4 wt.% (blue) under dry and SO_2 -free condition, 5 vol.% H_2O present condition, and 5 vol.% H_2O +20 ppm SO_2 present condition. 2500 ppm CH_4 , 10 vol.% O_2 , 5 vol.% H_2O when present, 20 ppm SO_2 when present, balanced with N_2 . GHSV=150,000 ml/h \cdot g_{cat}⁻¹.

As shown in Fig.3, the presence of 5 vol.% H_2O causes significant deactivation to the catalysts compared with the activity in the absence of H_2O . A further addition of 20 ppm SO_2 to the reaction stream causes more deactivation and results in even lower conversion. For the influence of Rh loading, the activity is enhanced as increasing the Rh loading from 1 wt.% to 2 wt.%, while the performance of 4 wt.% Rh/zeolite is similar to that of 2 wt.% Rh/zeolite catalyst. When taking both the CH_4 removal efficiency and the cost of the catalyst into consideration, 2 wt.% Rh/zeolite catalyst was selected as the most promising catalyst for removing of CH_4 from the engine exhausted gas. Therefore, the influence of operation temperature and SO_2 concentration was further studied over 2 wt.% Rh/zeolite catalyst and the results are shown in Fig.4.

As shown in Fig.4, the 2 wt.% Rh/zeolite was tested at 450, 475, and 500 °C separately with addition of SO_2 and increasing the SO_2 concentration from 1 ppm to 20 ppm at each temperature. As increasing the operation temperature from 450 °C to 500 °C, the finalized conversion of CH_4 in the presence of 1 ppm

SO₂ after 48 h increases from 27 % to 79 %. At each operation temperature, increase in SO₂ concentration causes decrease in CH₄ conversion, the conversion of CH₄ decreased from 58 % to 28 % as increasing the SO₂ concentration from 1 ppm to 20 ppm at 475 °C. As indicated by Fig.4, it is possible to obtain a high CH₄ removal efficiency by elevating the operation temperature and decreasing the SO₂ concentration in the exhausted gas. The SO₂ concentration in the real natural gas fuelled engine can be limited to around 1 ppm, allowing for a high CH₄ removal efficiency on this homemade 2 wt.% Rh/zeolite catalyst.

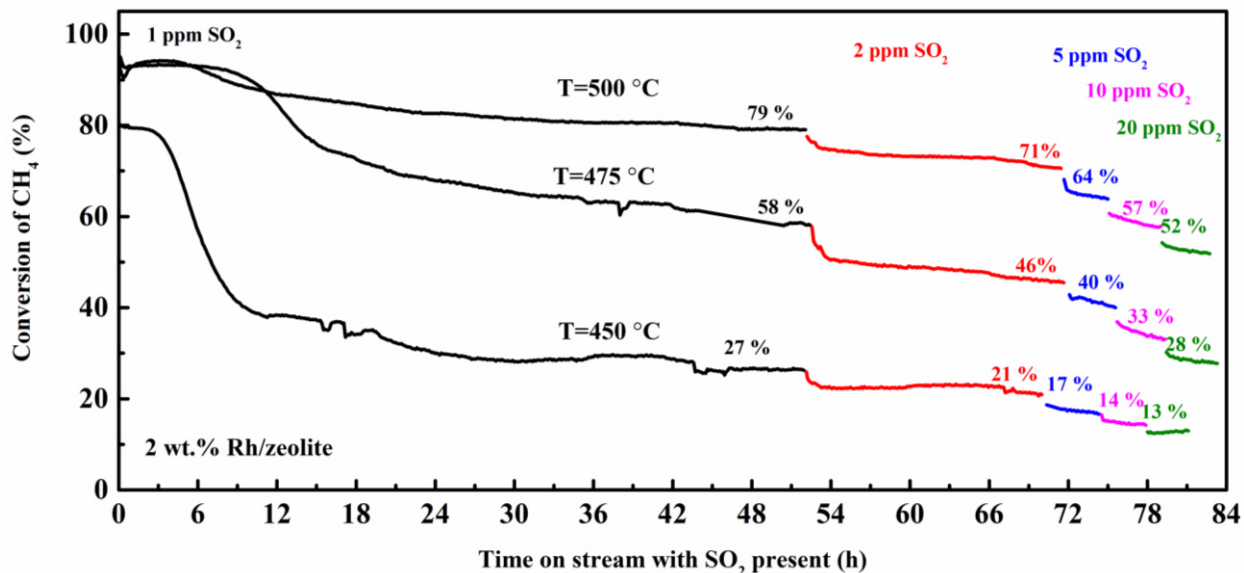


Fig. CS4.4. Conversion of CH₄ over 2 wt.% Rh/zeolite catalyst at 450, 475, and 500 °C in the presence of 1 ppm (blank), 2 ppm (red), 5 ppm (blue), 10 ppm (pink), and 20 ppm (olive) SO₂. 2500 ppm CH₄, 10 vol.% O₂, 5 vol.% H₂O, 1-20 ppm SO₂ when present, balanced with N₂. GHSV=150,000 ml/h·g_{cat}.

Regeneration of the poisoned catalyst

After SO₂ poisoning at 475 °C, the conversion of CH₄ decreased from 95 % to 28 %, further on, the poisoned catalyst was regenerate by removing SO₂ from the reaction gas to regenerate at the operation temperature (475 °C) and then regenerate at higher temperatures (500, 550, and 600 °C). After regeneration at each temperature, the catalytic bed was cooled to 475 °C to measure the activity of the regenerated catalyst. The temperature of the catalytic bed and the conversion of CH₄ during and after regeneration were shown in Fig.5. The conversion of CH₄ can be restored from 28 % to 71 % by just removing SO₂ from the reaction stream for 12 h at 475 °C. Which indicates that the deactivation caused by 20 ppm SO₂ was partially reversible. The conversion can be further restored to 74 %, 80 %, and 84 % after regeneration at 500, 550, and 600 °C, respectively. The activity cannot be regenerated to the activity of the fresh catalyst (95 %), which indicates the irreversible deactivation caused by running in the presence of SO₂.

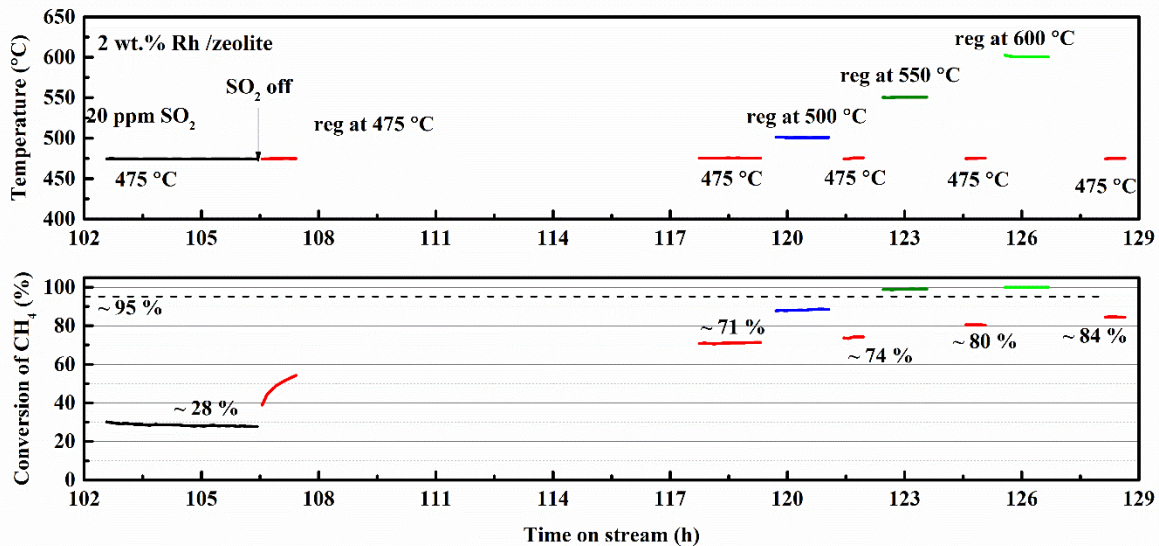


Fig. CS4.5. Influence of regeneration temperature on the activity of regenerated catalyst. 2500 ppm CH₄, 10 vol.% O₂, 5 vol.% H₂O, 1-20 ppm SO₂ when present, balanced with N₂. GHSV=150,000 ml/h · g_{cat}. (the experimental data during 107-118 h was lost due to the computer issue)

Conclusions

As a conclusion, the Rh/zeolite catalyst is the most promising catalyst to be used in the real natural gas fueled engine exhausted gas condition to remove CH₄. A Rh loading of 2 wt.% was selected among 1 wt.%, 2 wt.%, and 4 wt.% when taking both the CH₄ removal efficiency and the cost of the catalyst into consideration. In the presence of both H₂O and SO₂, it is possible to obtain a high CH₄ conversion by increasing the operation temperature to 475-500 °C and limiting the SO₂ concentration to a low level. The SO₂ in the real exhausted gas comes from lube oil and odour stuff which end up with a SO₂ concentration in the range 1-2 ppm. It makes the 2 wt.% Rh/zeolite promising to be used in the real engine exhausted gas to mitigate CH₄ emission. Thermal regeneration by removing SO₂ from the reaction gas can partly restore the activity but there are irreversible deactivation cannot be easily regenerated. A more efficient regeneration method is still being sought.

[Case study 5. Korean catalyst study.](#)

Pt/Pd bimetallic catalyst with improved activity and durability for lean-burn CNG engines

Abstract

Compressed natural gas (CNG) has been regarded as an alternative fuel for current fossil fuels such as gasoline and diesel. Recently the increasing interest in shale gas is drawing more attention to CNG vehicles of which number is expected to increase. Exhaust gas from CNG engines with lean combustion contains relatively low nitrogen oxides and particulate matters compared to conventional fossil fuel based engines. However, high amount of unburned methane, which has much higher greenhouse warming potential than CO₂, limits the wide use of CNG.

Pd-based catalysts have been studied for a long time for the combustion of methane that is a main constituent of CNG. Pd is reported to be more active for combustion of methane as a main, compared to other precious metals. However the durability of Pd-based catalysts has been a concern so far. However, in the present study, we developed an improved Pd-based catalyst for CNG engines by introducing Pt and promoters to enhance methane oxidation activity at low temperature and long term durability. Pt was more active to oxidize paraffinic hydrocarbons that comprise ~10% of total hydrocarbons in exhaust gas from lean burn CNG engines. Exotherm resulting from the paraffinic hydrocarbon oxidation by Pt could promote the remaining methane oxidation by Pd. Furthermore, potential causes for the deactivation of Pd-based catalyst were investigated from the various points of Pd-sintering by high temperature exposure, PdO decomposition, sulfation and coking, and the formation of new Pd containing compound.

Further, the root causes for the deactivation was investigated from the points of thermal and non-thermal routes. Based on the investigation some key factors were concluded and using these results new generation catalysts were designed. Majorly, two factors attributed for the improved performance, i) optimal support material and ii) optimal characteristics of Pd. Better Pd dispersion were achieved by selecting support with optimal surface property. Along with Pd-Pt alloying, electronic modifiers such as OSC and promoters were effective to make CNG catalyst more durable. In conclusion, optimal use of support material for Pd/Pt and promoters to keep Pd stable were identified as key factors for the design of more active and durable catalyst.

Experimental

Catalysts preparation and aging

Reference Pd-based and newly developed CNG catalysts were prepared by applying wash-coat onto cordierite honeycomb substrates (400cpsi/6.5mil). 1Pt/5Pd ratio was adopted for the sample preparation for activity test and characterization. Hydrothermal aging before activity testing was performed at 750 °C for 10hrs with 10% water.

Table CS5.1. Summary of prepared catalysts.

Catalyst	Key concept
Ref. CNG	Reference
CNG-A	Optimal Pt/Pd location
CNG-B	CNG-A + new support
CNG-C	CNG-B + Optimal OSC
CNG-D	CNG-C + additive

Catalytic activity test

Catalytic activity tests were performed in a fixed-bed reactor equipped with an electrically heated furnace. Cored catalysts with 1" diameter and 2" length were located vertically in the rig. Temperatures were monitored using a K-type thermocouple placed in the inlet and outlet position of the cored catalyst. Main feed condition of CH₄ oxidation was 5000ppm CH₄, 10% O₂, 5% H₂O, 5% CO₂ under N₂ balance and GHSV=60,000 1/h. Feed condition were also adjusted when needed. Catalyst inlet temperature was heated from room temperature to 500°C for CH₄ light-off test and maintained at 450°C for durability test. Total HC was detected using FID equipped analyzer (Thermo, 51C-HT, USA). NDIR equipped analyzer (Simens Oxymat6) was used for CO and NO_x measurement.

Catalyst Characterization

Diffuse Reflectance Infrared Fourier Transform (DRIFT) spectra of the samples were recorded using a Nicolet 6700 spectrometer equipped with a MCT detector and a diffuse reflectance cell (Harrick CHC-CHA-3). The spectra of 64 scans were collected with a resolution of 2 cm⁻¹. About 20 mg of the catalyst powder was placed in the cell and pretreated at 400°C for 30 min in a flow of N₂ (40 ml/min) in order to remove water in the catalyst. The system was cooled down to room temperature and the background spectrum was recorded. The catalyst was then subjected to feed stream for methane oxidation reaction, CH₄ 5000 ppm, 10 vol.% O₂, N₂ balance.

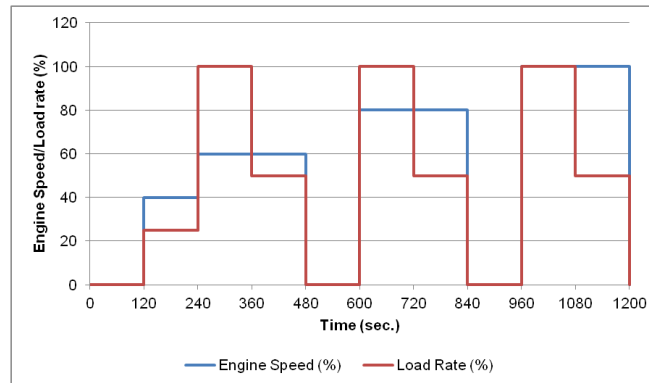
CO-chemisorption was performed using BELCAT instrument in order to measure the PGM dispersion. About 50 mg of catalyst powder was used for the experiment.

Two kinds of TG/DSC experiments were performed. First one was a consecutive heating-up and cooling-down test for PdO decomposition study. Secondly soot oxidation test using mixture of 0.2g catalyst powder and 0.04g soot was placed into a crucible. Soot burning temperature was determined by increasing temperature to 900°C.

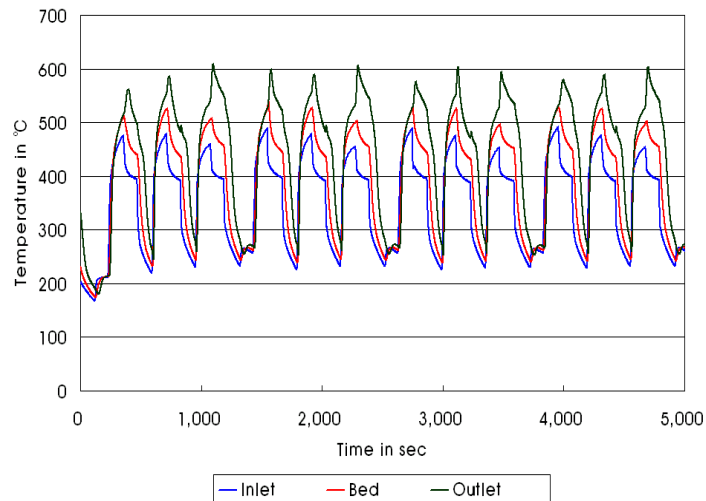
RESULT AND DISCUSSION

Durability of Pd-based CNG catalyst

The durability of Pd-based CNG catalyst with 10.6g/L, PGM ratio 1Pt/5Pd, 10.5”*6” (400/6.5) was evaluated at 6L CNG engine using Seoul-10 as shown in Figure 1. Used evaluation mode has 3 phases with difference engine speed and load rate. Maximum temperature during on cycle test of Seoul-10 mode was about 600°C. THC conversion was monitored with Seoul-10 aging time. The THC conversion dropped significantly as the aging time increased from 100% at fresh state to 40% after 50-hrs aging (Figure 2).



(a)



(b)

Figure CS5.1. (a) Seoul-10 mode for evaluation and (b) temperature profiles of Seoul-10 mode for aging

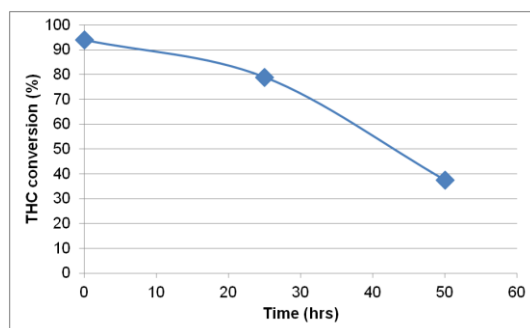


Figure CS5.2. THC conversion of reference catalyst with aging time of Seoul-10 mode. Engine: 6L (360 hp) CNG engine, Catalyst size & PGM : 10.5”D*6”L (400/6.5), 2 bricks, 10.6g/L

Catalyst deactivation mechanism

Others have investigated the deactivation mechanism of CH₄ oxidation catalysts. Potential causes are suggested such as PdO decomposition to Pd at high temperature and its hysteresis in Pd to PdO formation at low temperature, sulfation, coking and water inhibition.

To determine the thermal deactivation, the reference catalyst was aged at 700°C and 750°C for 10 hrs. Both aged catalysts out performed engine bench aged sample for 50hrs using Seoul-10 mode

(Figure 3).

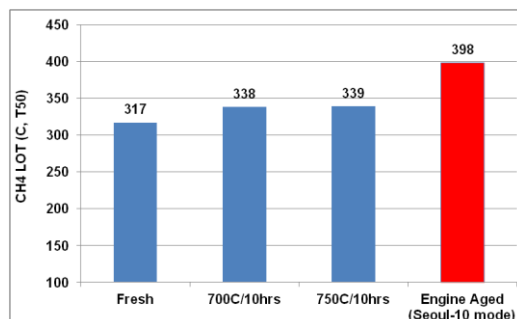


Figure CS5.3. THC oxidation activities of furnace and engine-bench aged catalysts, Catalyst size & PGM : 1”D*2”L (400cps/6.5mil) core, 1.6g/L, Feed : 5000ppm CH₄, 5% O₂, 5% H₂O, N₂ balance, GHSV=50,000 1/h

Figure 4 shows the thermal gravity analysis (TGA) pattern of the engine-bench aged catalyst. No remarkable weight loss was not observed at 400 to 500°C (reaction temperature). And PdO decomposition took place around 850°C.

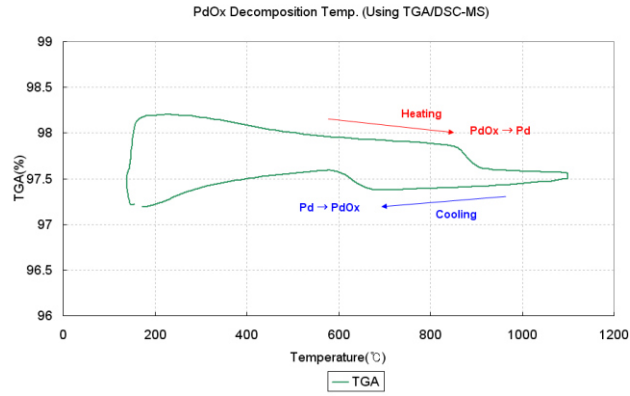


Figure CS5.4. Thermo-gravimetric pattern of engine bench aged reference catalyst with consecutive heating and cooling

Considering the temperature profile of CNG catalyst during aging with maximum temperature of about 600°C (Figure 1), the contribution of thermal routes to CNG catalyst deactivation seems to be minimal through either Pd sintering or PdO decomposition.

Figure 5 shows the elemental mapping images of engine-bench aged catalyst. The S concentration was not so high that sulfation might not be a main cause for the deactivation of aged catalyst.

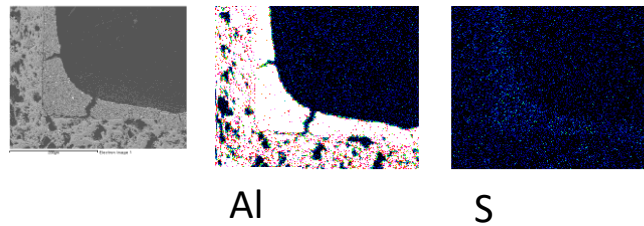
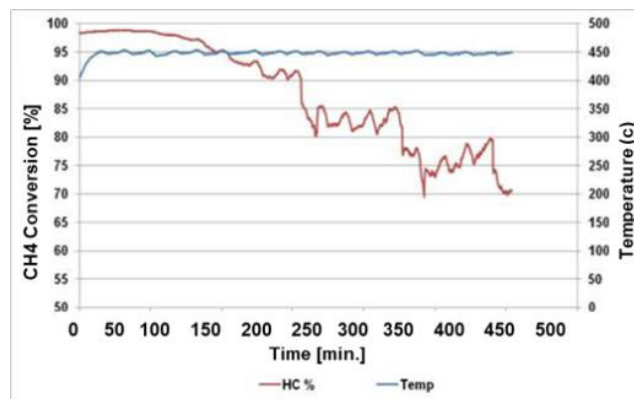
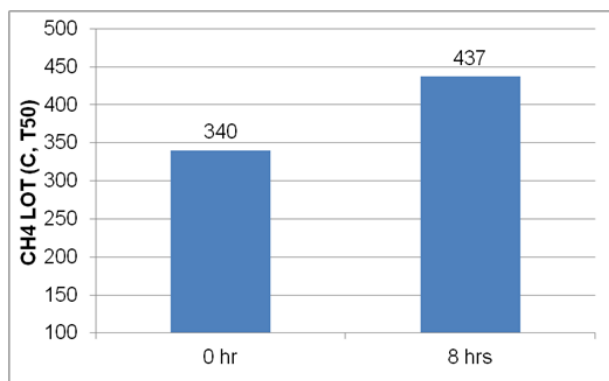


Figure CS5.5. EDS elemental mapping images of engine bench aged reference catalyst



(a)



(b)

Figure CS5.6. CH₄ oxidation activity of reference catalyst at 450°C (a) CH₄ conversion with time-on-stream, (b) light-off temperatures of fresh and after 8 hrs operated catalyst.

To investigate further, catalysts were deactivated under simulated condition of CH₄, O₂ and steam at 450°C using hydrothermally aged reference catalyst at 750°C for 10hrs. THC conversion began with 98% and started to decline after 1.5hrs and dropped to 70% after 8 hrs (figure 6-a). Also, THC LOT50 significantly increase about 100°C higher compared to fresh catalyst (figure 6-b). This strongly indicates the deactivation is not directly associated with sulfation, because the simulated feed did not contain any sulfur species.

In-situ DRIFTS works have been carried out to investigate the change in Pd. Powder sample, placed onto drift cell, were heated to 450°C under N₂ flow and kept at the temperature for 10 hours under 80 ml/min feed comprising of 5000 ppm CH₄, 10% O₂ and N₂ balance. DRIFTS spectra of reference catalyst were recorded before and after the CH₄ oxidation reaction. After the CH₄ oxidation reaction, a strong hydroxyl group peak presumably bonded to Pd was observed in the corrected spectrum using the one obtained before CH₄ reaction (Figure 7). As Lisa and Charles reported, this strongly suggests Pd(OH)_x formation might be a root cause for the deactivation of reference CNG catalyst under lean environment in the mid-temperature range.

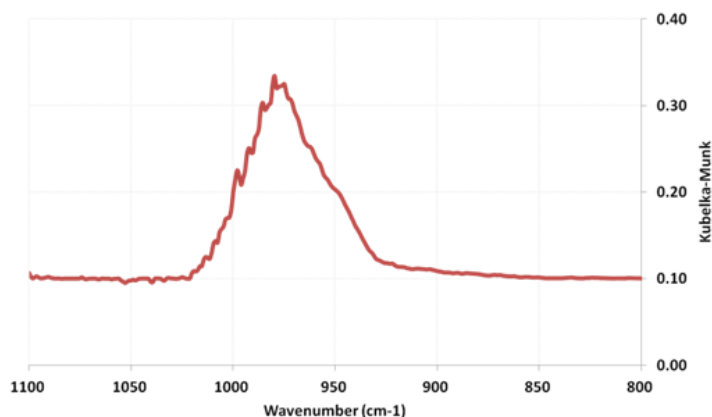


Figure CS5.7. DRIFTS spectrum of after CH₄ oxidation

Factors effecting the catalysts deactivation:

To know the effect of H₂O and intermediate species like HCHO, an experimental study was carried and found that both of these compounds (H₂O and HCHO) effected the durability of catalysts. With increase of steam from 5 to 10%, a substantial deactivation noticed even from first hour. Figure 8 illustrates the delta T, represents the exothermic temperature occurred due to reaction, after five hours of reaction with 10%H₂O there was no much exotherm (ΔT) means the catalyst deactivated. Figure 9 represents the role HCHO in the feed, addition of HCHO strongly effected the durability of catalysts. Considering these two major factors effective the catalysts deterioration design and process of metal oxide are carried.

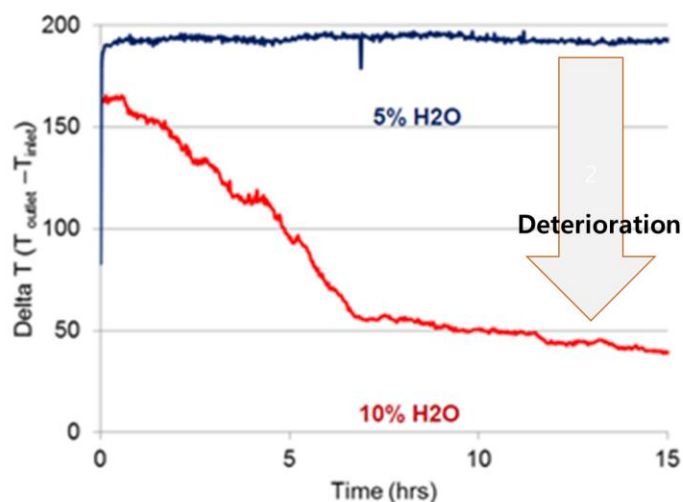


Figure CS5.8: H₂O effect on durability of catalysts aged at 750°C/25h.
Feed: 5,000ppm CH₄, 15% O₂, 5 or 10% H₂O, SV : 60,000 l/hr

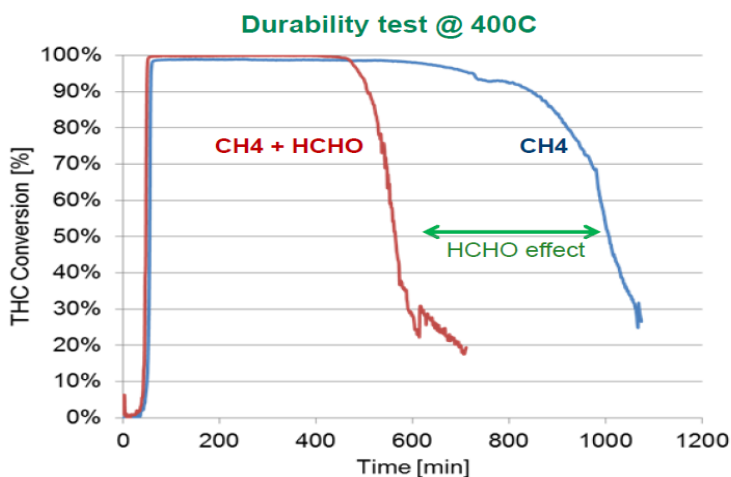


Figure CS5.9: HCHO effect on durability of catalysts aged at 750°C/25h
Feed: 5,000ppm CH₄, 0 or 1400ppm HCHO, 10% O₂, 10% H₂O, N₂ balance @ 400°C

Development of new CH₄ oxidation catalyst with improved durability

To improve CH₄ oxidation under lean environment, Pd stabilization has been tried by alloying with Pt, and using optimal support material for better Pd dispersion and gas diffusion.

Effective Pt-Pd alloying

Typical exhaust gas from CNG engines contains NMHC (Non Methane Hydrocarbon) that covers about 10% of total hydrocarbon. In general, the complete oxidation of CH₄ requires temperature higher than 450°C while NMHCs can be oxidized at relatively at lower temperature. Pt is also known to be more active for paraffinic NMHC oxidation. The reference catalyst contains Pt as well as Pd to utilize the exotherm generated by Pt catalyzed NMHC oxidation for Pd catalyzed CH₄ oxidation.

An optimal process has been developed to make Pt-Pd alloy better for Pd stabilization against water induced deactivation, resulting into catalyst CNG-A. Figure 10 shows the THC conversions of reference and CNG-A catalysts before and after hydrothermal aging. CNG-A was much better than reference catalyst at 450°C.

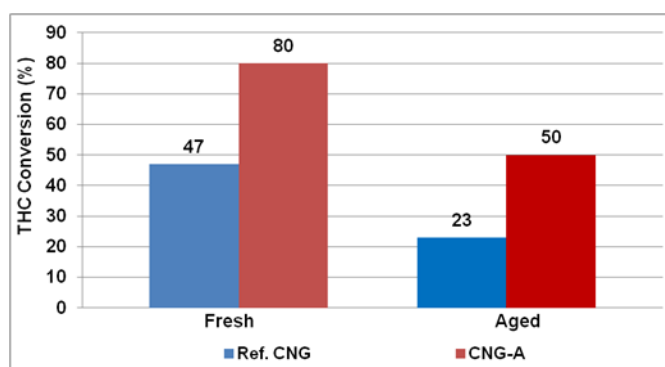


Figure CS5.10. THC conversions of reference and CNG-A catalyst, Catalyst size & PGM : 1”D*2”L (400cpsi/6.5mil) core, 2.5g/L(1Pt/5Pd), Feed : 1000ppm THC(82% CH₄, 3% C₃H₈, 15% C₂H₆), 400ppm CO, 300ppm NO, 8% O₂, 5% CO₂, 10% H₂O, N₂ balance, GHSV=48,000 1/h

PGM support material

Pd dispersion is one of key factors for the intrinsic activity of CH₄ oxidation and highly depends on the characteristics of the support material. Through screening the various kinds of alumina based support materials, a new support material was found for Pd support. As shown in Figure 11, the new support material increased Pd dispersion (blue bar and left Y axis), measured by CO-chemisorption, significantly after aging at 1,050°C for 12hrs.

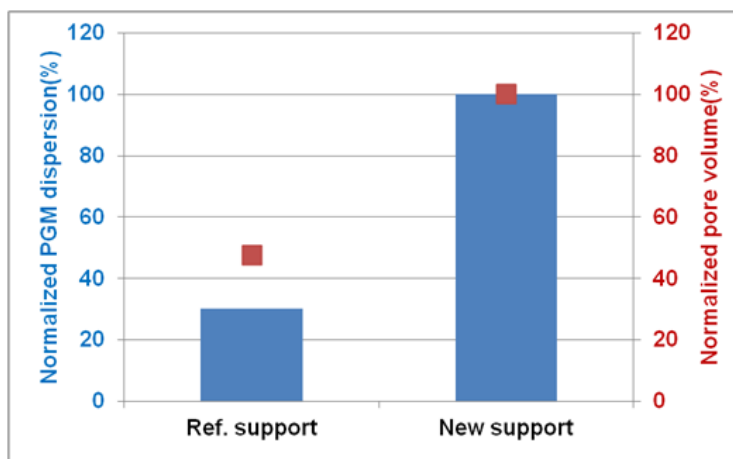


Figure CS5.11. Pd dispersion by CO-chemisorption after aged at 1050°C/12hrs

Figure 12 show the TEM images of smaller Pd particles in new support material after aging at 1,050°C for 12hrs (Figure 12). Pd particles were in size of 200~250 nm in case of reference support while 50~200 nm in case of new support.

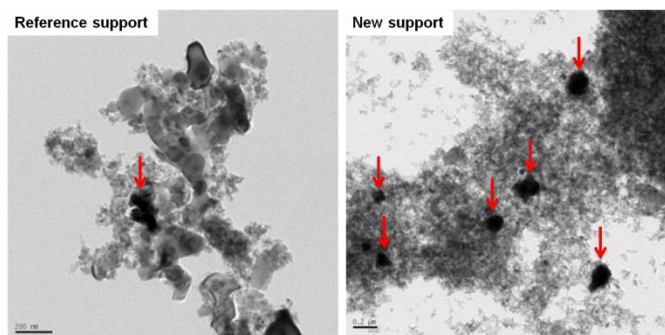


Figure CS5.12. TEM images of Pd on reference and CNG-B supports

The effect of improved Pd dispersion could be confirmed in Figure 13 showing the light-off performance of CNG-A and CNG-B prepared by new process described earlier. CNG-B with the new support material was 41°C better in T50 (THC) than CNG-A due to the improved Pd dispersion.

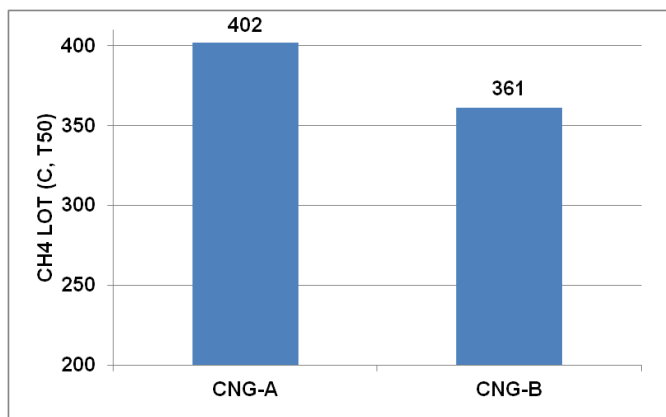


Figure CS5.13. Light-off performance of CNG-A and CNG-B catalysts

Effect of OSC material

The OSC (Oxygen Storage Component) has been well known as a key component of modern three-way catalysts. And its active oxygen species can oxidize soot at low temperature. The soot burning activity of OSC could be used as an indicator for its interaction with Pd and Pt. Soot burning temperatures with different OSC materials are shown in Figure 14. The temperature determined by TG/DSC measurement using the mixture of 0.2g catalyst and 0.02g soot under 90 ml/min, air flow. All OSC samples were aged at 900°C for 10hrs with 10% water.

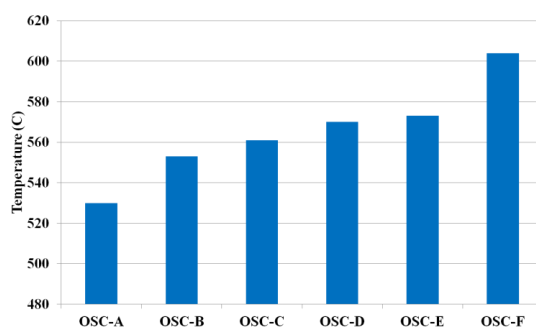


Figure CS5.14. Soot burning temperature with different OSC materials

OSC-F was used for reference and CNG-A and B catalysts. CNG-C sample was made by using OSC-A. More active OSC-A lowered light-off temperature of CH4 by 11°C (Figure 15).

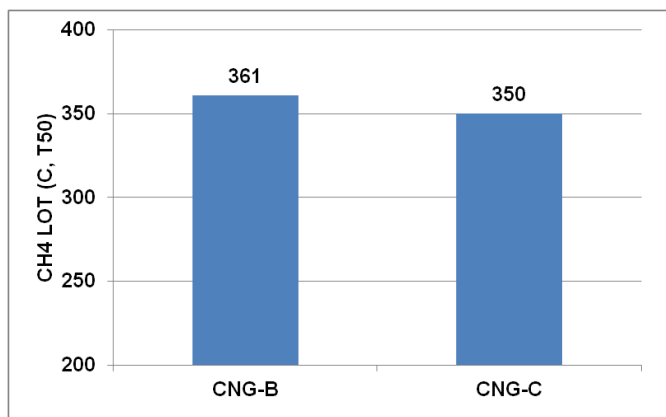


Figure CS5.15. Effect of OSC type to CH4 oxidation activity

New promoter for Pd

Various promoters were tested to modify the electronic property of Pd for improvement the catalytic performance and durability, especially under water feeding condition. When promoter A was added to CNG-C, the catalytic activity was significantly improved (Figure16).

Finally, CNG-D as a new CNG catalyst operating under lean environment was developed by applying new process and materials to reference CNG catalyst. The catalyst showed big improvement in CH4 oxidation and durability. Figure 17 shows THC conversion with time-on-stream at 450°C. Compared to the reference, CNG-D was much more durable. The activity of CNG-D was maintained until 38hrs while the reference catalyst survived for 4 hrs.

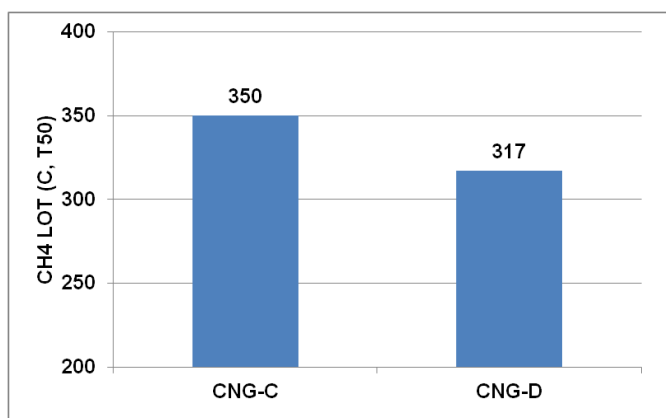


Figure CS5.16. Effect of promoter A (CNG-D) on CH4 oxidation activity

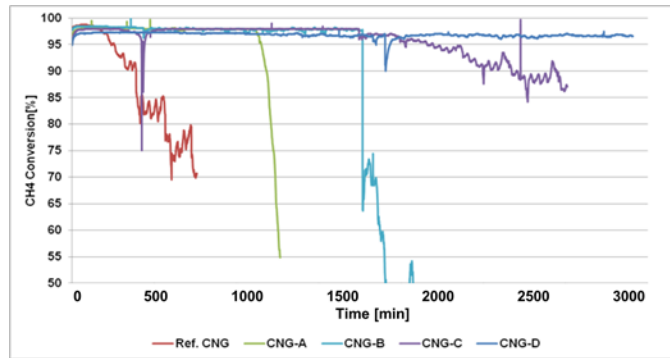


Figure CS5.17. CH4 oxidation activity with time-on-stream at 450°C

Summary/Conclusions

CNG is an attractive alternative for conventional liquid fuel. The lean burn engines based on CNG are able to be easily adapted to heavy duty vehicles, whereas it is essential to remove unburned CH₄ by use of the aftertreatment technologies. Low temperature activity and long term durability of Pd-based catalysts have been challenges in the aftertreatment system. In this study, we found some key factors which led to enhance the activity and durability of current Pd-based CNG catalyst. Two critical contributions were from optimal support material and optimal characteristics of Pd. Pd dispersion were achieved by selecting support with optimal surface property. Pd-Pt alloying and the use of electronic modifiers such as OSC and promoters were effective to make CNG catalyst more durable.

Case study 6. Finnish catalyst study.

Methane catalyst study as a part of 'CENGE - Controlling Emissions of Natural Gas Engines' project

In order to oxidize methane, a highly efficient catalyst is needed. One significant challenge in the development of methane oxidation catalysts for lean NG applications is the catalyst deactivation, since e.g. both sulphur and water have been found to inhibit the oxidation of methane [44-45].

Experimental

The research facility included a passenger car gasoline engine that was modified to run with natural gas. The selection of driving conditions was based on the emission levels. The target was to mimic the emission levels of a relevant power plant engine. Acceptable carbon monoxide and nitrogen oxide levels were achieved with engine adjustments. However, in order to achieve acceptable hydrocarbon levels, HC additions into the exhaust gas were also made. The engine with the test facility was presented in detail in [46] and a simplified schematic in Figure 1. The engine was operated with a lean air-to-fuel mixture.

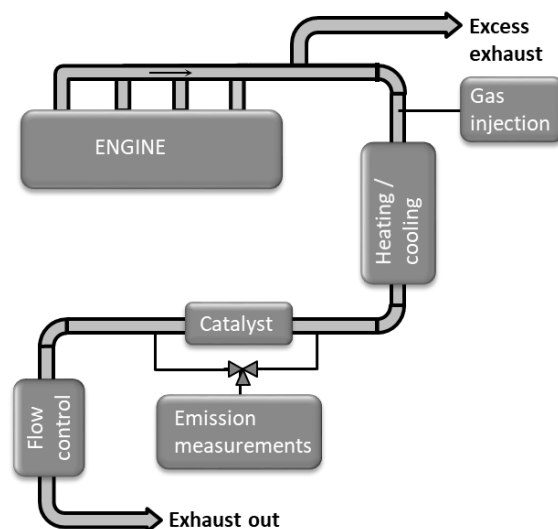


Figure CS6.1 A schematic of the research facility.

Natural gas from the Nord Stream pipeline has high methane content. In the present study, the gas analysis results were: 97.2 % methane, 1.37 % ethane, 0.17 % propane, 0.07% other hydrocarbons, 0.9 % nitrogen and 0.2 % carbon dioxide. The sulphur content of the gas was below 1.5 ppm. The lubricating oil sulphur content was 1760 mg/kg, density was 852.3kg/m³ and viscosity at 100°C was 12.0 mm²/s.

The methane oxidation catalyst (MOC) utilized platinum-palladium (1:4) as active metals on a tailored coating developed for lean NG applications and supported on a metallic substrate. The volume of MOC was 1.69 dm³.

In order to study the performance of catalysts, the exhaust gas temperature and the space velocity are essential parameters. In the test facility of the present study, the exhaust gas temperature and the exhaust gas flow were adjustable [46]. Studies were conducted in an exhaust gas temperature range of 350 to 500°C and with two exhaust gas flows (80kg/h and 40kg/h). The higher temperatures are needed for methane oxidation, and would also mean that the catalyst placement in any real application would be first in line downstream of the engine, even pre-turbocharger. Before conducting any actual tests, the catalyst was preconditioned by ageing for 48 hours in mode 1 (with an exhaust gas temperature of 400 °C and exhaust flow of 80kg/h).

The emission measurement setup consisted of a chemiluminescence detector (CLD), used to measure the NO_x (NO, NO₂) and a non-dispersive infrared (NDIR) analyser to measure CO and CO₂. An FTIR (Fourier transform infrared spectroscopy) analyser was used to measure water, methane, NH₃ and HNCO concentrations. The FTIR as well as the sampling line and the filter prior to the FTIR spectrometer were heated to 180 °C. In addition, methane, ethane, propane and ethylene components were measured from a diluted exhaust gas sample with a gas chromatograph (GC). The sample for GC measurement was taken from the FTIR output, utilizing a T-branch diluter and a tracer (Sulphur hexafluoride, SF₆) to define the exact dilution ratio. This was observed to be 9-13. All these measurements of gaseous emissions were made upstream and downstream of the catalyst setups.

Results

The measured methane concentrations (in mode 1) are shown in Figure 2 as a function of the exhaust temperature measured upstream of the catalyst. The MOC had a minor decreasing effect on the methane at ~400°C, but at ~500°C approximately 50% methane decrease was observed. Furthermore, the lower exhaust flow studied at 450°C increased the methane conversion from 38% (measured with 80kg/h exhaust flow) to 65% (with 40kg/h). These results have been presented in [47].

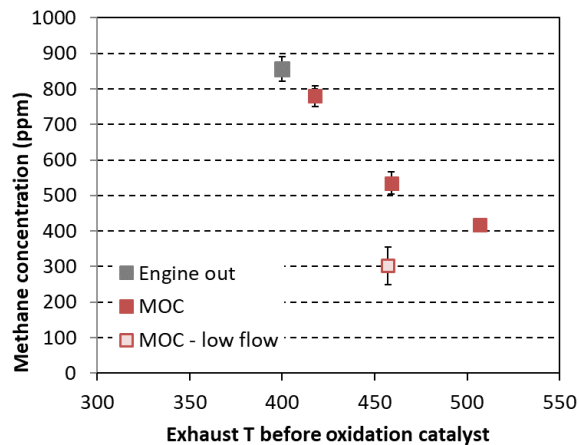


Figure CS6.2 Methane concentration measured upstream (engine out) and downstream of the MOC at three different exhaust temperatures and two exhaust flows (normal flow 80kg/h, low flow 40kg/h).

The effect of sulphur on the methane oxidation catalyst performance can be crucial, since as little as 1 ppm SO₂ present in the exhaust has already been found to inhibit the oxidation of methane (e.g. [44-45]). In this study we did not observe any significant change in the catalyst performance during the tests. The possible SO₂ originates from the sulphur in natural gas and the lubricating oil. Assuming that all this sulphur (from gas and oil) ends up as SO₂, the SO₂ present in the exhaust gas would still be below 0.2 ppm in the driving modes of the present study. Furthermore, the test times in the present study were rather short, only tens of hours (after the 48h preconditioning), which might be too short to observe any significant catalyst deactivation by the sulphur amount in the present study.

Methane catalyst regeneration study as a part of ‘Hercules’ project

The SO₂ and water present in the exhaust gas has found to inhibit the oxidation of methane and therefore a regeneration procedure needs to be developed in order to maintain the catalyst efficiency. In this work the regeneration of a methane oxidation catalyst (MOC) by H₂ was studied.

Experimental

Prior to experiments the catalyst was preconditioned by ageing for 48 h in the selected driving mode with an exhaust gas temperature of 400 °C and exhaust flow of 80 kg/h. The actual experiments were performed at 500°C with an additional experiment at 550°C. The catalyst set-up is presented in Figure CS6.3 Set-up. and the engine out exhaust gas composition at the selected driving mode is presented in Table 2.

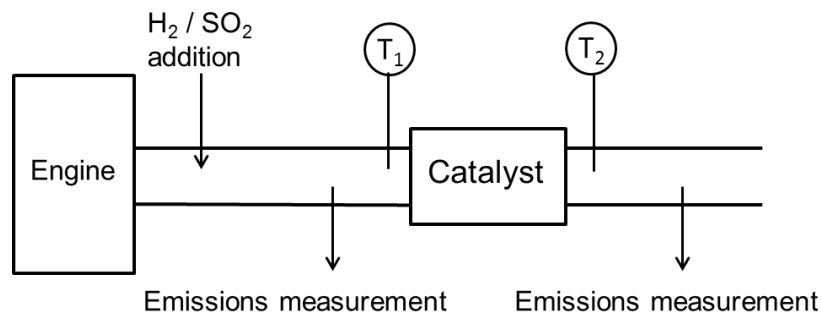


Figure CS6.3 Set-up.

Table CS6.1 Engine out emissions at the selected driving mode in the beginning of the experiments

Torque	Speed	Power	NO _x	CH ₄	CO	CO ₂	O ₂
70 Nm	2700 rpm	20 kW	230 ppm	740 ppm	420 ppm	6.9 %	5.6 %

The experiments included a 190 h at the same driving mode (see Table 3). During the experiments, additional SO₂ was fed into the catalyst in 20 h periods until 80 h was reached following with a longer period of 70 h and again continued with 20 h periods until 190 h was reached. This SO₂ fed (together with the sulphur from the natural gas and lubricating oil) lead to an SO₂ level of 1.5 ppm in the exhaust gas. After each 20 h, H₂ was fed into the catalyst at concentrations of 2-2.5% in order to study how the catalyst regenerates. Specifically, after the first three '20 h ageing' periods 2% of H₂ was fed for 15 min, while the following regenerations were done with 2.5% H₂. After the 190 h ageing one additional 20 h ageing was done at higher exhaust temperature of 550 °C following by regeneration with 2% H₂.

Table CS6.2 Description of the experiment.

Exhaust temperature	500 °C
20 h ageing periods	SO ₂ level in exhaust 1,5 ppm
Regeneration in 20h periods:	H ₂ addition:
	20h 2 % H ₂ for 15 min
	40 h 2 % H ₂ for 15 min
	60 h 2 % H ₂ for 15 min
	80 h 2.5 % H ₂ for 15 min
	150 h 2.5 % H ₂ for 30 min
	170 h 2.5 % H ₂ for 30 min
	190 h 2.5 % H ₂ for 30 min
Total ageing time	190 h
Additional	+ 20 h ageing at 550 °C followed by regeneration with 2% H ₂

In general, emission measurements we done in the beginning of the experiment, after the 20 h ageing, after the regeneration phase, again after the next 20 h ageing and so on. Every time after the regeneration, the emissions were monitored for 4 hours before the next 20 h ageing period.

Emission measurements included a Horiba PG-250 analyser used to measure NO_x, CO, CO₂, and O₂. CO and CO₂ were measured by non-dispersive infrared, NO_x by chemiluminescence and O₂ by a paramagnetic measurement cell. Exhaust gas was dried with gas-cooler before it was measured by Horiba.

Online SO₂ emissions were determined by a Rowaco 2030 1 Hz FTIR Spectrometer equipped with an Automated MEGA-1 (miniMEGA) sampling system. The detection limit for SO₂ was 2.5 ppm. An agilent

490 MicroGC was used to measure the hydrocarbons and hydrogen. The detection limits for ethane, ethene, and propane were approximately 2 ppm, for methane 10 ppm, and 100 ppm for hydrogen. In addition, multiple gaseous components were measured by two Gaset DX-4000 FTIR spectrometers, one placed upstream and the other downstream of the catalyst.

Results

During the ageing experiment the exhaust temperatures before and after the catalyst were followed. During the regeneration periods the added H₂ was found to react (oxidize) in the catalyst leading to remarkable temperature increase. The temperature downstream the catalyst was increased by 140 °C and 165 °C, at H₂ injection of 2% and 2.5%, respectively (Figure 4). The temperatures before the catalyst stayed constant regardless of hydrogen injection, as was targeted.

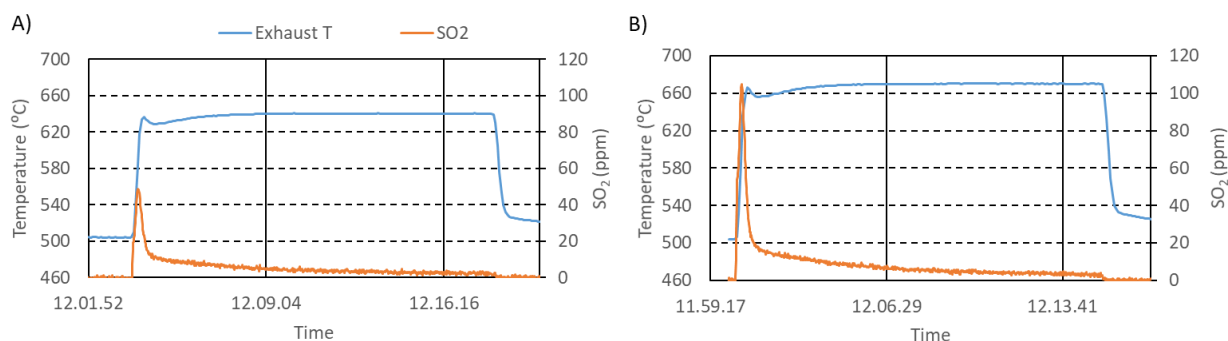


Figure CS6.4 Exhaust temperature and SO₂ measured downstream of the catalyst during the regenerations A) with 2% H₂ and B) with 2.5% H₂.

At each regeneration phase (i.e. H₂ addition) SO₂ was found to release from the catalyst since a sharp peak of SO₂ was measured downstream of the catalyst by FTIR. The SO₂ release seemed to depend also on the amount of added H₂ since at the higher H₂ amount also a higher SO₂ peak was observed (Figure 4).

An earlier study, done with the same engine facility, showed that the temperature increase alone (i.e. without any H₂ addition) did not release any SO₂ from the catalyst (Heikkilä 2017). Also earlier, a total reduced sulphur thermal converted was utilized to convert any H₂S release to SO₂, but since no hydrogen sulfide (H₂S) was observed in the earlier study, the converted was not utilized in present study.

As targeted by the regeneration procedure, the H₂ addition and the following SO₂ release, was found to have an effect also on the methane efficiency of the catalyst. The methane conversion after the first 20 h ageing was found to be 37% (see Figure 5). After the following regeneration (2% H₂) the conversion was found to be 44%. However, after the next 20 h ageing the conversion was decreased to level of 33%. Again, the methane conversion was recovered by the regeneration but resulted to lower level (i.e. 41%) than after the first regeneration (i.e. 44%). During the third ageing and regeneration process the same conversion decrease continued. However, after the fourth 20 h ageing the conversion seemed to maintain the same level that was observed after the third ageing. Following with a regeneration done by increased H₂ addition (2.5%) the conversion ended up to higher level than after the earlier regeneration.

The fifth ageing was a longer ageing of 70 h after which the methane conversion was found to decrease near to 21% while the following regeneration recovered the conversion to the level of 31%. The following two '20 h ageing and regeneration' -cycles resulted to nearly same methane conversion levels. This indicates that the catalyst is stabilized or saturated with the SO₂ meaning that no more SO₂ can be stored in the catalyst.

At the end (after 190 h), the temperature was increased from 500 °C to 550 °C and a significant increase was also found in the methane conversion which increased from 29% to 53%. One more ageing (20 h) was performed at this higher temperature resulting to methane conversion of 42% but the following regeneration recovered the conversion to nearly same level than before the ageing.

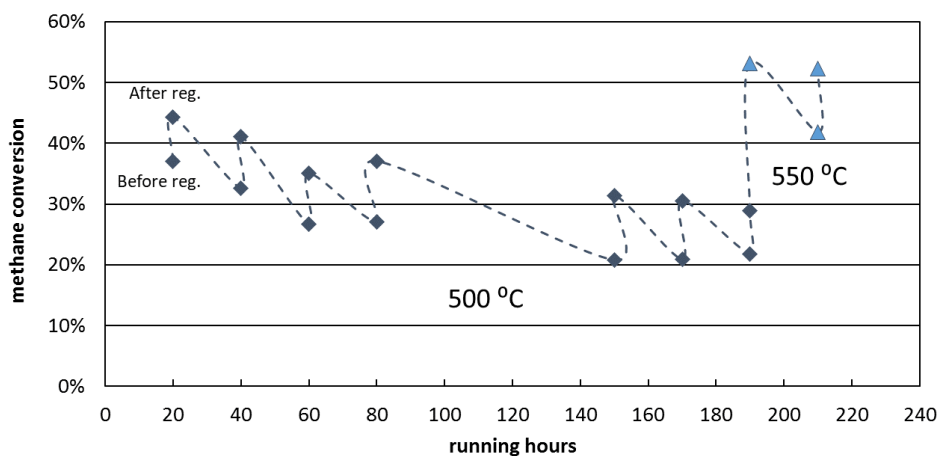


Figure CS6.5 Methane conversion during the whole 190 h ageing at 500 °C, measured after the ageing period (before the regeneration) and after the regeneration (before next ageing), and additional 20 h ageing at 550 °C.

Case study 7. Outside engine emissions (Swedish study)

Summary

AVL MTC AB has on the commission of The Swedish Transport Administration (STA) carried out measurements of methane leakage from methane fueled city buses. The amount of tested vehicles was 60. Twelve of the tested vehicles (15%) did not have any leakage. Thirty buses (50 %) did have leakage at fuel filling fittings corresponding to 2.9 ug/ day on average. There were no leakage from the gas tanks and roof fittings and only 3 % of the vehicles did have a diffuse, not quantified, increased level in the engine room. The major source of methane was inside the tailpipe corresponding to 0.88 mg /day and bus. The result indicates the major contribution of methane originates from slip during driving.

Introduction

There has been much discussions about the climate impact of increased natural gas usage. It is true that methane burns cleaner than other fossil fuels but methane leaking during the production, delivery and use of the gas has the potential to undo much of the greenhouse gas benefits we think we're getting when methane gas is substituted for other fuels.

According to EDF (Environmental Defense Fund) methane is more than 100 times more potent at trapping energy than carbon dioxide (CO₂), the principal contributor to man-made climate change. When considering its conversion to carbon dioxide over time its impact on an integrated weight basis is 84 times more potent after 20 years and 28 times more potent after 100 years.

Leaks and releases occur throughout the gas supply chain. If not minimized, methane leaks could undermine the greenhouse gas advantage methane gas offers and causes major trouble for the climate. However leaks can be detected, measured and reduced. In present study leakage from city buses in Stockholm were investigated. The fuel in Stockholm area consist of B50, i.e. 50 % bio methane and 50 % natural gas.

Gas leak detector for leak detection.

A Snooper mini was used for checking accessible gas lines for leakage. Leaks was determined based on detection at connection points, e.g. fittings, flanges, connections and gas regulator fittings The gas concentration was displayed in the ppm range (1 – 5000) and then calculated to g/day using the volume and estimated leakage rate.



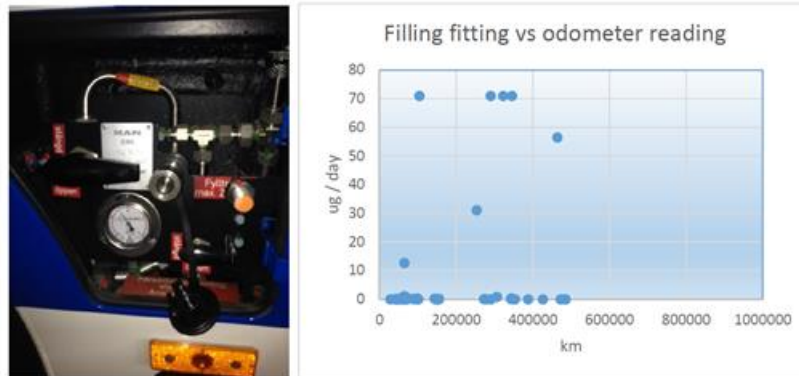
Picture 1. Methane leak measuring device.

Filling fittings

Each bus has two gas filling fittings. One at the front of the vehicle and one beside the of the entrance door. Each filling fitting consist of ten splices. Out of the 62 tested buses leakage was detected on 30 vehicles (48 %). The relatively high rate are due to wear since the buses are filled on daily bases. The

average amount emitted from these buses, four high emitters omitted, are calculated to 2.92 μg per day.

However, four of the busses were above the detection limit of the instrument i.e. more than 71 μg per day. No correlation between driving distance and methane emissions could be seen, Figure 1.



Picture 2. Gas filling fittings.

Figure CS7.1. Filling fitting leakage.

Gas tank and roof fittings.

The CNG gas tanks were located at the roof of the vehicles and consist of more than 100 fittings. No leakage were detected on all of the tested busses. However, one vehicle did have a diffuse increased level of 20 ppm under the cover of the gas bottles. The place for the leakage were not identified. The result indicates that fittings on the roof and gas bottles are not a major issue.

Engine room

The engine room consist of approximately 20 visible fittings. Two busses, 3 % of the tested vehicles, did have a diffuse increased level of 15 – 20 ppm. The leakage was not found and thus not quantified. The result indicates that fittings in the engine room are not a major issue.



Picture 3 a -e. Gas bottles and roof fittings.



Picture 4 a -b. Engine room fittings.

Exhaust pipe.

Methane levels were measured directly outside the tail pipe on parked vehicles. None of these measurements reveals any leakage outside the pipe. However, 24 % of the busses did have methane inside the tail pipe, suggesting that the leakage occurs during the start phase of the engine. This emission corresponds to 0.88 mg/ day in average. No correlation between driving distance and methane emissions could be seen, Figure CS7.2.

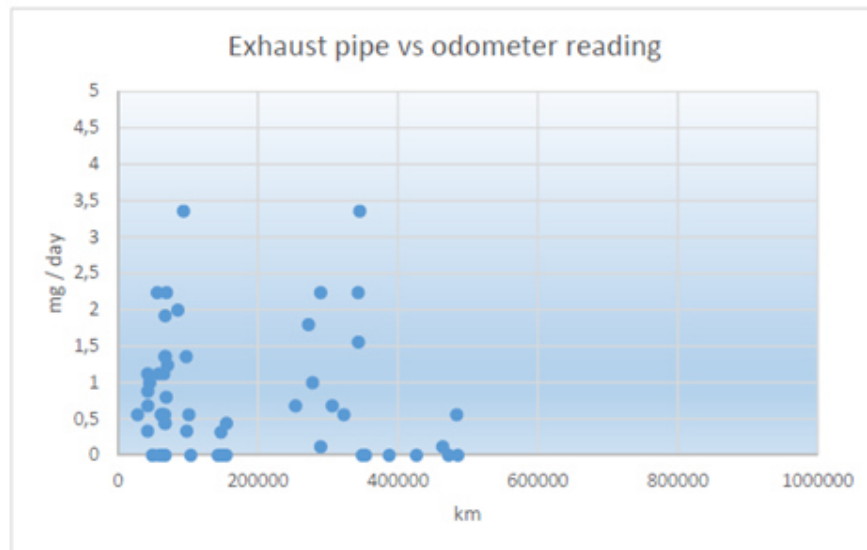


Figure CS7.2. Exhaust pipe leakage

Appendix

Table 1. Euro VI vehicles methane leakage. Filling fitting max 71 ug/day. Exhaust pipe max 28 mg/day.

Reg #	Odometer	Year	Exhaust pipe (mg/day)	Filling Fittings (ug/day)	Engine room (ppm)	Roof fittings (ppm)	Gas tank (ppm)	Class	Comment
EKY 492	42138	2014	1,1	0,14	0	0	0	EVI	
EKY 589	42465	2014	0,7	0	0	0	0	EVI	Measurement one
EKY 589	42609	2014	0,9	0	0	0	0	EVI	Measurement two
RHZ 071	45227	2014	1,0	0	0	0	0	EVI	
EKY 401	42204	2014	0,3	0	0	0	20	EVI	Measurement one
EKY 401	61968	2014	0,6	0,92	0	0	0	EVI	Measurement two
EHY 903	58246	2014	1,1	0	0	0	0	EVI	
ELA 874	65400	2014	MAX	0,63	0	0	0	EVI	Measurement one
ELA 874	101241	2014	0,6	0	0	0	0	EVI	Measurement two
EHZ 070	65360	2014	1,1	0	0	0	0	EVI	Measurement one
EHZ 070	67849	2014	1,4	0,49	0	0	0	EVI	Measurement two
ELA 870	97521	2014	1,4	0,35	0	0	0	EVI	
EKY 373	98054	2014	0,3	0	0	0	0	EVI	
ELA 800	70645	2014	1,2	0	0	0	0	EVI	
ELA 887	103872	2014	0,0	MAX	0	0	0	EVI	
EKY 388	67334	2014	0,4	0	0	0	0	EVI	
EKY 522	61924	2014	0,6	0,35	0	0,6	0	EVI	
XKM 199	66501	2014	0,6	0,28	0	0	0	EVI	
EKY 377	64198	2014	0,6	0,35	0	0	0	EVI	Measurement one
EKY 377	93499	2014	3,4	0	0	0	0	EVI	Measurement two
EKY 780	66849	2014	1,4	0,85	0	0	0	EVI	
ELA 911	67432	2014	0,0	0,49	0	0	0	EVI	
ELA 934	64223	2014	0,0	1,13	0	0	0	EVI	
EKY 568	69248	2014	2,2	0	0	0	0	EVI	
EHY 912	68805	2014	0,8	0,071	0	0	0	EVI	
EKY 789	67381	2014	1,9	0,92	0	0	0	EVI	Measurement one
EKY 789	85595	2014	2,0	0,14	0	0	0,14	EVI	Measurement two
DHZ 201	64467	2014	0,0	12,71	0	0	0	EVI	
EKY 388	67334	2014	0,4	0,49	0	0	0	EVI	
RBC 022	59740	2014	0,0	0	0	0	0	EVI	
URT 054	55997	2014	2,2	0	0	0	0	EVI	
HZL 909	49943	2014	0,0	0	0	0	0	EVI	
MBC 594	49072	2014	0,0	0	0	0	0	EVI	
EKH 533	142890	2014	0,0	0,21	0	0	0	EVI	
Average	68742	2014	0,88	0,75	0	0	0	EVI	

Table 2. Euro VI vehicles methane leakage. Filling fitting max 71 ug/day. Exhaust pipe max 28 mg/day.

Reg #	Odometer	Year	Exhaust pipe (mg/day)	Filling fittings (ug/day)	Engine room (ppm)	Roof fittings (ppm)	Gas tank (ppm)	Class	Comment
UPG 720	483671	2004	0,6	0	0	0	0	EEV	
ALM 760	272185	2009	1,8	0,071	0	0	0	EEV	
CJX 870	343221	2010	2,2	0,071	0	0	0	EEV	Measurement one
CJX 870	305993	2010	0,7	0,85	0	0	0	EEV	Measurement two
TDY 445	289516	2009	2,2	0	0	0	0	EEV	Measurement one
TDY 445	289516	2009	0,1	MAX	0	0	0	EEV	Measurement two
UPG 680	426191	2004	0,0	0	0	0	0	EEV	
ALM 812	27786	2009	0,6	0	0	0	0	EEV	
BED 353	277985	2009	1,0	0	0	0	0	EEV	
CJX 789	345246	2010	3,4	MAX	0	0	0	EEV	
UPG 710	472400	2004	0,0	0	0	0	0	EEV	
UPG 770	463846	2004	0,1	56,5	0	0	0	EEV	Measurement one
UPG 770	485336	2004	0,0	0	0	0	0	EEV	Measurement two
UPG 810	4787919	2004	4,5	28,2	0	0	0	EEV	
UPG 780	4545029	2004	0,0	0,57	0	0	0	EEV	
TFJ 532	253391	2009	0,7	31,1	0	0	0	EEV	
CRB 090	353386	2011	0,0	0	0	0	0	EEV	
CRO 350	349024	2011	0,0	0	0	0	0	EEV	
CDL 251	387233	2009	0,0	0	0	0	0	EEV	
DWZ 284	146582	2013	0,0	0	0	0	0	EEV	
WUC 539	150333	2012	0,0	0	0	0	0	EEV	
XYJ 062	154550	2012	0,0	0	60	0	0	EEV	
DWZ 151	154896	2013	0,4	0,14	0	0	0	EEV	
RKS 916	147076	2012	0,3	0	0	0	0	EEV	
DFT 505	343267	2011	1,6	0,28	30	0	0	EEV	
CJY 002	322456	2010	0,6	MAX	0	0	0	EEV	
Average	637617	2009	0,80	5,1	3	0	0	EEV	

6. Conclusions

The mechanisms behind the formation of unburned methane in natural gas engines have been described, based on state of the art from the literature. A model, TECMU, for the formation mechanisms has been developed in order to verify the understanding of these mechanisms (Case Study 1). The model has been evaluated and calibrated experimentally against measurements of unburned methane emissions from a 4-stroke medium speed dual fuel engine (Case Study 1) and a single cylinder spark ignited research engine operating on natural gas (Case Study 2). The work has resulted in a detailed understanding of methane formation mechanisms. It is concluded, that there are a number of items of special importance. These include: misfire/bulk quenching, wall quenching, crevice volumes, post oxidation and valve timing/overlap. It is also concluded that particularly low-pressure dual fuel engines are associated with high values of methane emissions. An easy and effective methane emission reducing measure on the involved 4-stroke medium speed engine was to adjust the valve timing. The investigations have, furthermore, shown that both the crevice and the quench layer mechanisms are important for the engine methane slip at moderately lean operation, and the post oxidation is certainly important, at least in relation to the crevice material. It was also found that the quench layer mechanism is very important at leaner operation, and the post oxidation was almost eliminated at leaner operation. Since the unburned methane emissions origins from areas near the combustion chamber walls the sensible way to go now is towards direct injection of natural gas/bio-methane in order to reduce emissions.

Methane was applied as fuel with and without hydrogen admixture in a Euro-4 vehicle with stoichiometric operated, naturally aspirated, manifold injected 4 cylinder engine with an engine capacity of 2.0 l. Blending of hydrogen into natural gas was investigated on this vehicle. The blending of hydrogen into the CNG is not readily feasible in terms of materials, as both the gas network and the gas-carrying components in the vehicle must be designed for this. However, operation in conventional CNG vehicles would lead to significantly lower pollutant emissions than those already present in CNG operation. NO_x emissions could be practically eliminated in the entire operating range, and T.HC emissions, which mainly consist of methane could also be reduced by an average of one third. However, the volumetric energy density, which decreases by almost 30% with an H₂ content of 25 mole %, would be operationally disadvantageous. It could be compensated by increasing the pressure to 350 bar. For future combustion processes with diluted mixture formation (lean or EGR operation), H₂ blending could be an interesting option due to the difficult ignition of (diluted) methane gases.

Catalytic after treatment of methane was investigated in two different cases:

- 1) A series of Rh/zeolite catalysts design for oxidation of exhaust CH₄ were tested. 1 wt.% Rh/zeolite catalyst had higher activity compared with the commercial catalyst under same operation condition. The activity of the Rh/zeolite catalyst can be significantly enhanced by elevating the operation temperature to 475 °C and limiting the SO₂ concentration to a low level. It seems promising to be used in the real engine exhausted gas condition where the SO₂ concentration is 1-2 ppm. Regeneration by removing SO₂ from the reaction gas can partly restore the catalyst activity, but a more efficient regeneration method is still being sought.
- 2) Another case investigated the Pd based catalyst performance. Pd is believed to be the best converting precious metal for methane catalysts. In this study, some key factors were found,

which led to enhance the activity and durability of current Pd-based CNG catalyst. Two critical contributions were from optimal support material and optimal characteristics of Pd. Pd dispersion were achieved by selecting support with optimal surface property. Pd-Pt alloying and the use of electronic modifiers such as OSC and promoters were effective to make CNG catalyst more durable.

Regeneration of the catalysts used is an important issue, and a regeneration method by hydrogen was studied. With a catalyst aged to a conversion efficiency of 37%, it was possible to maintain this level, and even increase the efficiency after regeneration and ageing again applying regeneration gases containing 2,5% hydrogen.

Finally, a number of vehicles were tested for tailpipe methane emissions as well as other methane emissions. The results of this investigation indicates that the major contribution of methane originates from slip during driving, i.e. tailpipe emissions.

7. References

- [1] IPCC, 2013. "Climate Change 2013: The Physical Science Basis", Working Group I Contribution to the Fifth Assessment Report of the Intergovernmental Panel on Climate Change, <https://www.ipcc.ch/report/ar5/wg1/>
- [2] <https://www.dieselnet.com/standards/eu/hd.php>
- [3] "Alternative Fuels for Marine Applications: Future Marine Fuels Study", IEA Advanced Motor Fuels TCP – Annex 41. Final report, May 2013.
- [4] "Enhanced Emission Performance and Fuel Efficiency for HD Methane Engines", IEA Advanced Motor Fuels TCP – Annex 39. Final report, May 2014.
- [5] Dyer, TM, "On the Sources of Unburned Hydrocarbon Emissions from Lean-Burn Engines". VDI Symposium on Lean-Burn Engines, Wolfsburg, West Germany, December, 1985.
- [6] Bechtel, JH and Blint, RJ "Structure of a Laminar Flame-Wall Interface by Laser Raman Spectroscopy". Applied Physics Letters, Vol. 37, No. 6, pp. 576-578, 1980.
- [7] Blint, RJ and Bechtel, JH, "Flame/Wall Interface: Theory and Experiment", Combustion Science and Technology, Vol. 27,, pp 87-95, 1982.
- [8] Westbrook, CK et. al. "A Numerical Study of Laminar Wall Quenching" Combustion and Flame, Vol. 40, pp 81-99, 1981.
- [9] Wentworth, JT "The Piston Crevice Volume Effect on Exhaust Hydrocarbon Emissions" Combustion Science and Technology, Vol. 4, pp 97-100, 1971.
- [10] Adamczyk, AA et. al. "A Combustion Bomb Study on the Hydrocarbon Emissions from Engine Crevices". Combustion Science and Technology, Vol. 33, pp 261-277, 1983.
- [11] Namazian, M and Heywood, JB ""Flow in the Piston-Cylinder-Ring Crevices of a Spark-Ignition Engine: Effects on Hydrocarbon Emissions, Efficiency and Power" SAE Technical Paper Series, Paper no. 820088, 1982.
- [12] Quader, AA "Lean Combustion and Misfire Limit in Spark Ignition Engines". SAE Technical Paper Series, Paper no. 741055, 1974.
- [13] Jensen, TK and Schramm, J "A Three Zone Heat Release Model for Combustion Analysis in a Natural Gas SI Engine. SAE Technical Paper Series, Paper no. 2000-01-2802, 2000.
- [14] Ogawa, H et al , " Improvement of Combustion and Emissions in a Dual Fuel Compression Ignition Engine with Natural Gas as the Main Fuel", SAE Technical Paper Series, paper no. 2015-01-0863, 2015
- [15] Jespersen MC, "Experimental investigation of methane slip sources from spark ignited natural gas engines". PhD thesis, Technical University of Denmark, Dep. Of Mechanical Engineering, 2019.

- [16] C. K. Westbrook and F. L. Dryer, "Simplified reaction mechanisms for the oxidation of hydrocarbon fuels in flames," *Combustion Science and Technology*, vol. 27, pp. 31-43, 1981.
- [17] Jensen, MV and Schramm, J. "Numerical analysis of methane slip source distribution in a four-stroke dual-fuel marine engine", Technical University of Denmark, Dep. Of Mechanical Engineering, 2019 (to be published in journal).
- [18] Kikusato A, et al, "Study on Improving Thermal Efficiency of a Natural Gas Engine by Highly Dispersed Pilot Diesel Spray" *JSAE Technical Paper Series*, paper no. 20164416, 2016.
- [19] Meng F, et al, "Conversion of Exhaust Gases from Dual-Fuel (Natural Gas-Diesel) Engine under Ni-Co-Cu/ZSM-5 Catalyst", *SAE Technical Paper Series*, paper no. 2017-01-0908, 2017
- [20] <http://www.naturalhy.net/>
- [21] C. Skalla, *Gemischbildung und Verbrennung von Wasserstoff/Methan-Gemischen in Pkw-Anwendungen*, 2012, Institut für Verbrennungskraftmaschinen und Thermodynamik, TU Graz, Graz
- [22] O. Florisson, D. Pinchbeck, *NATURALHY: first step in assessing the potential of the existing natural gas network for hydrogen delivery*, 2009
- [23] Soltic P. et al; *Micro-thermal CMOS-based gas quality sensing for control of spark ignition engines; Measurement* 91 (2016)
- [24] Biffiger H. et al; *Effects of split port/direct injection of methane and hydrogen in a spark ignition engine; International journal of hydrogen energy* (2015)
- [25] Corro, G., Cano, C. & Fierro, J. L. G. Promotional effect of C2-C4 hydrocarbon on CH4 oxidation on sulfated Pt/r-Al2O3 catalysts. *J. Mol. Catal. A Chem.* **281**, 179–183 (2008).
- [26] Su, S. C., Carstens, J. N. & Bell, A. T. A Study of the Dynamics of Pd Oxidation and PdO Reduction by H 2 and CH 4. *Sci. York* **135**, 125–135 (1998).
- [27] Castellazzi, P. *et al.* Role of Pd loading and dispersion on redox behaviour and CH4 combustion activity of Al2O3 supported catalysts. *Catal. Today* **155**, 18–26 (2010).
- [28] Roth, D., Gélin, P., Primet, M. & Tena, E. Catalytic behaviour of Cl-free and Cl-containing Pd/Al2O3 catalysts in the total oxidation of methane at low temperature. *Appl. Catal. A Gen.* **203**, 37–45 (2000).
- [29] Lovón-quintana, J. J., Santos, J. B. O., Lovón, A. S. P., La-salvia, N. & Valenc, G. P. Low-temperature oxidation of methane on Pd-Sn / ZrO 2 catalysts. **411**, 117–127 (2016).
- [30] Tao, F. F. *et al.* Understanding complete oxidation of methane on spinel oxides at a molecular level. *Nat. Commun.* **6**, 7798 (2015).
- [31] Cargnello, M. *et al.* Exceptional Activity for Methane Combustion over Modular Pd@CeO2 Subunits on Functionalized Al2O3. *Science (80-.)*. **337**, 713–717 (2012).
- [32] Chen, J., Arandiyán, H., Gao, X. & Li, J. Recent Advances in Catalysts for Methane Combustion. *Catal. Surv. from Asia* **19**, 140–171 (2015).
- [33] Choudhary, T. V., Banerjee, S. & Choudhary, V. R. Catalysts for combustion of methane and lower

- alkanes. *Appl. Catal. A Gen.* **234**, 1–23 (2002).
- [34] Mahara, Y. *et al.* Time Resolved in situ DXAFS Revealing Highly Active Species of PdO Nanoparticle Catalyst for CH₄ Oxidation. *ChemCatChem* **10**, 3384–3387 (2018).
- [35] Schmal, M. *et al.* Methane oxidation - effect of support, precursor and pretreatment conditions - in situ reaction XPS and DRIFT. *Catal. Today* **118**, 392–401 (2006).
- [36] Miller, J. B. & Malatpure, M. Pd catalysts for total oxidation of methane: Support effects. *Appl. Catal. A Gen.* **495**, 54–62 (2015).
- [37] Escandon, L. S., Ordonez, S., Vega, A. & Diez, F. V. Oxidation of methane over palladium catalysts: Effect of the support. *Chemosphere* **58**, 9–17 (2005).
- [38] Monai, M. *et al.* Phosphorus poisoning during wet oxidation of methane over Pd@CeO₂/graphite model catalysts. *Appl. Catal. B Environ.* **197**, 271–279 (2015).
- [39] Monai, M. *et al.* The effect of sulfur dioxide on the activity of hierarchical Pd-based catalysts in methane combustion. *Appl. Catal. B Environ.* **202**, 72–83 (2017).
- [40] Gremminger, A. *et al.* Sulfur poisoning and regeneration of bimetallic Pd-Pt methane oxidation catalysts. *Applied Catal. B, Environ.* **218**, 833–843 (2017).
- [41] Lou, Y. *et al.* Low-temperature methane combustion over Pd/H-ZSM-5: active Pd sites with specific electronic properties modulated by acidic sites of H-ZSM-5. *ACS Catal.* acscatal.6b01801 (2016). doi:10.1021/acscatal.6b01801
- [42] Jones, J. M. *et al.* Sulphur poisoning and regeneration of precious metal catalysed methane combustion. *Catal. Today* **81**, 589–601 (2003).
- [43] Corti E. *et al.*; Spark advance real-time optimization based on combustion analysis; *Journal of Engineering for Gas Turbines and Power* (2011)
- [44] Lambert, J. K.; Kazi, M. S.; Farrauto, R. J. Palladium catalyst performance for methane emissions abatement from lean burn natural gas vehicles. *Applied Catalysis B: Environmental* 1997, **14**, 211-223.
- [45] Ottinger, N.; Veele, R.; Xi, Y.; Liu, Z. G. Desulfation of Pd-based oxidation catalysts for lean-burn natural gas and dual-fuel applications. SAE Tech. Pap. Ser. 2015, SAE paper 2015-01-0991.
- [46] Murtonen, T.; Lehtoranta, K.; Korhonen, S.; Vesala, H. Imitating emission matrix of a large natural gas engine opens new possibilities for catalyst studies in engine laboratory. In: CIMAC congress, June 6-10, 2016.
- [47] Lehtoranta, K., Murtonen T., Vesala H., Koponen P., Alanen J., Simonen P., Rönkkö T., Timonen H., Saarikoski S., Maunula T., Kallinen K., Korhonen S. Natural gas engine emission reduction by catalysts. *Emiss. Control Sci. Technol.* 2017, **3** (2) 142-152.
- [48] Heikkilä, S. 2017. Methane slip abatement by hydrogen addition. Master's thesis, University of Vaasa.

- [49] R. Amirante, E. Distaso, P. Tamburrano and R. D. Reitz, "Laminar flame speed correlations for methane, ethane, propane and their mixtures, and natural gas and gasoline for spark-ignition engine simulations", *International Journal of Engine Research*, vol. 18, pp. 951-970, 2017.
- [50] J. B. Heywood, "Internal Combustion Engine Fundamentals", McGraw-Hill, 1988.
- [51] www.cambustion.com/sites/default/files/instruments/HFR500/Cambustion500seriesgasanalyzers.pdf